PREPARATION AND CHARACTERIZATION OF POLYCHLOROPRENE/MODIFIED CLAY NANOCOMPOSITES

by

SAMSON MASULUBANYE MOHOMANE (B.Sc. Hons.)

Submitted in accordance with the requirements for the degree

MASTER OF SCIENCE (M.Sc.)

Department of Chemistry

Faculty of Natural and Agricultural Sciences

at the

UNIVERITY OF THE FREE STATE (QWAQWA CAMPUS)

SUPERVISOR: PROF A.S. LUYT

April 2010

DECLARATION

I declare that the dissertation hereby submitted by me for the Master of Science degree at the University of the Free State is my own independent work and has not previously been submitted by me at another university/faculty. I furthermore cede copyright of the dissertation in favour of the University of the Free State.

_____ _____

Mohomane S.M. (Mr) Luyt A.S. (Prof)

DEDICATIONS

I would like to dedicate this book to my mother, my siblings and my fiancée, and most importantly the Almighty One.

ABSTRACT

Nanocomposites are a new class of mineral-filled plastics that contain relatively small amounts (<10%) of nanometer-sized clay particles. Production of rubber-based nanocomposites involves melt mixing the base polymer and layered silicate powders that have been modified with quaternary ammonium salts. In this study, new nanocomposite materials were produced from polychloroprene rubber (PCP) as the matrix and organically modified montmorillonite clays as fillers by using a two-roll mill. PCP was mixed with the clays in contents of 2.5, 5, and 10 phr. Five types of clays (Cloisite 15A, 20A, 25A, 10A and 93A) were investigated during this study and their influence on the thermal and mechanical properties of the rubber was compared.

The degree of exfoliation or intercalation of the organoclays in the PCP nanocomposites was investigated using x-ray diffraction spectroscopy (XRD) and transmission electron microscopy (TEM). The results for Cloisite 93A and 15A depicted an exfoliated structure and a well-dispersed morphology in the polymer matrix at all filler contents, while complete exfoliation was not observed for the other clays, especially at higher clay contents. The tensile modulus was found to increase with an increase in clay content for all the nanocomposites, while tensile strength and elongation at break decreased. The initial stage of thermal degradation was accelerated with the incorporation of organoclays. The TGA results show that Cloisite 15A and 93A have a significant influence on the PCP degradation mechanism, even at low clay contents. The properties of the PCP/clay nanocomposites were also determined by dynamic mechanical analysis (DMA) and stress relaxation. Cloisite 15A and 93A containing nanocomposites were generally found to have better properties than the other samples. This could be due to these clays having stronger interactions with the PCP rubber.

ABBREVIATIONS

CBS	N-cyclohexylbenzothiazole-2-sulfenamide
CEC	Cation exchange capacity
CSBR	Carboxylated styrene butadiene rubber
DMA	Dynamic mechanical analysis
DSC	Differential scanning calorimetry
EPDM	Ethylene-propylene diene rubber
GC	Gas chromatography
HCI	Hydrogen chloride
IIR	Isobutylene–isoprene rubber
LDPE	Low density polyethylene
LFRP	Living free radical polymerization
MA	Maleic anhydride
MgO	Magnesium oxide
MMT	Montmorillonite
MR’Cs	Molecular remote controls
NBR	Nitrile butadiene rubber
NR	Natural rubber
OMLS	Organically modified layered silicate
PCN	Polymer clay nanocomposites
PCP	Polychloroprene
PE	Polyethylene
phr	per hundred of rubber by mass
PLS	Polymer layered silicates
PMMA	Polymethylmethacrylate
PNC	Polymer nanocomposites
PP	Polypropylene
PS	Polystyrene
PVC	Polyvinylchloride
PVDC	Poly(vinylidene chloride)

SBR	Styrene butadiene rubber
SiO_2	Silica
TEM	Transmission electron microscopy
TGA	Thermogravimetric analysis
TPU	Thermoplastic polyurethane
US	United States
XPS	X-ray photoelectron spectroscopy
XRD	X-ray diffraction
ZnO	Zinc oxide

TABLE OF CONTENTS

LIST OF TABLES

LIST OF FIGURES

Chapter 1: Introduction

1.1 Polymer nanocomposites background

A polymer composite is a combination of a polymer matrix and a strong reinforcing phase, or filler. Polymer composites provide desirable properties unavailable in matrix or filler materials alone [1]. Polymer nano-composites are a new class of composites derived from nano-scale inorganic particles with the dimensions ranging from 1 to 100 nm. Owing to the high aspect ratio of the fillers, the mechanical, thermal, flame retardant and barrier properties of polymers may be enhanced without a significant loss of clarity, toughness or impact strength [2]. Nano-particles or fillers such as silica [3], carbon nano-tubes [4], calcium carbonate [5] and clay [6] have been used to prepare nano-composites. In the past decade, extensive research has focused on polymer nano-composites in hopes of exploiting the unique properties of materials in the nano-sized regime [7-9]. A general conclusion has been drawn that nano-composites show much improved mechanical properties over their micro-sized similar systems [10-12]. The mechanical performance of composites is mainly dependent upon the properties of the matrix and reinforcement, and their mutual interaction [13-15].

1.2 Polymer/clay nanocomposites

Polymer–clay nanocomposites (PCN) are one of the important modern technologies for both scientific challenges and industrial applications because of the capability of generating new polymer properties [18]. It is known that the addition of very small amounts of clay brings about an improvement in the mechanical properties, increased gas barrier properties, reduced moisture adsorption, improved thermal stability, and superior flame/heat resistance when compared to their micro- and macrocomposite counterparts and their neat polymer matrices at very low loadings [16-22]. Clay fillers such as montmorillonite, saponite, kaolinite, mica and hectorite are the mostly used clays for the production of PCN [23]. Nylon 6/clay is the first example of such a clay nano-composite [24]. Other polymer/clay nano-composites, involving polymetric matrices such as polyamide [25], polyurethane [26], polyisoprene rubber [27], polyethylene (PE) [28], polypropylene (PP) [29], polystyrene (PS) [30], polyvinyl chloride (PVC) [31], epoxy resin [32], unsaturated polyester resin [33] and silicone elastomers [34] have been investigated. Although clay nano-composites have been prepared for many

thermoplastics and thermosetting polymers, rubber nano-composites constitute only a minor proportion of the available literature [35].

Polymer nano-composites prepared with montmorillonite clay have been studied extensively in the recent years. They generally show improved mechanical properties, because of fairly large aspect ratios [36-38]. These improvements result from the incorporation of thin (1 nm) silicate lamellae that exhibit both high surface area (up to 10^3 m^2 g^{-1}) and large aspect ratios (often greater than 100) which, when combined with their high tensile modulus (>100 GPa), produce efficient reinforcement of a polymer matrix [39]. These nanocomposites also effectively improve gas barrier properties, probably due to the tortuous diffusional path, better filler dispersion and lower fractional free volume of montmorillonite [40]. The incorporation of montmorillonite clay into the polymer matrix enhances thermal stability by acting as a superior insulator and mass transport barrier to the volatile products generated during decomposition [41].

1.3 Rubber/clay nanocomposites

Rubber-based nanocomposites have been receiving increased attention because they often exhibit remarkable improvements in material properties when compared to the virgin polymer or conventional composites [42]. The papers so far published for various rubbers filled with nanoclay reported strong interactions between the rubber matrices and the organo-modified clays, resulting in higher degrees of intercalation using mechanical and/or solution mixing methods [43-44]. Some studies demonstrated that the uniform distribution of nano-scaled filler particles into a rubber matrix, with reasonably good interfacial bonding strength, could lead to a rubber nano-composite with improved mechanical and gas barrier properties [45]. Several rubber/clay nanocomposites, such as natural rubber (NR)/clay, nitrile rubber (NBR)/clay, ethylene–propylene–diene rubber (EPDM)/clay, and styrene butadiene rubber (SBR)/clay, were successfully prepared and possess improved gas barrier properties [46]. Isobutylene–isoprene rubber (IIR) has the best gas barrier property among the general rubbers. Nevertheless, in some fields, such as aerospace, aircraft, and high vacuum systems, IIR does not meet the extremely high gas barrier requirements. It is expected that dispersing nano-clay layers in an IIR matrix could effectively reduce the gas permeability [47].

For many years clays consisting of nano-layered silicate have been widely used as non-reinforcing filler for rubber, to save rubber consumption and reduce the cost. Besides higher gas barrier performance and somewhat better fire-resistance, most of the developed rubber/clay nanocomposites exhibit much higher tensile strength than the corresponding matrix; generally the ratio is at least three times. This surprising reinforcement of nano-clay is attributed to the formation of an oriented region of rubber molecules between nano-dispersed particles during stretching [48-49].

1.5 Research objectives

The objective of this work was to examine the morphology, thermal, and mechanical properties of polychloroprene rubber (PCP)/clay nanocomposites. In this study, the aim was to produce nanocomposite material from PCP matrix and with the addition of organically modified montmorillonite (MMT) clay as filler. Another aim was to study the effect of different modified organoclays, and to observe the effects of clay content on sample properties, e.g, thermal, mechanical and morphological properties of PCP/clay nanocomposite systems. These systems have not been investigated before. Since there is a lack of information available on PCP/clay nanocomposites, these systems should be investigated in other to exploit their properties which could be academically and industrially useful. The samples were prepared by mixing the organoclay and PCP on a 2-roll mill followed by vulcanization. The thermal and mechanical properties, as well as the morphology of the nano-composites, were investigated by using thermogravimetric analysis (TGA), dynamic mechanical analysis (DMA), tensile testing, stress relaxation, x-ray diffraction (XRD) and transmission electron microscopy (TEM).

1.6 Thesis overview

In Chapter 2 a literature survey relevant to polymer nano-composite research, and a general review of related literature, are provided. Chapter 3 describes the preparation of the PCP/nano-clay samples, as well as the techniques used to characterize the samples. In Chapter 4 the experimental results are presented, and the thermal and mechanical properties are discussed in relation to the observed morphologies. Chapter 5 summarizes the conclusions drawn from this research, with some recommendations for future research.

1.7 References

1. M. Bahrami, S. Ranjbarian. Production of micro- and nano-composite particles by supercritical carbon dioxide. Journal of Supercritical Fluids 2007; 40:263–283.
2. B.W. Jo, S.K. Park, D.K. Kim. A mechanical properties of nano-MMT reinforced polymer composite and polymer concrete. Construction and Building Materials 2008; 22:14–20.
3. Q. Liu, Y. Zhang, H. Xu. Properties of vulcanized rubber nanocomposites filled with nanokaolin and precipitated silica. Applied Clay Science 2008; 07:1317-1388.
4. Y. Termonia. Structure property relationships in nanocomposites. Polymer 2007; 48:6948-6954.
5. M. Avella, S. Cosco, M.L Lorenzo, E.D. Pace, M.E. Errico, G. Gentile. Nucleation activity of nanosized $CaCO_3$ on crystallization of isotactic polypropylene, in dependence on crystal modification, particle shape, and coating. European Polymer Journal 2006; 42:1548-1557.
6. C. Lu, Y.M. Mai. Permeability modelling of polymer-layered silicate nanocomposites. Composites Science and Technology 2007; 67:2895-2902.
7. S. Su, D.D. Jiang, C.A. Wilkie. Methacrylate modified clays and their polystyrene and poly(methyl methacrylate) nanocomposites. Polymer for Advanced Technologies 2004; 15:225-231.
8. D. Gersappe. Molecular mechanisms of failure in polymer nanocomposites. Physical Review Letters 2002; 89:5830- 5834.
9. P.H.T. Vollenberg, D. Heikens. Particle size dependence of the young's modulus of filled polymers. Polymer 2000; 50:1656-1662.
10. E. Reynaud, T. Jouen, C. Gauthier, G. Vigier, J. Varlet. Nanofillers in polymeric matrix: A study on silica reinforced PA6. Polymer 2001; 42:8759-8768.
11. C.L. Wu, M.Q. Zhang, M.Z. Rong, K. Friedrich. Tensile performance improvement of low nanoparticles filled-polypropylene composites. Composites Science and Technology 2002; 62:1327-1340.
12. J.S. Shelley, P.T. Mather, K.L. DeVries. Reinforcement and environmental degradation of nylon-6/clay nanocomposites. Polymer 2001; 42:5849-5858.
13. M.Z. Rong, M.Q. Zhang, S.L. Pan, B. Lehmann, K. Friedrich. Analysis of the interfacial interactions in polypropylene/silica nanocomposites, Polymer 2003; 53:176-183.

14. Y. Brechet, J.Y. Cavaille, E. Chabert, L. Chazeau, R. Dendievel, L. Flandin, C. Gauthier. Polymer based nanocomposites: Effect of filler-filler and filler-matrix interactions. Advanced Engineering Materials 2001; 3:571-577.
15. M.S. Sreekala, J. George, M.G. Kumaran, S. Thomas. The mechanical performance of hybrid phenol-formaldehyde-based composites reinforced with glass and oil palm fibers. Composites Science and Technology 2002; 62:339-345.
16. Y.L. Lu, Z. Li, Z.Z Yu, M. Tian, L.Q. Zhang, Y.M. Mai. Microstructure and properties of highly filled rubber/clay nanocomposites prepared by melt blending. Composites Science and Technology 2007; 67:2903–2913.
17. S. Takahashi, H.A. Goldberg, C.A. Feeney, D.P. Karim, M. Farrell, K. O'Leary, D.R. Paul. Gas barrier properties of butyl rubber/vermiculite nanocomposite coatings. Polymer 2006; 34:3083–3093.
18. W. Dong, X. Zhang, Y. Liu, H. Gui, Q. Wang, J. Gao, Z. Song, J. Lai, F. Huang, J. Qiao. Effect of rubber on properties of nylon 6/unmodified clay/rubber nanocomposites. European Polymer Journal 2006; 42:2515–2522.
19. J. Gonzalez, J.I. Eguiazabal, J. Nazabal. Rubber-toughened polyamide 6/clay nanocomposites. Composites Science and Technology 2006; 66:1833–18431.
20. D. Homminga, B. Goteris, S. Hoffman, H. Reynaers, G. Groeninckx. Influence of shear flow on the preparation of polymer layered silicate nanocomposites. Polymer 2005; 46: 9941-9954.
21. B.N. Jang, C.A. Wilkie. The thermal degradation of polystyreme nanocomposites. Polymer 2005; 46:2933-2942.
22. M. Elexander, P. Dubois, T. Sun, J.M. Garces, R. Jerome. Polyethylene-layered silicate nanocomposites prepared by the polymezation-filling technique synthesis and mechanical properties. Polymer 2002; 43:2123-2132.
23. X. Yi, H.L. Duan, Y. Chen, J. Wang. Prediction of complex dielectric constants of polymer-clay nanocomposites. Physics Letters 2007; 372:68–71.
24. T.N. Blanton, D. Majumdar, S.M. Melpolder. Microstructure in clay-polymer composites. Advances in X-ray Analysis 2000; 42:562-568.
25. A.N. Wilkinson, Z. Man, J.L. Stanford, P. Matikainen, M.L. Clemens, G.C. Lees, C.M Liauw. Tensile properties of melt intercalated polyamide-montmorillonite nanocomposites. Composites Science and Technology 2007; 67:2933-2942.

26. W. Chen-Yang, Y.K. Lee, Y.T. Chen, J.C. Wu. High improvement in the properties of exfoliated PU/clay nanocomposites by the alternative swelling process. Polymer 2007; 48:2969-2979.
27. Z. Peng, L.X. Kong, S.D. Li, Y. Chen, M.F. Huang. Self-assembled natural rubber/silica nanocomposites: Its preparation and characterization. Composites Science and Technology 2007; 67:3130–3139.
28. J. Golebiewski, A. Rozanski, J. Dzwonkowski, A. Galeski. Low density polyethylene–montmorillonite nanocomposites for film blowing. European Polymer Journal 2008; 44:270–286.
29. N. Muksing, M. Nithitanakul, B.P. Grady, R. Magaraphan. Melt rheology and extrudate swell of organo bentonite-filled polypropylene nanocomposites. Polymer Test 2008; 46:361-365.
30. G.H. Wang, L.M. Zhang. Reinforcement in thermal and viscoelastic properties of polystyrene by in-situ incorporation of organophilic montmorillonite. Applied Clay Science 2007; 38:17–22.
31. L. Szazdi, A. Pozsgay, B. Pukanszky. Factors and processes influencing the reinforcing effect of layered silicates in polymer nanocomposites. European Polymer Journal 2007; 43:345–359.
32. N. Hameed, P.A. Sreekumar, B. Francis, W. Yang, S. Thomas. Morphology, dynamic mechanical and thermal studies on poly(styrene-co-acrylonitrile) modified epoxy resin/glass fibre composites. Composites 2007; 38:2422–2432.
33. Y. Li, Y. Zhang, Y. Zhang. Morphology and mechanical properties of HDPE/SRP/elastomer composites: effect of elastomers polarity. Polymer Test 2004; 23:83–90.
34. W.G. Hwang, K.H. Wei, C.M. Wu. Preparation and mechanical properties of nitrile butadiene rubber/silicate nanocomposites. Polymer 2004; 45:5729–5734.
35. M. Arroyo, M.A. Lopez-Manchado, J.L. Valentıno, J. Carretero. Morphology/behaviour relationship of nanocomposites based on natural rubber/epoxidized natural rubber blends. Composites Science and Technology 2007; 67:1330–1339.
36. C.M. Chang, J. Wu, J. Li, Y. Cheung. Polypropylene/calcium carbonate nanocomposites. Polymer 2002; 43:2981-2992.
37. Y. Xu, S. Van Ho. Mechanical properties of carbon fiber reinforced epoxy/clay nanocomposites. Composites Science and Technology 2008; 68:854–861.

38. H.A. Stretza, D.R. Paula, P.E. Cassidy. Poly(styrene-co acrylonitrile)/montmorillonite organoclay mixtures: a model system for ABS nanocomposites. Polymer 2005; 46:3818–3830.
39. A.N. Wilkinson, Z. Man, J.L. Stanford, P. Matikainen, M.L. Clemens, G.C. Lees, C.M. Liauw. Tensile properties of melt intercalated polyamide-6-montmorillonite nanocomposites. Composites Science and Technology 2007; 67:3360–3368.
40. S. Lin-Gibson, H. Kim, G. Schmidt, C.C. Han, E.K. Hobbie. Shear-induced structure in polymer–clay nanocomposite solutions. Journal of Colloidal Interface and Science 2004; 274:515-525.
41. J. Lee, T. Takekoshi, E. Giannelis. Fire retardant polyetherimide nanocomposites. Journal of Materials Science and Engineering 1997; 457:513-518.
42. Q. Liu, Y. Zhang, H. Xu. Properties of vulcanized rubber nanocomposites filled with nanokaolin and precipitated silica. Applied Clay Science 2007; 169:1317-1388.
43. G. Mathewa, J.M. Rhee, Y.S. Lee, D.H. Park, C. Nah. Cure kinetics of ethylene acrylate rubber/clay nanocomposites. Journal of Industrial Engineering and Chemistry 2008; 14:60–65.
44. Y. Wang, H. Zhang, Y. Wu, J. Yang, L. Zhang. Preparation and properties of natural rubber/rectorite nanocomposites, European Polymer Journal 2005; 41:2276-2783.
45. X.Y. Zhao, P. Xiang, M. Tian, H. Fong, R. Jin, L.Q. Zhang. Nitrile butadiene rubber/hindered phenol nanocomposites with improved strength and high damping performance. Polymer 2007; 48:6056-6063.
46. Y. Liang, Y. Wang, Y. Wu, Y.Lu, H. Zhang, L. Zhang. Preparation and properties of isobutylene–isoprene rubber (IIR)/clay nanocomposites. Polymer Test 2005; 24:12–17.
47. Y. Liang, W. Cao, Z. Li, Y. Wang, Y. Wu, L. Zhang. A new strategy to improve the gas barrier property of isobutylene-isoprene rubber/clay nanocomposites. Polymer Test 2007; 45:3285-3290.
48. S. Tobias, S. Halbach, R. Mulhaupt. Boehmite-based polyethylene nanocomposites prepared by in-situ polymerization. Polymer 2008; 49:867-876.
49. Q.X. Jia, Y.P. Wu, Y.O. Wang, M. Lu, L.Q. Zhang. Enhanced interfacial interaction of rubber/clay nanocomposites by a novel two-step method. Composites Science and Technology 2008; 68:1050–1056.

Chapter 2: Literature survey

2.1 Fillers

Fillers are, in general, solid substances that are embedded in polymers to reduce cost or improve performance. We can distinguish between nonfunctional (extender) fillers, that are mainly used to reduce costs, and functional fillers, that improve properties or generate new properties in the composites. Crucial parameters in determining the effect of fillers on the properties of composites are the filler geometry (size, shape, structure, aspect ratio), surface characteristics, filler origin and how well the material is dispersed in the polymer matrix. The inclusion of fillers into polymers leads to an increase in modulus and a decrease in toughness. In general, the effectiveness of reinforcing fillers in composites is inversely proportional to the size and directly proportional to the aspect ratio of the filler [1-3].

Traditional fillers display average characteristic sizes in the range of several microns. However, due to the development of nanosized fillers, the specific influence of the nanometric size in the reinforcement mechanisms has to be addressed. Composite materials based on nano-sized fillers, the so-called nanocomposites, are presently studied because they may have unusual combinations of properties. These unusual properties are a consequence of the extremely large specific interfacial area (hundreds of $m^2\ g^{-1}$), and may be related to the very short distances between the reinforcing fillers (about 10^{-8} m) that are close to the characteristic size of the macromolecular coils. In addition, strong reinforcing effects may be observed at very low volume fractions for fillers with very large aspect ratios, when the percolation of the fillers occurs [4-5].

2.1.1 Structure and properties of layered silicates

Clays have been recognized as potentially useful filler materials in polymer matrix composites because of their high aspect ratio and plate morphology. Clay minerals are hydrous aluminum silicates and are generally classified as phyllosilicates, or layered silicates. Silica (SiO_2) is a main component of a tetrahedral sheet, while an octahedral sheet comprises diverse elements such as aluminium (Al), magnesium (Mg), and iron (Fe). A natural stacking of tetrahedral and octahedral sheet occurs in specific ratios and modes, leading to the formation of the 2:1 layered silicates. The phyllosilicate clays include mica, smectite,

vermiculite, and chlorite. The smectite group can be further divided into montmorillonite (MMT), saponite and hectorite species [6]. The chemical formulae and values of the cation exchange capacity (CEC) for MMT, hectorite, and saponite are given in Table 2.1 and structure of a 2:1 phyllosilicate in Figure 2.1. Their crystal structure consists of layers made up of two tetrahedrally coordinated silicon atoms fused to an edge-shared octahedral sheet of either aluminum or magnesium hydroxide. The layer thickness is around 1 nm, and the lateral dimensions of these layers may vary from 30 nm to several microns or larger, depending on the particular layered silicate. Stacking of the layers leads to a regular van der Waals gap between the layers called the interlayer or gallery [7].

Isomorphic substitution within the layers (for example, Al^{3+} replaced by Mg^{2+} or $Fe^{2+,}$ or Mg^{2+} replaced by Li^{1+}) generates negative charges that are counterbalanced by alkali and alkaline earth cations situated inside the galleries. This type of layered silicate is characterized by a moderate surface charge known as CEC, and generally expressed as mequiv/100 gm. This charge is not locally constant, but varies from layer to layer, and must be considered as an average value over the whole crystal. [7].

Table 2 .1 Chemical formula and characteristics of commonly used clays

2:1 phyllosilicates	Chemical formula	CEC / (mequiv/ 100 g)	Particle length / nm
Montmorillonite	$M_x(Al_{4-x}Mg_x)Si_8O_{20}(OH)_4$	110	100–150
Hectorite	$M_x(Mg_{6-x}Li_x)Si_8O_{20}(OH)_4$	120	200–300
Saponite	$M_xMg_6(Si_{8-x}Al_x)Si_8O_{20}(OH)_4$	86.6	50–60

M, monovalent cation; x, degree of isomorphous substitution (between 0.5 and 1.3)

Two particular characteristics of layered silicates that are generally considered for polymer layered silicate (PLS) nanocomposites are: (1) The ability of the silicate particles to disperse into individual layers, and (2) the ability to fine-tune their surface chemistry through ion exchange reactions with organic and inorganic cations. These two characteristics are, of course, inter-related since the degree of dispersion of layered silicate in a particular polymer matrix depends on the interlayer cation [8-9].

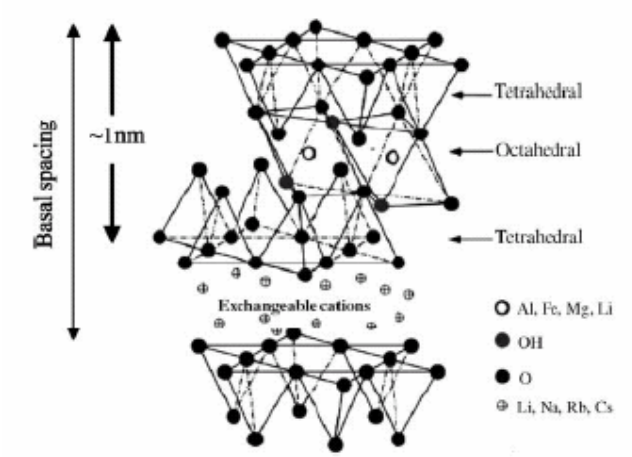

Figure 2.1 Structure of 2:1 phyllosilicates [8]

2.1.2 Organically modified layered silicate (OMLS)

Clays have been extensively used in the polymer industry either as reinforcing agent to improve the physico-mechanical properties of the final polymer or as a filler to reduce the amount of polymer used in the shaped structures, i.e. to act as a diluent for the polymer, thereby lowering the high cost of the polymer systems. The efficiency of the clay to modify the properties of the polymer is primarily determined by the degree of its dispersion in the polymer matrix, which in turn depends on the clay's particle size. However, the clay nanolayers are not easily dispersed in polymers due to their preferred face-to-face stacking tactoids. Dispersion of tactoids is further hindered by the fact that clays are hydrophilic in nature, and are therefore incompatible with the majority of polymers that are primarily hydrophobic. In order to achieve a better dispersion of MMT clay platelets in a polymer matrix, the organophilic modification (usually with an organic ammonium salt) of MMT have commonly been used in order to enhance compatibility between the matrix polymer and the clay. To overcome this incompatability between the polymer and clay, compatibilizing agents are used to try to alleviate the interfacial adhesion between the polymer and filler [10-11]. The first compatibilizing agents used in the preparation of polyamide 6-clay hybrids nanocomposites were amino acids [12]. Numerous other kinds of compatibilizing agents have since been used in the synthesis of nanocomposites. The most popular are alkyl ammonium ions, because they can be easily exchanged with the ions situated between the layers. Silanes

have been used because of their ability to react with the hydroxyl groups situated possibly at the surface and at the edges of the clay layers.

2.1.2.1 Alkylammonium ions

Montmorillonites exchanged with long chain alkylammonium ions can be dispersed in polar organic liquids, forming gel structures with high liquid content. Alkylammonium ions can easily be intercalated between the clay layers and offer a good alternative to amino acids for the synthesis of nanocomposites based on polymer systems other than polyamide 6. The most widely used alkylammonium ions are based on primary alkylamines put in an acidic medium to protonate the amine function. Their basic formula is CH_3–$(CH_2)_n$–NH_3^+ where n is between 1 and 18. It is interesting to note that the length of the ammonium ions has a strong impact on the resulting structure of nanocomposites. The cation-exchange process of linear alkylammonium ions is shown in Figure 2.2. Depending on the layer charge density of the clay, the alkylammonium ions adopt different structures between the clay layers (monolayers, bilayers, pseudotrimolecular layers, and paraffin type monolayers). The alkylammonium ions adopt a paraffin type structure (clay with high layer charge density) and the spacing between the clay layers increases by about 10 Å. Alkylammonium ions permit to lower the surface energy of the clay so that organic species with different polarities can get intercalated between the clay layers [13-18].

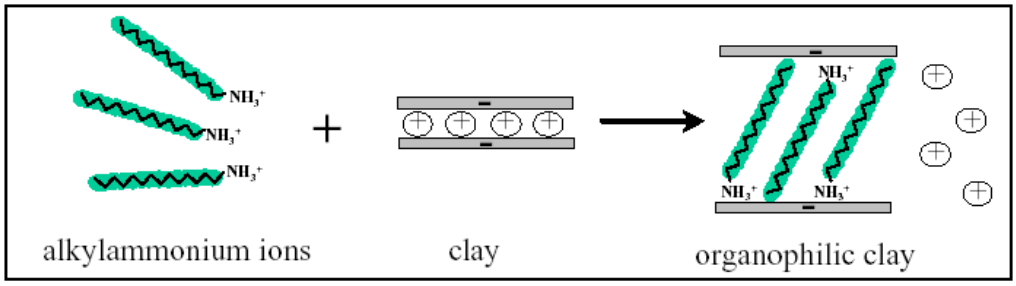

Figure 2.2 The cation-exchange process of linear alkylammonium [18]

2.1.2.2 Amino acids

Amino acids are molecules that consist of a basic amino group (-NH_2) and an acidic carboxyl group (-COOH). In an acidic medium, a proton is transferred from the -COOH group to the intramolecular -NH_2 group. A cation-exchange is then possible between the formed -NH_3^+

and a cation (i.e. Na^+, K^+) intercalated between the clay layers so that the clay becomes organophilic. A wide range of amino acids ($H_3N^+(CH_2)^{n-1}COOH$) have been intercalated between the layers of montmorillonite. Amino acids were successfully used in the synthesis of polyamide 6 – clay hybrids because their acid function has the ability to polymerise with α-caprolactam intercalated between the layers. Thus, this intragallery polymerisation delaminates the clay in the polymer matrix and a nanocomposite is formed [20-21].

2.2 Polymer nanocomposites

Polymer nanocomposites have become an important area studied more widely in academic, government and industrial laboratories. These types of material were first reported as early as 1950 [22]. However, it was not widespread until the period of investigation on this type of structures by Toyota researchers [23-27]. This early work of the Toyota group was based on the formation of nanocomposites where montmorillonite was intercalated with ε-caprolactam *in situ*. Polymer nanocomposites may be defined as structures that are formed by infusing layered-silicate clay (filler) into a thermosetting or thermoplastic polymer matrix, in which at least one dimension of the dispersed particles is in the nanoscale. The matrix is the continuous phase, and the reinforcement constitutes the dispersed phase. It is the behaviour and properties of the interface that generally control the properties of the composite [28]. The property improvements of clay-based nanocomposites are due to the nanoscale nature of the formed system resulting in a high surface area of montmorillonite (750-800 m^2/g) and high-aspect ratio (about 100 to 15000). At these very small sizes, the properties of nanocomposites depend not only on the properties of the two materials that form them, but also on the way these materials interact together at the molecular level. The interfaces between the matrix and reinforcement are maximized in nanocomposites. Hence, the properties of the composites, such as shear strength and flexural strength that are especially dependent on interfacial strengths, are greatly improved [29]. The principal properties that layered silicates can bring to a polymer composite include improved stiffness [30-32], thermal stability [33], oxidative stability [34], reduced flammability [35], and barrier properties [36]. The main attraction is that, because of the high surface area and aspect ratio, these benefits are potentially obtainable at much lower volume fractions than with most other fillers [37].

2.2.1 Morphologies of polymer nanocomposites

In the open literature, polymer/clay nanocomposites (PCN) are generally classified into three groups according to their structures: nanocomposites with intercalated, exfoliated, or mixed (intercalated and exfoliated) morphologies (Figure 2.3). This depends on the nature of the components (polymer matrix, layered silicate and organic cation). Conventional composites may contain clay with the layers un-intercalated in a face-to-face aggregation; here, the clay platelet aggregates are simply dispersed with macroscopic segregation. These phase separated composites have the same properties as traditional micro composites. Intercalated clay composites are intercalation compounds of a definite structure formed by the insertion of one or more molecular layers of the organic compound into the clay host galleries. The result is a well ordered multilayer structure of alternating polymeric and inorganic layers. Exfoliated clay or delamination composites have singular clay platelets dispersed in a continuous organic phase. The delamination configuration is of particular interest, because it maximizes the polymer-clay interactions, making the entire surface of the layers available for interaction with the polymer. This should lead to the most significant changes in mechanical and physical properties. Many efforts have therefore been made to investigate this type of nanocomposites [38-39].

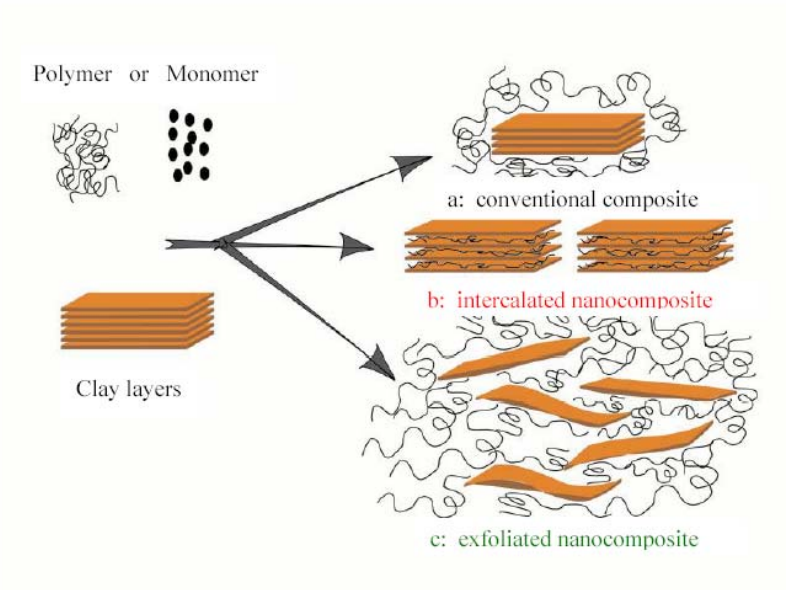

Figure 2.3 Schematic illustrations of three types of polymer nanocomposites [40].

2.3 Polymer-filler interphase

An area of polymer nanocomposite structure that has always garnered attention is the region near the interface of the polymer matrix and the filler. Despite the large variety of polymer nanocomposite systems, a common thread among all the systems is the existence of a phase border between the matrix and filler and the formation of an interphase layer between them. As seen in Figure 2.4, the interphase layer extends well beyond the adsorption layer of the matrix chains' bound surface. Because of the differences in structure, properties of the polymer at the interphase can differ dramatically from those in the bulk polymer. The interphase structure and properties are important to the overall mechanical properties of the composite, because its distinct properties control the load transfer between matrix and filler. A weak interface results in low stiffness and strength, but high resistance to fracture, whereas a strong interface produces high stiffness and strength but often a low resistance to fracture, i.e. brittle behaviour [41].

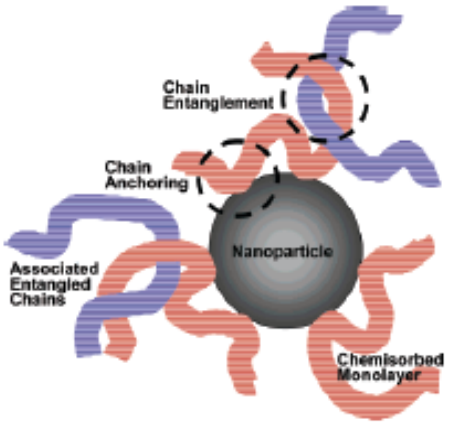

Figure 2.4 Schematic representation of the interphase region between a filler and a polymer matrix [41].

The concept of interphase is not unique to nanocomposites, but because of the large surface area of nanoparticles, the interphase can easily become the dominating factor in developing the properties of nanocomposites. A 1 nm thick interface surrounding micro particles in a composite represents as little as 0.3% of the total composite volume. However, a 1 nm thick interphase layer on nanoparticles can reach 30% of the total volume [40]. As shown in Figure 2.4., the interphase has a characteristic structure consisting of flexible polymer chains, typically in sequences of adsorbed segments (point contacts, i.e., anchors or trains) and unadsorbed segments, such as loops and tails, which in turn are entangled with other chains in their proximity and which are not necessarily bound to the surface. Interphase thickness for a

specific particle-polymer system does not have a constant size because the interphase has no well defined border with the bulk polymer. The effective value of the thickness depends on chain flexibility, the energy of adsorption, and the extent of chain entanglements, which are determined by the surface energies of the polymer and the nanoparticles. Because of conformational limitations brought by the particles, in addition to other restrictions on chain conformation, only a relatively small number of segments within a chain are directly bound to the surface. If all areas of the surface are capable of adsorption, then the polymer segments, for a reasonably flexible polymer chain, are readily adsorbed on the surface, resulting in short loops and a flat (i.e. dense) layer close to the surface. If the chain segments have weak interaction with the surface or if the chain is rigid, the loops and tails extend further into the matrix and form a region of lower density. Therefore, the strength of the interaction of a polymer molecule with the surface of the nanoparticles controls both the polymer molecular conformations at the surface and the entanglement distribution in a larger region surrounding the nanoparticles. Hence, a higher degree of entanglements will result in a larger number of polymer chains that are associated with a given nanoparticle, of which only a fraction are actually anchored to the surface [41-42].

2.4 Preparation methods

Polymer clay nanocomposites can be synthesized by three methods.

2.4.1 Melt intercalation

Polymer melt intercalation is an approach to produce nanocomposites by using a conventional polymer extrusion process. The nanocomposites are formed by heating a mixture of polymer and layered silicate above the glass transition or melting temperature of the polymer. It involves the diffusion of polymer chains into the space between the organoclay layers or galleries with different degrees of exfoliation [43-44]. If the layer surfaces are sufficiently compatible with the chosen polymer, the polymer can separate the clay layers and form either an intercalated or an exfoliated nanocomposite [45].

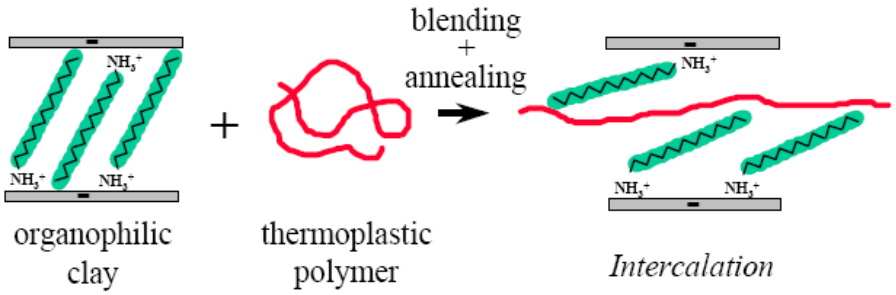

Figure 2.5 Schematic representation of the melt intercalation method [55].

Melt intercalation is an environmentally friendly technique, as it does not require any solvent. It is also commercially attractive due to its compatibility with existing processing techniques. However, the resulting morphology of the nanocomposites is often an intercalated structure rather than the preferred exfoliated state [46].

2.4.2 Solution intercalation

In this method the polymer is dissolved in an appropriate solvent (a solvent capable of dissolving the polymer and swelling the clay), in which the nano-clay is dispersed. Intercalation of polymer chains into the clay galleries occurs from solution. The operating temperatures are typically low. The solvent is then removed by evaporation or by precipitation in a non-solvent, after which uniform mixing of the polymer and layered silicate is achieved [48-49]. This method is useful for only a few polymers, for which suitable solvents are available. This route is also preferred for polymers that require high processing temperatures at which the organoclay may degrade.

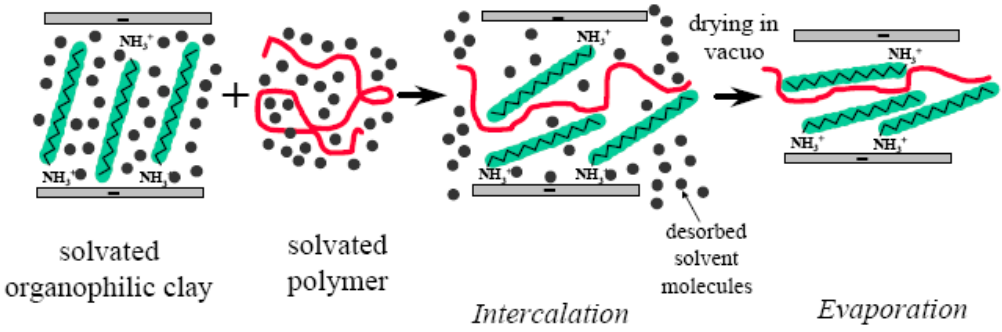

Figure 2.6 Schematic representation of the solution intercalation method [55].

The solution intercalation method involves the use of large amounts of organic solvents, which is usually environmentally unfriendly; therefore, it is not an ideal way to prepare commercial nanocomposites. However, since the solution method gives good control of the homogeneity of the constituents, it helps to understand the intercalation process and nanocomposite morphology. It also leads to a better understanding of the structure and dynamics of the intercalated polymers in these nanocomposites, which can provide molecular insight and lead to the design of materials with desired properties [50].

2.4.3 *In-situ* polymerization

The *in situ* polymerization of monomers in the presence of nanofillers is a promising approach for a more homogeneous distribution due to the close contact of the polymer and filler during synthesis. This method often gives better filler dispersion than melt intercalation, especially at higher filler contents [51]. In this method, the nano-dimensional clay is first dispersed in the liquid monomer, which is then polymerized resulting in an expanded interlayer distance. Polymerization can be initiated by heat or by a suitable initiator [52]. The monomer may also be intercalated with the help of a suitable solvent, and then polymerized as illustrated in the scheme in Figure 2.7.

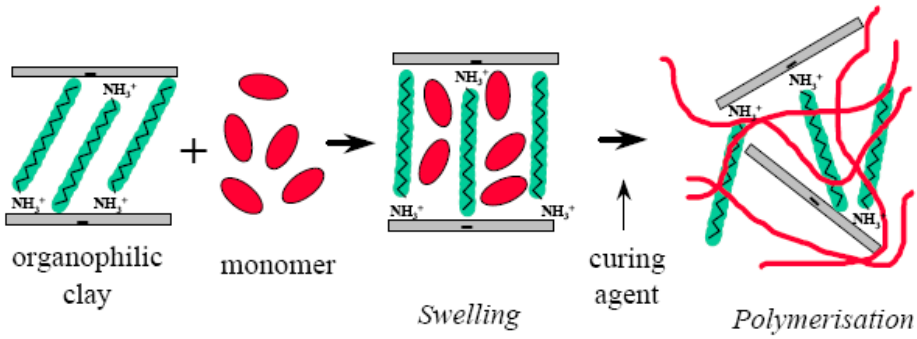

Figure 2.7 Schematic representation of the *in situ* polymerization method [55].

Nylon nanocomposites are commonly synthesized by *in situ* polymerization [53-55]. *In situ* polymerization of a monomer very often produces nearly exfoliated nanocomposites.

2.5 Polymer-clay nanocomposites

Polymer nanocomposites containing a small amount (< 5 wt %) of layered silicate frequently

exhibit remarkably improved mechanical and materials properties when compared to those of conventional polymer composites. The main reason for these improved properties in nanocomposites is the stronger interfacial interaction between the matrix and layered silicate, compared with conventional filler-reinforced systems [56-63]. A lot of experimental work has been done in the area of polymer matrix nanocomposites, but there is yet no consensus on how nano-sized inclusions affect material properties. This is partly due to the novelty of the area, challenges in the processing of nanocomposites, lack of systematic experimental results, and scarcity of theoretical studies. Moreover, some material properties were studied more in-depth than other, leaving gaps in the knowledge on nanocomposite behaviour. The following sections will cover some of the experimental results that are available to-date and identify the trends that can be obtained from these results.

2.5.1 Mechanical behaviour

Since the Toyota group first reported the excellent reinforcement performance of montmorillonite in Nylon 6 in 1987, smectite clays, mainly montmorillonite and hectorite, have been increasingly selected as fillers in polymer composite research and industrial applications. They showed that inserting as little as 4.7 wt.% clay into Nylon 6 doubled both the elastic modulus and strength of the Nylon/clay nanocomposites [64-66].

Sharif *et al.* [67] prepared and studied the properties of natural rubber/clay nanocomposites. They found that the silicate reinforced systems, prepared by melt mixing natural rubber (NR) with various amounts of organoclay, had superior moduli compared to pristine NR. The modulus increased as a function of organoclay loading. Even at a low loading of organoclay, the tensile modulus increased considerably above that of the unfilled NR. Valadares *et al*. [68] observed similar mechanical improvements using natural rubber–montmorrilonite nanocomposites prepared by melt mixing. Their findings were attributed to a good dispersion of the clay (i.e. pronounced intercalation without agglomeration) accompanied with strong interfacial adhesion between the matrix and the filler. The large increase in strength and modulus was not accompanied by a decrease in impact resistance, which is usually the case with polymers filled with silica, calcium carbonate and other inorganic particles.

In other clay-reinforced rubber nanocomposite systems prepared through melt intercalation [69], the tensile strength increased by more than 100%, with only a slight effect on the

elongation at break when compared to pristine nitrile butadiene rubber (NBR). The tear strength also increased considerably for all NBR/clay nanocomposites at low filler contents, compared to neat NBR. In another study of NBR/silicate nanocomposites [70], the authors also observed improvement in the mechanical performance at low filler loading. This was believed to be due to an improved chemical compatibility and the formation of strong interfacial interactions such as hydrogen bonding and/or other chemical bonding.

Liang *et al.* [71] studied the properties of isobutylene–isoprene rubber (IIR)/clay nanocomposites prepared by melt and solution intercalation. They found an improvement in tensile strength, as well as stress and tear strength compared to unfilled IIR. The tensile strength of the nanocomposite filled with 3 phr of clay was nearly twice that of the pure IIR vulcanizate. This high reinforcement effect implied a strong interaction between the matrix and the clay interface and a good dispersion of MMT in the composites. In ethylene propylene rubber (EPR)/clay nanocomposites prepared by melt intercalation, the incorporation of organophilic montmorillonite resulted in raising the tensile modulus and lowering the elongation at break. The tensile modulus of EPR filled with 6 phr layered silicate was similar to that of 30 wt.% carbon black filled EPR [72].

Wan *et al.* [73] studied the effect of different clay treatments on the morphology and mechanical properties of polyvinylchloride (PVC)/clay nanocomposites. They found that the mechanical properties, especially stiffness and impact strength, of PVC/MMT nanocomposites were significantly improved at low MMT loadings. They concluded that the homogeneous dispersion of MMT throughout the polymeric matrix was more important than complete exfoliation to create a material with improved mechanical properties. Therefore, the intercalated structure of the PVC/MMT nanocomposites may be favourable to enhance the mechanical properties. All improvements in the tensile properties of rubber nanocomposites were mainly due to the intercalation of rubber chains into layered-silicate galleries, which provided strong interaction between the rubber matrix and the organoclay [74-75].

2.5.2 Thermal behaviour

The thermal stability of polymeric materials is usually studied by thermogravimetric analysis (TGA). The weight loss due to the formation of volatile products after degradation at high temperatures is monitored as a function of temperature. When the heating occurs under an

inert gas flow, non-oxidative degradation occurs, while the use of air or oxygen allows oxidative degradation of the samples [76]. Several authors recently drew attention to the thermal stabilization observed for nanocomposites, in particular polymer/clay nanocomposites.

Lopez-Manchado *et al* [77] found that the addition of organoclay shifted the thermal decomposition temperature of natural rubber to higher values, which indicated the enhancement of the NR/organoclay nanocomposite thermal stability compared to that of unfilled NR. NR nanocomposites filled with 10 wt.% fluorohectorite (synthetic layered clay) were more thermally stable at 450 °C than those filled with 10 wt.% bentonite (natural layered clay) due to better clay dispersion and stronger interaction between the NR matrix and the clay layers. Peprnicek *et al.* [78] observed an improvement in the thermal stability of PVC nanocomposites reinforced with clay. The main degradation temperature shifted towards a higher value when organophilic MMT was used compared to the unmodified MMT clay used in another study by the same authors [79]. It was concluded that organophilic treatment improves the thermal stability of PVC/clay nanocomposites, due to better interactions between the PVC matrix and the clay. These led to the formation of a continuous char layer, which protects the inner polymer materials from flame, restrict the thermal motion of the polymer in a confined space, and delay the emission of volatile decomposition products [80].

In a thermal study by Morgan *et al.* [81], where polystyrene/clay nanocomposites were investigated, some interesting trends with regard to the onset of decomposition were observed. As the loading of organoclay increased, the onset temperature of decomposition decreased. Since the organic modifier on the clay is thermally unstable above 200 °C, this suggests that the early decomposition observed by TGA is the organic modifier decomposing before the base polymer. Therefore, as the amount of organoclay is increased in the nanocomposites, more organic modifier will decompose, pushing the onset of decomposition to lower temperatures. Jitendra *et al.* [82] found that the incorporation of clay into PVC enhances the rapid decomposition and reduces the maximum decomposition rate and onset temperature of degradation. The presence of quaternary ammonium ions in the nanocomposites was responsible for the acceleration of the polymer decomposition in the initial stage. It is believed that these ions initiate the degradation mechanism by the formation of radicals.

Generally, the incorporation of clay into the polymer matrix was found to enhance the thermal stability by acting as a superior insulator and mass transport barrier to the volatile products generated during decomposition [80-82].

2.5.3 Morphology

For the greatest property enhancement in polymer-clay nanocomposite systems, it is generally believed that the clay layers should disperse as single platelets throughout the polymer matrix. This is termed exfoliation. To attain such a dispersion of clay platelets, the polymer should first penetrate in between the clay platelets (intercalation). This intercalation is possible if both the polymer and the clay layers have polar groups that have favourable interaction. If the polymer and clay are incompatible, the clay platelets remain as large stacks without any polymer chains entering the regions between the clay platelets (gallery spaces), which creates large regions of pure polymer in the nanocomposite, leading to poor properties [83-84].

Mathew *et al.* [85] studied the effect of organoclay dispersion on the cure behaviour of ethylene acrylate rubber (EAR)/clay nanocomposites prepared through melt mixing. The organoclay-filled EAR composites showed a fairly good dispersion composed of a mixture of intercalated and exfoliated clay layers at relatively low clay contents (below 10 phr), but a partial re-aggregation of clay took place at higher clay contents. Wang *et al.*, in their investigation of the morphology and mechanical properties of polyamide 6 (PA 6)/ethylene–propylene–diene copolymer grafted with maleic anhydride (EPDM-*g*-MA)/organoclay ternary nanocomposites, observed the disappearance of the characteristic clay (001) peak in the nanocomposites [86]. The authors attributed the finding to the complete exfoliation of the clay plates in either PA 6 or EPDM-*g*-MA. In another study of the x-ray diffraction patterns of PVC/MMT at various filler contents, Wan *et al*. [87] found a decrease in the magnitude of the (d_{001}) diffraction peak with an increase in organofiller content. The increase in *d*-spacing observed from XRD can also be linked with interactions between the organoclay and polymer, and normally demonstrates a good level of dispersion at nanometer level. This suggests that the PVC chains intercalated into the interlayers of Na^+-MMT. Pluart *et al.* [88] also found an increase in the *d*-spacing in their investigation of the influence of organophillic treatment on the reactivity, morphology and fracture properties of epoxy/montmorillonite nanocomposites. This behaviour can be due to a good interaction between the epoxy matrix and the clay at the interphase region.

Gatos *et al.* [89] showed that the cation exchange capacity (CEC) of the silicates could have an impact on the clay basal spacing when mixed with nitrile rubber. Two organoclays were used in this study, MMT organoclay (high CEC) and FHT organoclay (low CEC). After compounding, the MMT-nanocomposites had a d-spacing of 3.85 nm while the FHT-nanocomposites had a mean value of 3.54 nm, indicating more effective intercalation into MMT-nanocomposites. Lee *et al*. [90] compared the TEM images of nanocomposites with respectively Cloisite 15A and Cloisite 25A using a polymethylmethacrylate (PMMA)/ poly(styrene-*co*-acrylonitrile) (SAN) blend as the matrix. The overall shapes and sizes of the domains in the images look similar, but the domain sizes were generally a little bit larger for the Cloisite 15A nanocomposites than for those of Cloisite 25A. The difference between Cloisite 25A and Cloisite 15A is that the latter has longer chains attached to the quaternary ammonium ion, and also has a larger modifier concentration.

Zheng *et al.* [91] investigated the behaviour of ethylene–propylene–diene rubber (EPDM)/OMMT nanocomposites prepared *via* a simple melt-mixing process using three kinds of OMMT modified by different surfactants. The modifiers used were sodium montmorrilonite (Na-MMT), C18a (MMT-C18a) and C18b (MMT-18b). They found that the basal spacing of Na-MMT in the EPDM/Na-MMT composite did not change, indicating that only a few EPDM chains might have entered into the Na-MMT galleries. They observed broad peaks in the XRD patterns for the EPDM/MMT-C18a and EPDM/MMT-C18b composites, indicating that intercalation of the EPDM chains into the OMMT interlayers had occurred, and that some of the OMMT was possibly exfoliated into the EPDM matrix. Since the alkylammonium-based MMT had polar groups of the surfactant with a different aliphatic polar nature to EPDM, such a system is not at theta conditions, and there is a favourable excess enthalpy to promote MMT dispersion in the EPDM matrix. In the case of MMT-C18a and MMT-C18b, a lack of surfactant polar groups (in MMT-C18a) or a lack of insufficient polarity (in MMT-C18b) might have impeded further delamination of the OMMTs, and intercalated nanocomposites were formed. Therefore the polarity of the MMT layer surface, and the interaction between EPDM and MMT, are seen as important factors influencing the morphology development of EPDM/MMT nanocomposites.

The morphology of isobutylene-isoprene (IIR)/organic modifier clay nanocoposites was studied by Liang *et al*. [92]. Low magnification TEM photographs showed that the clay layers

were homogeneously dispersed in the IIR matrix, and in some areas in the polymer matrix the intercalated silicate layers were locally stacked up to hundreds of nanometers in thickness, while the high-magnification TEM images revealed that there were some single exfoliated clay layers in the IIR matrix besides the intercalated clay layers.

Zhang *et al*. [93] looked at the effect of the double bond and the length of the alkyl chains on the formation of exfoliated polystyrene (PS)/clay nanocomposites by comparing PS/2-methacryloyloxyethyloctayldimethylammoniumbromide – modified - montmorillonite nano-composites (MOABM) and PS/hexadecyldimethylammonium bromide-modified mont-morillonite nanocomposites (HABM). The length of the alkyl chain of MOABM is shorter than that of HABM, and the structure of the PS/MOABM nanocomposites were found to be exfoliated, and that of PS/HABM nanocomposites intercalated. Chavarria *et al.* [94] compared the behaviour of dimethyl bis(hydrogenated-tallow) ammonium chloride organoclay ($M_2(HT)_2$: shorter alkyl tail) and trimethyl hydrogenated-tallow ammonium chloride organoclay ($M_3(HT)_1$: longer alkyl tail) and their dispersion using a thermoplastic polyurethane (TPU) matrix. They found that $M_2(HT)_2$ led to a small number of large, extended tactoids, while $M_3(HT)_1$ produced a larger number of small, elongated tactoids. The length of the alkyl tail also seems to affect the clay dispersion, with the shorter alkyl tail producing lower clay dispersion than the longer alkyl tail.

2.6. Polychloroprene

PCP is among the most important chlorinated polymers, together with poly(vinyl chloride) (PVC) and poly(vinylidene chloride) (PVDC). Although PCP is considered to be a synthetic rubber due to its physical properties, its behaviour during thermal degradation shows some analogies with that of PVC [95]. The structure of PCP can be modified by copolymerizing chloroprene with sulfur and/or 2,3-dichloro-1,3-butadiene to yield a family of materials with a broad range of chemical and physical properties. It is soluble in solvents with various evaporation rates and has no known health hazards. It has a low glass-transition temperature and exhibits easy bond formation and high bond strength to many substrates [96-97]. It is generally unstable in air and will discolour upon reaction with oxygen [98].

TGA analysis of PCP showed that the degradation of PCP occurs in two stages, with the maximum rate of weight loss occurring in the 357–365 °C region. The first degradation step is

the elimination of hydrogen chloride (HCl) and some minor gaseous compounds. Approximately 90% of the available chlorine is lost as HCl. Dehydrochlorination occurs less readily in PCP than in PVC, unless oxygen is present. HCl elimination is not autocatalytic in the absence of air. The loss of HCl is thought to occur by a nonradical intramolecular mechanism, as opposed to the 'unzipping' radical chain process that is thought to occur in PVC [98-99].

An x-ray photoelectron spectroscopic (XPS) investigation by Hao *et al.* [100] showed that the loss of chlorine in both crosslinked and virgin polymers began at about 200 °C. However, at 370 °C the crosslinked system retains more chlorine than the virgin material. This is presumably due to the rigidity of the crosslinked system preventing the facile loss of chlorine. This is then followed by the second stage of degradation which occurs in the range 400–550 °C. In this stage the decomposition of the residue occurs to yield hydrocarbons similar to those produced in PVC degradation. During this stage, the residue degrades further yielding gaseous and liquid fractions and a black carbonaceous char. In a study characterizing virgin and crosslinked PCP and polyisoprene after degradation in argon and in air, Jiang *et al.* [101] showed that PCP produced higher char after the main step of thermal oxidative decomposition. The crosslinked PCP was less thermally stable than the virgin polymer.

It can be seen from the summary above that most of the research on PCP involved the investigation of the thermal stability and degradation mechanisms of the polymer. No references could be found on general material properties of PCP, or on the use of PCP as a composite matrix. This thesis will therefore investigate the physical properties of PCP and its clay nanocomposites, and compare it with trends of available results on rubber nanocomposites.

2.7. References

1. W. Hohenberger. Fillers and reinforcements / Coupling agents. Plastics Additives Handbook. Hanser Publishers: Munich. p.901-943 (2001).
2. R. Stephen, C. Ranganathaiah, S. Varghese, K. Joseph, S. Thomas. Gas transport through nano and micro composites of natural rubber (NR) and their blends with

carboxylated styrene butadiene rubber (XSBR) latex membranes. Polymer 2006; 47:858-870.

3. H. Mahfuz, A. Adnan, V.K. Rangari, S. Jeelani, B.Z. Jang. Carbon nanoparticles/ whiskers reinforced composites and their tensile response. Composites: Part A 2004; 35:519-527.
4. C.J. Chou, A.E. Read, E.I. Garcia-Meitin, C.P. Bosnyak. Polymer nanocomposites. Journal of Applied Polymer Science 1995; 55:119-121.
5. E. Chabert, M. Bornert, E. Bourgeat-Lami, J.Y. Cavaillé, R. Dendievel, C. Gauthier, J.L. Putaux, A. Zaoui. Filler–filler interactions and viscoelastic behavior of polymer nanocomposites. Materials Science and Engineering 2004; 38:320-330.
6. S.R. Suprakas, M. Okamoto. Polymer/layered silicate nanocomposites: a review from preparation to processing. Progress in Polymer Science 2003; 28:1539-1641.
7. T. Lan, P.D. Kaviratna, T.J. Pinnavaia. Epoxy self-polymerization in smectite clays. Journal of Physics and Chemistry of Solids 1996; 57:1005-1010.
8. S.C. Tjong. Structural and mechanical properties of polymer nanocomposites. Materials Science and Engineering R: Reports 2006; 53: 73-197.
9. J. Zhang, R.K. Gupta, C.A. Wilkie. Controlled silylation of montmorillonite and its polyethylene nanocomposites. Polymer 2006; 47:4537-4543.
10. A. Rehab, N. Salahuddin. Nanocomposite materials based on polyurethane intercalated into montmorillonite clay. Materials Science and Engineering A 2005; 399:368-376.
11. C.D. Munzy, B.D. Butler, H.J.M. Hanley, F. Tsvetkov, D.G. Pfeiffer. Clay platelet dispersion in a polymer matrix. Materials Letters 1996; 28:379-384.
12. A. Usuki, M. Kawasumi, Y. Kojima, A. Okada, T. Kurauchi, O. Kamigaito. Synthesis of nylon 6-clay hybrid. Journal of Materials Science 1993; 8:1179-1184.
13. T. Lan, P.D. Kaviratna, T.J. Pinnavaia. Mechanism of clay tactoid exfoliation in epoxy-clay nanocomposites. Journal of Materials Science 1995; 7:2144-2150.
14. R. Maharaphan, W. Lilayuthalert, A. Sirivat J.W. Schwank. Preparation, structure, properties and thermal behavior of rigid-rod polyimide/montmorillonite nanocomposites. Composites Science and Technology 2001; 61:1253-1264.
15. A.J. Brunner, A. Necola, M. Rees, P. Gasser, X. Kornmann, R. Thomann, M. Barbezat. The influence of silicate-based nano-filler on the fracture toughness of epoxy resin. Journal of Engineering Fracture Mechanics 2006; 16:2336-2345.

16. S. Su, D.D. Jiang, C.A. Wilkie. Novel polymerically-modified clays permit the preparation of intercalated and exfoliated nanocomposites of styrene and its copolymers by melt blending. Polymer Degradation and Stability 2004;83:333-346.
17. P.C. LeBaron, Z. Wang, T.J. Pinnavaia. Polymer-layered silicate nanocomposites: an overview. Applied Clay Science 1999; 15:11-29.
18. Kirk-Othmer Encyclopedia of Chemical Technology", 4th ed, Vol. 6, John Wiley and Sons, Inc.: New York, p.381-409 (1993).
19. L. Le Pluart, J. Duchet, H. Sautereau. Epoxy/montmorillonite nanocomposites: influence of organophilic treatment on reactivity, morphology and fracture surface. Polymer 2005; 46:12267-12278.
20. A. Funck, W. Kaminsky. Polypropylene carbon nanotube composites by in situ polymerization. Composites Science and Technology 2007; 67:906-915.
21. F. Perrin-Sarazin, M.T. Ton-That, M.N. Bureau, J. Denault. Micro- and nano-structure in polypropylene/clay nanocomposites. Polymer 2005; 46:11624-11634.
22. H.R. Dennis, D.L. Hunter, D. Chang, S. Kim, J.L. White, J.W. Cho, D.R. Paul. Effect of melt processing conditions on the extent of exfoliation in organoclay-based nanocomposites. Polymer 2001; 42:9513-9522.
23. Y. Kojima, A. Usuki, M. Kawasumi, A. Okada, T. Kurauchi, O. Kamigaito. Synthesis and properties of nylon-6/clay hybrids. Journal of Applied Polymer Science 1993; 31: 983-986.
24. K. Yano, A. Usuki, A. Okada, T. Kurauchi, O. Kamigaito. Synthesis and properties of polyimide-clay hybrid. Journal of Applied Polymer Science 1993; 31:2493-2498.
25. Y. Kojima, A. Usuki, M. Kawasumi, Y. Fukushima, A. Okada, T. Kurauchi, O. Kamigaito. Mechanical properties of nylon 6 clay hybrid. Journal of Materials Research 1993; 5:1179-1184.
26. P.B. Messersmith, E.P. Giannelis. Synthesis and barrier properties of poly-(ε-caprolactone)–layered silicate nanocomposites. Journal of Polymer Science, Part A. Polymer Chemistry 1995; 33:1047-1057.
27. K. Yang, Y. Huang, J.Y. Dong. Efficient preparation of isotactic polypropylene/montmorillonite nanocomposites by in situ polymerization technique. Polymer 2007; 48:6254-6261.
28. S. Choi, I.S. Kim. Filler-polymer interactions in filled polybutadiene compounds. European Polymer Journal 2002; 38:1265-1269.

29. F.L. Jin, S.J. Park. Interfacial toughness properties of trifunctional epoxy resins/calcium carbonate nanocomposites. Materials Science and Engineering 2008; 10:190-193.
30. K. Wang, C. Wang, J. Li, J. Su, Q. Zhang, R. Du, Q. Fu. Effects of clay on phase morphology and mechanical properties in polyamide 6/EPDM-g-MA/organoclay ternary nanocomposites. Polymer 2007; 48:2144-2154.
31. K. Wang, L. Chen, M. Kotaki, C. He. Preparation, microstructure and thermal mechanical properties of epoxy/crude clay nanocomposites. Composites 2007; 38:192-197.
32. Y. Xu, S.V. Hoa. Mechanical properties of carbon fiber reinforced epoxy/clay nanocomposites. Composites Science and Technology 2008; 68:854-861.
33. D. Wu, L. Wu, L. Wu, M. Zhang. Rheology and thermal stability of polylactide/clay nanocomposites. Polymer Degradation and Stability 2006; 91:3149-3155.
34. A. Leszczynska, J. Njuguna, K. Pielichowski, J.R. Banerjee. Polymer/montmorillonite nanocomposites with improved thermal properties. Thermochimica Acta 2007; 453:75-96.
35. J. Zhang, C.A. Wilkie. Preparation and flammability properties of polyethylene-clay nanocomposites. Polymer Degradation and Stability 2003; 80:163-169.
36. Y.L. Lu, Z. Li, Z.Z. Yu, M. Tian, L.Q. Zhang, Y.M. Mai. Microstructure and properties of highly filled rubber/clay nanocomposites prepared by melt blending. Composites Science and Technology 2007; 67:2903-2913.
37. Y.P. Wu, Y.Q. Wang, H.F. Zhang, Y.Z. Wang, D.S. Yu, L.Q. Zhang, J. Yang. Rubber–pristine clay nanocomposites prepared by co-coagulating rubber latex and clay aqueous suspension. Composites Science and Technology 2005; 65:1195-1202.
38. T.N. Blanton, D. Majumdar, S.M. Melpolder. Microstructure of clay-polymer composites. Advances in X-Ray Analysis 2000; 42:562-568.
39. P.H.T. Vollenberg, D. Heikens. Particle size dependence of the Young's modulus of filled polymers: preliminary experiments. Polymer 1989; 30:1656-1662.
40. P. Meneghetti, S. Qutubuddin. Synthesis, thermal properties and applications of polymer-clay nanocomposites. Thermochimica Acta 2006; 442:74-77.
41. D. Ciprari, K. Jacob, R. Tannenbaum. Characterization of polymer nanocomposite interphase and its impact on mechanical properties. Macromolecules 2006; 39:6565-6573.

42. K. Putz, R. Krishnamoorti, P.F. Green. The role of interfacial interactions in the dynamic mechanical response of functionalized SWNT-PS nanocomposites. Polymer 2007; 48:3540-3545.
43. A. Funck, W. Kaminsky. Polypropylene carbon nanotube composites by in situ polymerization. Composites Science and Technology 2007; 67:906-915.
44. M. Alexandre, P. Dubois. Polymer-layered silicate nanocomposites preparation, properties and uses of a new class of materials. Materials Science and Engineering. 2000; 28:1-63.
45. J.H. Lee, D. Jung, C.E. Hong, K.Y. Rhee, S.G. Advani. Properties of polyethylene-layered silicate nanocomposites prepared by melt intercalation with a PP-g-MA compatibilizer. Composites Science and Technology 2005; 65:1996-2002.
46. B. Lepoittevin, N. Pantoustier, M. Devalckenaere, M. Alexandre, C. Calberg, R. Jerome, C. Henrist, P. Dubois. Polymer/layered silicate nanocomposites by combined intercalative polymerization and melt intercalation. Polymer 2000; 44:2033-2040.
47. Y. Li, H. Ishida. Solution intercalation of polystyrene and the comparison with poly(ethyl methacrylate). Polymer 2003; 44:6571-6577.
48. Z. Shen, G.P. Simon, Y.B. Cheng. Comparison of solution intercalation and melt intercalation of polymer-clay nanocomposites. Polymer 2002; 43:4251-4260.
49. S. Filippi, E. Mameli, C. Marazzato, P. Magagnini. Comparison of solution-blending and melt-intercalation for the preparation of poly(ethylene-co-acrylic acid)/organoclay nanocomposites. European Polymer Journal 2007; 43:1645-1659.
50. X. Shi, Z. Gan. Preparation and characterization of poly(propylene carbonate)/montmorillonite nanocomposites by solution intercalation. European Polymer Journal 2007; 43:4852-4858.
51. K. Yang, Y. Huang, J.Y. Dong. Efficient preparation of isotactic polypropylene/montmorillonite nanocomposites by in situ polymerization technique via a combined use of functional surfactant and metallocene catalysis. Polymer 2007; 48: 6254-6261.
52. J. Tung, R.K. Gupta, G.P. Simon, G.H. Edward, S.N. Bhattacharya. Rheological and mechanical comparative study of in situ polymerized and melt-blended nylon 6 nanocomposites. Polymer 2005; 46:10405-10418.
53. R. Haggenmueller, F. Du, J.E. Fischer, K.I. Winey. Interfacial in situ polymerization of single wall carbon nanotube/nylon 6,6 nanocomposites. Polymer 2006; 47:2381-2388.

54. X. Zhang, T. Xie, G. Yang. Isothermal crystallization and melting behaviors of nylon 11/nylon 66 alloys by in situ polymerization. Polymer 2006; 47:2116-2126.
55. X. Kornmann. Synthesis and characterization of thermoset-clay nanocomposites, Ph.D. Thesis, Lulea University of Technology, Sweden, 2000. p.55.
56. Y.P. Wu, Q.X. Jia, D.S. Yu, L.Q. Zhang. Property modeling Young's modulus of rubber–clay nanocomposites using composite theories. Polymer Testing 2004; 23:903-909.
57. F.L. Jin, S.J. Park. Thermo-mechanical behaviors of butadiene rubber reinforced with nano-sized calcium carbonate. Materials Science and Engineering 2008; 478:406-408.
58. T. Peprnicek, A. Kalendova, E. Pavlova, J. Simonik, J. Duchet, J.F. Gerard. Poly(vinyl chloride)-paste/clay nanocomposites: Investigation of thermal and morphological characteristics. Polymer Degradation and Stability 2006; 91:3322-3329.
59. C. Wan, X. Qiao, Y. Zhang, Y. Zhang. Effect of different clay treatment on morphology and mechanical properties of PVC-clay nanocomposites. Polymer Testing 2003; 22:453-461.
60. F. Carrasco, P. Pages. Thermal degradation and stability of epoxy nanocomposites: Influence of montmorillonite content and cure temperature. Polymer Degradation and Stability 2008; 93:1000-1007.
61. C.M. Chang, J. Wu, J.X. Li. Polypropylene/calcium carbonate nanocomposites. Polymer 2002; 43:2981-2992.
62. G.C. Lees, C.M. Liauw, A.N. Wilkinson, Z. Man, J.L. Stanford, P. Matikainen , M.L. Clemens. Tensile properties of melt intercalated polyamide 6 – montmorillonite nanocomposites. Composites Science and Technology 2007; 67:3360-3368.
63. M. Lai, C.M. Chen. Preparation, structure, and properties of styrene–ethylene–butylene–styrene block copolymer/clay nanocomposites: Part III. Effectiveness of compatibilizers. European Polymer Journal 2007; 43: 2254-2264.
64. B. Chen, R.G.J. Evans. Elastic moduli of clay platelets. Scripta Materialia 2006; 54:1581-1585.
65. K. Hbaibeb, Q.X. Wang, Y.H.J. Chia, B. Cotterell. Modelling stiffness of polymer/clay nanocomposites. Polymer 2007; 48:901-909.
66. P. Potschke, B. Kretzschmar, A. Janke. Use of carbon nanotube filled polycarbonate in blends with montmorillonite filled polypropylene. Composites Science and Technology 2007; 67:855-860.

67. J. Sharifa, W.M. Yunusa, K.Z. Dahlanb, M.H. Ahmada. Preparation and properties of radiation crosslinked natural rubber/clay nanocomposites. Polymer Testing 2005; 24:211-217.
68. L.F. Valadares, C.A.P. Leite, F, Galembeck. Preparation of natural rubber-montmorillonite nanocomposites in aqueous medium: evidence for polymer-platelet adhesion. Polymer 2006; 47:672-678.
69. J. Sharifa, W.W. Yunusa, K.Z. Dahlanb, M.J. Ahmad. Preparation and properties of radiation crosslinked natural rubber/clay nanocomposites. Polymer Testing 2005; 24:211-217.
70. W.G. Hwang, K.H. Wei, C.M Wu. Preparation and mechanical properties of nitrile butadiene rubber/silicate nanocomposites. Polymer 2004; 45:5729-5734.
71. Y. Liang, W. Cao, Z. Lia, Y. Wang, Y. Wu, L. Zhang. A new strategy to improve the gas barrier property of isobutylene–isoprene rubber/clay nanocomposites. Polymer Testing 2008; 27:270-276.
72. Y. Wang, L. Zhang, C. Tang, D. Yu. Preparation and characterization of rubber-clay nanocomposites. Journal of Applied Polymer Science 2000; 78:1879-1883.
73. C. Wan, X. Qiao, Y. Zhang, Y, Zhang. Effect of different clay treatment on morphology and mechanical properties of PVC-clay nanocomposites. Polymer Testing 2003; 22 453-461.
74. Y.P. Wu, Q.X. Jia, D.S. Yu, L.Q. Zhang. Structure and properties of nitrile rubber (NBR)-clay nanocomposites by co-coagulating NBR latex and clay aqueous suspension. Journal of Applied Polymer Science 2003; 89:3855-3858.
75. H. Zheng, Y. Zhang, Z. Peng, Y, Zhang. A comparison between cure systems for EPDM/montmorillonite nanocomposites. Polymers 2004; 12:197-206.
76. M. Alexandre, P. Dubois. Polymer-layered silicate nanocomposites: preparation, properties and uses of a new class of materials. Materials Science and Engineering 2005; 28:1-63.
77. M.A. Lopez-Manchado, B. Herrero, M. Arroyo. Organoclay-natural rubber nanocomposites synthesized by mechanical and solution mixing methods. Polymer 2004; 53:1766-1772.
78. T. Peprnicek, A. Kalendova, E. Pavlova, J. Simonik, J. Duchet, J.F. Gerard. Poly(vinyl chloride)-paste/clay nanocomposites: Investigation of thermal and morphological characteristics. Polymer Degradation and Stability 2006; 91:3322-3329.

79. T. Peprnicek, J. Duchet, L. Kovarova, J. Malac, J.F. Gerard, J. Simonik. Poly(vinyl chloride)/clay nanocomposites: X-ray diffraction, thermal and rheological behaviour. Polymer Degradation and Stability 2006; 91:1855-1860.
80. J. Lee, T. Takekoshi, E. Giannelis. Fire retardant polyetherimide nanocomposites. Materials Science and Engineering 1997; 457:513-518.
81. D. Morgan, D. Joseph, H.J. Zhao, B. Alexander. Rheological characterization of polystyrene–clay nanocomposites to compare the degree of exfoliation and dispersion. Polymer 2005; 46:8641-8660.
82. K. Jitendra, K. Pandey, A. Reddy, P. Kumar, R.P. Singh. An overview on the degradability of polymer nanocomposites. Polymer Degradation and Stability 2005; 88: 234-250.
83. D.S. Chaudhary. R. Prasad. R.K. Gupta, S.N. Bhattacharya. Clay intercalation and influence on crystallinity of EVA-based clay nanocomposites. Thermochimica Acta 2005; 433:187-195.
84. S. Balakrishnan, P.R. Start, D. Raghavan, S.D. Hudson. The influence of clay and elastomer concentration on the morphology and fracture energy of preformed acrylic rubber. Polymer 2005; 46:1255-11262.
85. G. Mathew, J.M. Rhee, Y.S. Lee, D.H. Park, C. Nah. Cure kinetics of ethylene acrylate rubber/clay nanocomposites. Journal of Industrial and Engineering Chemistry 2008; 14:60-65.
86. K. Wang, C. Wang, J. Li, J. Su, Q. Zhang, R. Du, Q. Fu. Effects of clay on phase morphology and mechanical properties in polyamide 6/EPDM-g-MA/organoclay ternary nanocomposites. Polymer 2007; 48: 2144-2154.
87. C. Wan, X. Qiao, Y. Zhang, Y. Zhang. Effect of different clay treatment on morphology and mechanical properties of PVC-clay nanocomposites. Polymer Testing 2003; 22:453-461.
88. L. Pluart, J. Duchet, H. Sautereau. Epoxy/montmorillonite nanocomposites: influence of organophilic treatment on reactivity, morphology and fracture surface. Polymer 2005; 46:12267-12278.
89. K.G. Gatos, J. Karger-Kocsis. Effect of the aspect ratio of silicate platelets on the mechanical and barrier properties of hydrogenated acrylonitrile. European Polymer Journal 2007; 43:1097-1104.

90. M.H. Lee, C.H. Dan Jeong, H. Kim, J. Cha, S. Kim, Y. Hwang, C.H. Lee. Effect of clay on the morphology and properties of PMMA/poly(styrene-*co*-acrylonitrile)/clay nanocomposites prepared by melt mixing. Polymer 2006; 47:4359-4369.
91. H. Zheng, Y. Zhang, Z. Peng, Y. Zhang. Influence of clay modification on the structure and mechanical properties of EPDM/montmorillonite nanocomposites. Polymer Testing 2004; 23:217-223.
92. Y. Liang, Y. Wang, Y. Wu, Y. Lu, H. Zhang, L. Zhang. Preparation and properties of isobutylene-isoprene rubber (IIR)/clay nanocomposites. Polymer Testing 2005; 24:12-17.
93. W. A. Zhang, D. Z. Chen, H. Y. Xu, X. F. Shen, Y. E. Fang. Influence of four different types of organophilic clay on the morphology and thermal properties of polystyrene/clay nanocomposites prepared by using the γ-ray irradiation technique. European Polymer Journal 2007; 39:23213-2328.
94. F. Chavarria, D.R. Paul. Morphology and properties of thermoplastic polyurethane nanocomposites: Effect of organoclay structure. Polymer 2006; 47:7760-7773.
95. I. Aracil , R. Font, J.A. Conesa, A. Fullana. TG–MS analysis of the thermo-oxidative decomposition of polychloroprene. Journal of Analytical and Applied Pyrolysis 2007; 79:327–336.
96. J.A. Caballero, J.A. Conesa, I. Martin-Gullon, R. Font. Kinetic study of the pyrolysis of neoprene. Journal of Analytical and Applied Pyrolysis 2005; 74:231-237.
97. K. Zukiene, V. Jankauskaite. The effect of surface properties on the adhesion of modified polychloroprene used as adhesive. Journal of Adhesion Science and Technology 2005; 19:627-638.
98. C.M. Dicka, J.J. Liggata, E. Colin. Solid state ^{13}C NMR study of the char forming processes in polychloroprene. Polymer Degradation and Stability 2001; 74:397-405.
99. I. Aracil, R. Font, J.A. Conesa. Thermo-oxidative decomposition of polyvinyl chloride. Journal of Analytical and Applied Pyrolysis 2005; 74:215-223.
100. M.H. Yeh, W.S. Hwang, L.R. Cheng. Microstructure and mechanical properties of neoprene–montmorillonite nanocomposites. Applied Surface Science 2007; 253:4777-4781.
101. D.D. Jiang, G.F. Levchik, S.V. Levchik, C. Dick, J.J. Liggatc, C.E. Snape, C.A. Wilkie. Thermal degradation of cross-linked polyisoprene and polychloroprene. Polymer Degradation and Stability 2000; 68:75-82.

Chapter 3: Materials and methods

3.1 Materials

3.1.1 Elastomer

A G-type polychloroprene rubber was supplied by DuPont Dow Elastomer P.T.E. Ltd, India with the trade name Butaclor. Table 3.1 lists its specifications.

Table 3.1 Polychloroprene specifications

Physical form	Chips
Odour	Mild
Specific Gravity at 25/4°C, ASTM D7920-66 (1979)	1.23
Mooney Viscosity, ML 1+4 at 100°C, ASTM D1646-81	37-49

3.1.2 Nanoclays

The organoclays, Cloisite 10A, Cloisite 15A, Cloisite 20A, Cloisite 25A and Cloisite 93A were supplied by Southern Clay Products, Inc. (Texas, USA). More information on the different clays is presented in Table 3.1.

3.1.3 Curing agents

Magnesium oxide (MgO) was purchased from Merck Chemicals Limited (Kerala, India) and N-cyclohexylbenzothiazole-2-sulfenamide (CBS) was obtained from Rubber Chemicals (Kerala, India). CBS has a molar mass of 264.4 g mol^{-1} and appears as a light yellow powder. The chemical composition of MgO is shown in Table 3.2.

3.1.4 Activators

Zinc oxide (ZnO) and stearic acid were obtained from Merck Chemicals Limited (Kerala, India). Their chemical compositions are shown in Table 3.2.

Table 3.2 Properties of organoclays

Cloisite	Anion	XRD d-spacing (001) / Å	Organic modifier	Modifier concentration (mequiv./100gclay)
10A	Chloride	18.6	Dimethyl, benzyl, hydrogenated tallow, quaternary ammonium chloride (2MBHT)	125
15A	Chloride	31.5	Dimethyl, dehydrogenated tallow, quaternary ammonium chloride (2M2HT)	125
20A	Chloride	24.2	Dimethyl, dehydrogenated tallow, quaternary ammonium chloride (2M2HT)	95
25A	Methyl sulphate	19.2	Dimethyl, hydrogenated tallow, 2-ethylhexyl quaternary ammonium methyl sulfate (2MHTL8)	95
93A	Bisulphate	23.6	Methyl, dehydrogenated tallow ammonium bisulfate (M2HT)	90

Table 3.3 Chemical description of the curing materials

Zinc oxide pure	Magnesium oxide	Stearic acid
M = 81.37 g mol^{-1} Assay – 99% Water soluble – 0.3% Chloride – 0.02% Sulphate – 0.01% Heavy metals (as lead) – 0.01%	M = 44.30 g.mol^{-1} Assay – 97% Water soluble – 2% Chloride – 0.15% Sulphate – 0.5% Arsenic – 0.0003% Iron – 0.05% Lead – 0.0008% Loss of ignition – 8%	M = 284.48 g.mol^{-1} Acid value – 200-212 Sulphated ash – 0.1% Iodine value – 4 Density – 0.847 g cm^{-3} at 70 °C Melting point – 69.6 °C

3.2 Preparation of the nanocomposites

PCP rubber compounds were prepared on an open two roll mill at room temperature. The clay was first dried in a vacuum oven to remove any captured water. The PCP rubber was first masticated on a laboratory two-roll mill for 10 min in order to reduce the molar mass of the rubber. The reclaimed rubber was then re-added and the mastication process proceeded for a further 2 min. before starting the compounding process. All the vulcanization ingredients were then added to the rubber compound before the incorporation of the clay. A gum was also prepared from the recipe of rubber compounds but with the exclusion of organoclay. The recipes of the compounds are compiled in Table 3.3.

Table 3.4 Formulation of the nanocomposite compounds

Material	Amount
Polychloroprene	200 g
Zinc oxide	10 g
Magnesium oxide	4 g
Stearic acid	2 g
CBS	2 g
Organoclay content	5, 10 & 20 g

The vulcanization time, rate and kinetics were determined using an oscillating disc rheometer (Common Facility for Scientist (CFS), Rubber Technologies, Kerala, India). The curing behaviour was determined at 160 °C. The compounds were then melt pressed at 160 °C for 25 minutes using an INDEXPELL compression molder.

3.3 Characterization methods

Polymer characterization and analysis are considered to be a separate discipline of study in the field of polymers. It involves the investigation of the microstructure-property relationships of a polymeric material. Examination of microscopic details of the structure in order to understand the morphology, and measurement of the mechanical and thermal properties are

all part of the characterization process. The following analytical tools were employed for characterizing the samples:

3.3.1 X-ray diffractometry (XRD)

XRD gives quantitative data on the dispersion of the clay platelets. The clay platelets are arranged periodically in an intercalated system and thus a reflection from the clay platelets is observed in the XRD pattern. As more and more polymer chains enter the clay gallery, the clay spacing increases, shifting the clay peak to lower angles. The separation of the clay platelets also decreases the periodicity and hence reduces the intensity of the clay peak. For an exfoliated system the clay platelets are randomly dispersed and no clay peak is observed in the XRD pattern. The absence of a Bragg peak in the diffraction pattern does not necessarily mean that the clay is exfoliated. A disordered and immiscible sample, or other factors like low concentration of the clay in the region where the x-ray beam hits a non-uniformly dispersed sample, could fail to produce a Bragg reflection. Thus XRD can be used to characterize an incompatible or intercalated system, but could possibly give misleading data on the exfoliation [1].

XRD measurements were performed in a X'pert PRO (PANalytical) PN 3040/60 XRD: 45.0 kV, 40.0 mA, using the reflection mode at a scan rate of 4° min^{-1} with Cu-K_α radiation with wavelength = 0.154 nm. A 2θ geometry of 5 to 40° with a step size of 0.02° were used to measure the spectra.

3.3.2 Transmission electron microscopy (TEM)

TEM allows a qualitative understanding of the structure of the nanocomposite through direct observation. It enables the visualization of the internal structure of crystal samples and provides two-dimensional images magnified as high as 100,000 times by use of transmitted electrons. Because electrons can only travel a short distance through matter, samples must be very thin to enable acceptable image resolution. TEM also provides an actual image of the clay layers to permit the identification of the morphology of the nanocomposite. Usually both low magnification images, to show if the clay is well-dispersed or not, and high magnification images, to provide an identification of the morphology, are necessary. TEM is complementary to XRD, especially when peaks are not observed in XRD [2-3].

The samples were prepared using cryo-ultramicrotomy. They were mounted on cryo-pins and frozen in liquid nitrogen. Sections were cut at -100 ºC using a Reichert FCS (Leica, Vienna, Austria) attached to a Reichert Ultracut S Ultramicrotome. The sections (100-150 nm thick) were collected on copper grids and viewed in a LEO 912 Omega (Carl Zeiss NTS GmbH, Oberkochen, Germany) transmission electron microscope, with an energy filter, operating at 120 kV.

3.3.3 Thermogravimetric analysis (TGA)

Thermogravimetric analysis (TGA) is one of the members of the family of thermal analysis techniques used to characterize a wide variety of materials. Its principal uses include the measurement of a material's thermal stability and composition. TGA measures the amount and rate (velocity) of change in the mass of a sample as a function of temperature or time in a controlled atmosphere. The sample is placed in a pan held in a microbalance. The pan and sample are heated in a controlled manner and weight is measured throughout the heating cycle. The measurement is normally carried out in air or in an inert atmosphere, such as helium, argon or nitrogen, and the weight is recorded as a function of increasing temperature [1].

A Perkin-Elmer TGA7 thermogravimetric analyzer (Waltham, Massachusetts, U.S.A.) was used to investigate the degradation of the composites. Thermogravimetric analyses were done under flowing nitrogen (20 mL min^{-1}) gas. The instrument was computer controlled and calculations were done using Pyris software. Samples weighing between 5 and 10 mg were placed in platinum pans and analysed from 30 to 600 °C at a 10 °C min^{-1} heating rate.

3.3.4 Tensile testing

Tensile testing was performed to determine the elastic modulus, ultimate stress, and ultimate strain for all the systems. In tensile testing, a dumbbell shaped sample is placed in the grips of movable and stationary fixtures in a screw driven device, which pulls the sample until it breaks and measures applied load versus elongation of the sample. Tensile tests provide properties of Young's modulus, strength, and ductility of materials under tensile loadings.

These properties are often specified for a given material and used for comparison of materials, development of new materials, and quality control [4].

Analysis of the tensile properties was done using a Hounsfield H5KS universal testing machine from Redhill, United Kingdom. To ensure that a representative sample of each composition was tested, five tensile tests were performed for each material. The dimensions of the dumbbell shaped sample were as follows:

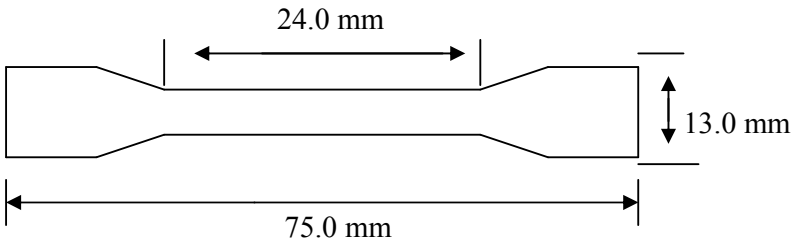

The instrument settings for the analyses were as follows:

Load range	250.0 N
Extension range	300.0 mm
Gauge length	24.0 mm
Speed	50.0 mm min^{-1}
Approach speed	0.02 mm min^{-1}

3.3.5 Stress relaxation

The tensile stress relaxation test is widely used to measure the mechanical properties of viscoelastic materials. By definition, stress relaxation refers to the decrease in stress at a constant deformation. When stress relaxation occurs, the stress needed to maintain a constant total deformation decreases as a function of time. Both physical and chemical processes are responsible for the stress decay upon constant deformation, including mechanisms such as disentanglement, chain slippage, chain and crosslink scission and formation of new crosslinks. At ambient conditions and/or short times, stress relaxation predominantly results from physical processes. At higher temperatures or in degradative environments, and/or for long time exposures, chemical processes dominate over physical processes [5-6].

The stress relaxation measurements were carried out on a Hounsfield H5KS universal tensile machine from Redhill, United Kingdom. Decreasing of stress was monitored for 90 minutes, and the stress monitoring was started immediately after the required strain was attained. The stress decay was monitored for a constant strain of 20% for all the measurements. The relaxation curves are shown as normalized curves with respect to initial stresses.

3.3.6 Dynamic mechanical analysis (DMA)

Dynamic mechanical analysis (DMA) of polymeric and composite materials is one of the most powerful techniques for studying structure-property relationships in that the damping behaviour of these materials is directly related to the molecular structure. DMA determines elastic modulus, loss modulus, and damping coefficient as a function of temperature, frequency, or time. These tests can be conducted over a wide temperature and frequency range to give information about a material's glass transitions, secondary transitions, and morphology [1].

DMA instrument, Perkin-Elmer Diamond DMA (Waltham, Massachusetts, U.S.A.) was used to assess the dynamic-mechanical performance of the nanocomposites prepared. Temperature ramp experiments were conducted using dual cantilever rectangular geometry with a temperature sweep from –100 to 100 °C at a 5 °C min^{-1} heating rate. The frequency used in the measurements was 1 Hz. Samples were cut into rectangular specimens of 20×13×3.5 mm dimensions.

.

3.3.7 Fourier-transform infrared (FTIR) spectroscopy

FTIR spectroscopy is a powerful tool to monitor the vibrational energy levels in the region of different molecules. The changes in chemical properties are usually followed by FTIR spectroscopy which is a very sensitive and non-destructive technique [7].

FTIR spectroscopy was performed using a Perkin Elmer Precisely multiscope connected to a Perkin Elmer Spectrum 100 FTIR spectrometer from Waltham, Massachusetts, U.S.A. Very thin layers of the samples were placed under the microscope and spectra of the desired areas were collected. The samples were scanned over a 400 - 4000 cm^{-1} wavenumber range at a resolution of 4 cm^{-1}. The FTIR spectra were recorded in the transmittance mode.

3.4 References

1. A.A. Bafna. Polyethylene-clay nanocomposites: processing-structure-property relationship. Phd thesis. University of Cincinatti: Cincinnati, Ohio, U.S.A. p.36-40 (2004).
2. Q. Sun, F.J. Schork, Y. Deng. Water-based polymer/clay nanocomposite suspension for improving water and moisture barrier in coating. Composites Science and Technology 2007; 67:1823-1829.
3. O. Monticelli, Z. Musina, S. Russo, S. Bals. On the use of TEM in the characterization of nanocomposites. Materials Letters 2007; 61:3446-3450.
4. Y.W. Cheng, D.T. Read, J.D. McColskey, J.E. Wright. A tensile-testing technique for micrometer-sized free-standing thin films. Thin Solid Films 2005; 485:426-432.
5. S. Mitra, A. Ghambari-Siahkali, K. Almdal. A novel method for monitoring chemical degradation of crosslinked rubber by stress relaxation under tension. Polymer Degradation and Stability 2006; 91:2520-2526.
6. M. Patel, P.R. Morell, J.J. Murphy. Continuous and intermittent stress relaxation studies on foamed polysiloxane rubber. Polymer Degradation and Stability 2005; 87:201-206.
7. S. Gunasekaran, R.K. Natarajan, A. Kala. FTIR spectra and mechanical strength analysis of some selected rubber derivatives. Spectrochimica Acta Part A: Molecular and Biomolecular Spectroscopy 2007; 68:323-330.

Chapter 4: Results and discussion

4.1 XRD and TEM

The degree of exfoliation or intercalation of the organoclays in the PCP nanocomposites was determined using x-ray diffraction spectroscopy (XRD) and transmission electron microscopy (TEM). The average size of the *d*- or basal spacing (d_{001}), which is the sum of the layer and interlayer distances between the clay platelets in the clay powders and nanocomposites, was determined from the 2θ position of the (d_{001}) diffraction peak of each material using Bragg's law, which is given in Equation 4.1.

$$n\lambda = 2d \sin \theta \qquad (4.1)$$

where

n = 1 and λ = 1.54056Å

TEM was used to visually observe the morphology of the clays in the PCP matrices. TEM images usually complement XRD data and also enable us to observe the nanocomposites' morphology at a nanometer scale. Table 4.1 summarizes the *d*-spacing values of the pure clays and the clays in the corresponding PCP nanocomposites, in cases where diffraction peaks were observed.

Table 4.1 The basal spacings of the clays determined from the d_{001} peaks in the XRD spectra of the samples

Sample	d_{001} / nm
Pure Cloisite 10A	27.2
PCP + 10 phr Cloisite 10A	52.5
Pure Cloisite 15A	48.0
Pure Cloisite 20A	36.0
Pure Cloisite 25A	29.8
PCP + 10 phr Cloisite 25A	51.9
Pure Cloisite 93A	36.2

Figure 4.1 represents the x-ray diffractograms of the pure Cloisite clays used in this study. Cloisite 15A has the largest basal spacing corresponding 48.0 nm, while Cloisite 20A has a

basal spacing of 36.0 nm. Both of them have the same organic modifier and anion (chloride anion), but differ in terms of the modifier concentration used. Cloisite 10A has a *d*-spacing of 27.2 nm. It is modified by the same anion as Cloisite 15A and 20A, but it has an aromatic functional group (benzyl group) attached to it. Cloisite 25A and 93A are modified by methyl sulphate and bisulphate anions respectively, and differ with the organic modifiers and their concentrations. They have basal spacings of 29.8 and 36.2 nm respectively.

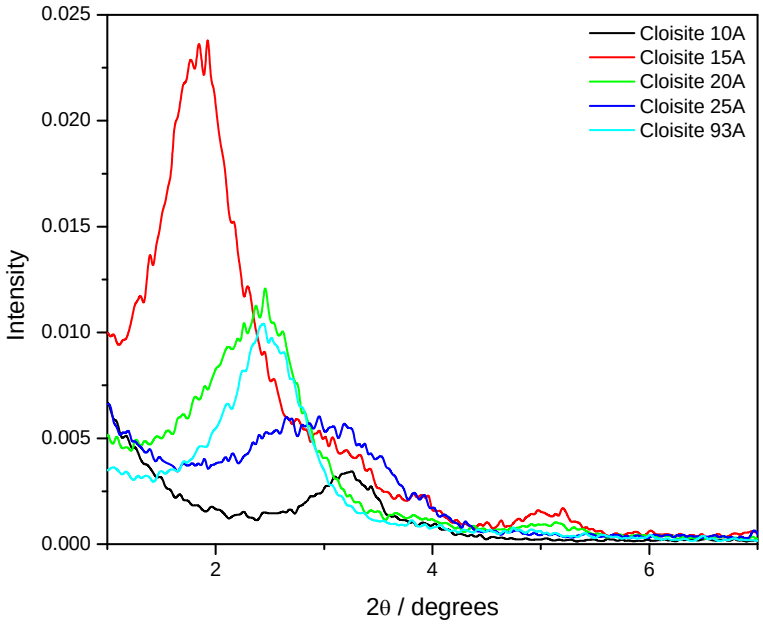

Figure 4.1 X-ray diffractograms of pure Cloisite clays

Figure 4.2 shows the x-ray diffractograms of the PCP nanocomposites formed with Cloisite 10A. For 2.5 and 5 phr clay no (001) diffraction peak is observed, which might indicate exfoliation of the clay in the PCP matrix. For the 10 phr clay containing sample, a weak diffraction peak seems to appear at $2\theta = 1.9°$ corresponding to a basal spacing of 52.5 nm. One may argue that the disappearance of the silicate diffraction peak from the XRD traces clearly prove complete exfoliation. Experience shows that complete exfoliation is rarely reached and the structure of the nanocomposites is rather complicated. The TEM photo for 5 phr filler content in Figure 4.3 shows individual silicate layers dispersed in the PCP matrix and some stacks of clay platelets. From these results, one could see that it is not possible to achieve complete exfoliation of silicate layers in the polymer matrix. The structure of the nanocomposites that is usually formed contains large particles, or tactoids with extended

gallery distances and individual exfoliated silicate layers [1,2]. The kinetics and extent of exfoliation depend on many factors, and the structure formed in the process is usually much more complicated than that of the traditional particulate filled microcomposites. The particle structure of the silicate, its gallery structure, exfoliation and the formation of a silicate network must be considered in nanocomposites, but some of these structural formations are completely neglected in most studies when determining the extent of exfoliation [3].

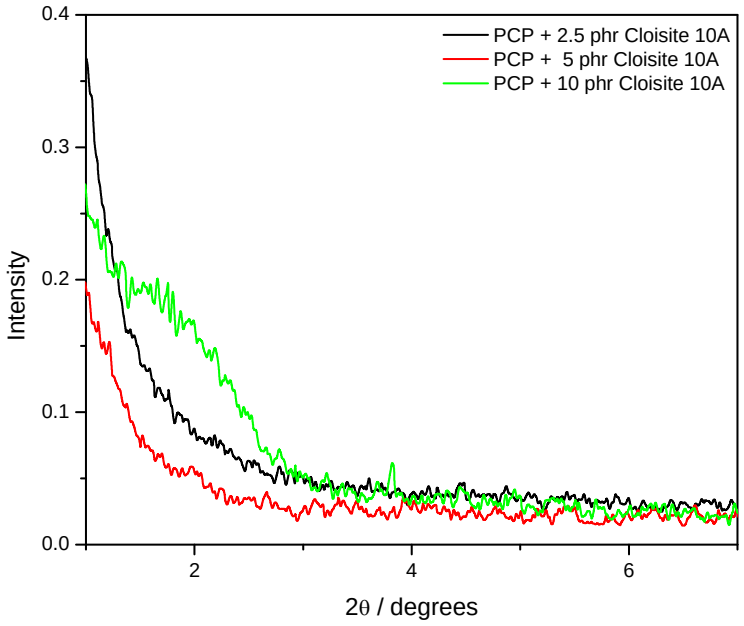

Figure 4.2 X-ray diffractograms of PCP/Cloisite 10A nanocomposites

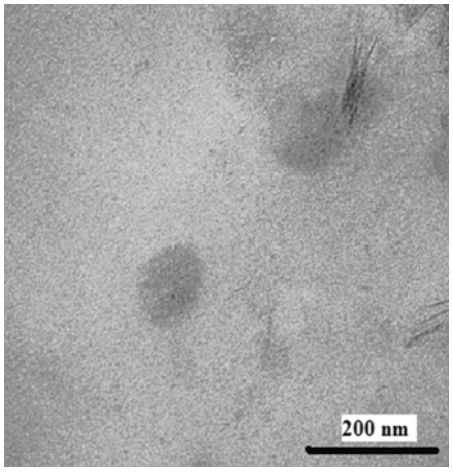

Figure 4.3 TEM micrograph of PCP + 5 phr Cloisite 10A (low magnification)

The x-ray diffractograms showed no diffraction peaks for all the samples when Cloisite 15A was used (Figure 4.4), indicating a high level of exfoliation. This may be due to an extensive layer separation associated with a high level of exfoliation of the silicate layers in the PCP matrix, which results in the eventual disappearance of any coherent x-ray diffraction from the distributed silicate layers in the PCP matrix [4]. However, the TEM micrographs in Figure 4.5 show that silicate tactoids still exist in the PCP matrix, indicating that complete exfoliation was not reached as the XRD predicted. Moczo *et al.* [3] also found that the disappearance of the clay reflection from the XRD pattern does not necessarily indicate complete exfoliation, and/or it does not show the extent of exfoliation. They concluded that even TEM micrographs do not give conclusive information about the morphology of the formed nanocomposites. It is therefore dangerous to draw general conclusions about the extent of exfoliation from XRD traces, and even from TEM micrographs.

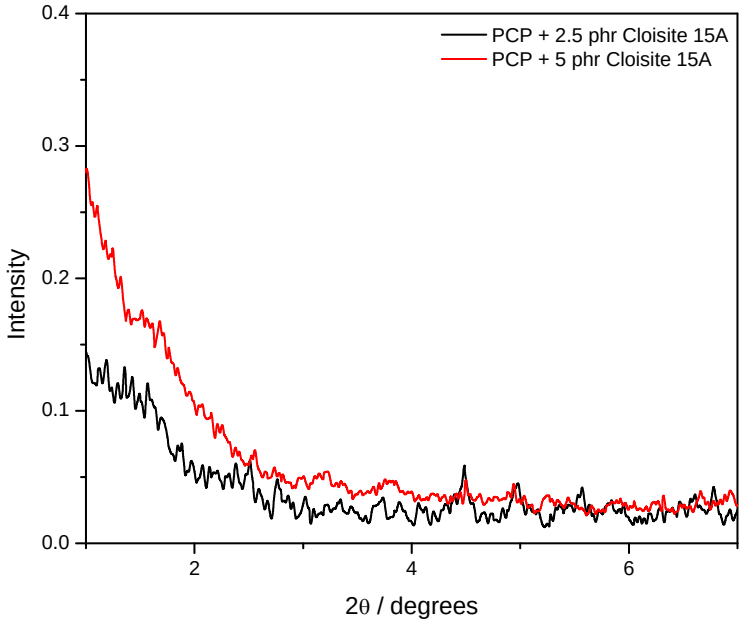

Figure 4.4 X-ray diffractograms of PCP/Cloisite 15A nanocomposites

This problem is further illustrated by Figure 4.6, where the x-ray diffractograms of Cloisite 20A containing samples are presented. No diffraction peaks are observed for all three the nanocomposites, which may indicate complete exfoliation of the clay in the PCP matrix. However, the TEM micrograph in Figure 4.7 shows a distinct particulate structure of the filler in the PCP matrix. We can safely state that in spite of the absence of the silicate reflection in

the corresponding XRD pattern, a completely exfoliated structure has not been achieved. Therefore the absence of a characteristic clay peak from the XRD spectrum of the nanocomposites cannot be considered as sufficient evidence that complete exfoliation has occurred, unless the angular range is explored beyond the low angle limit of the XRD [4].

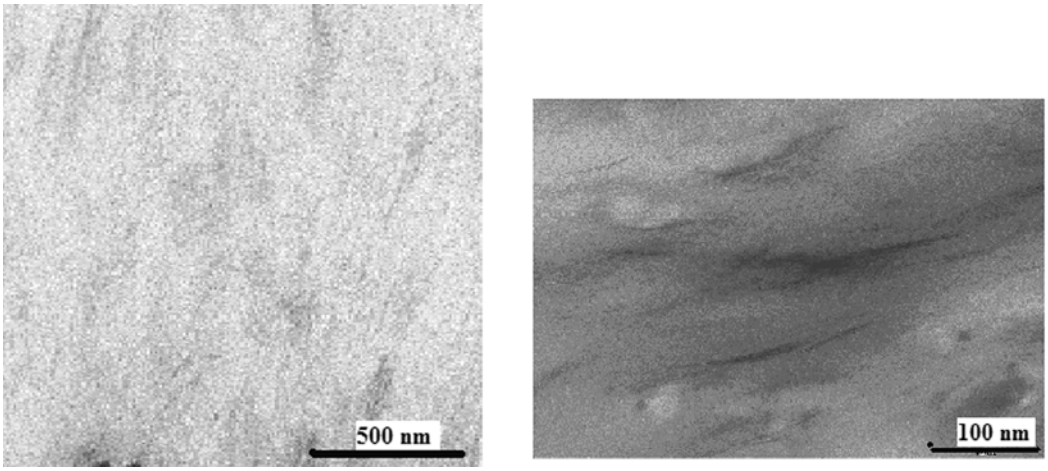

Figure 4.5 TEM micrographs of PCP + 5 phr Cloisite 15A: low magnification (left) high magnification (right)

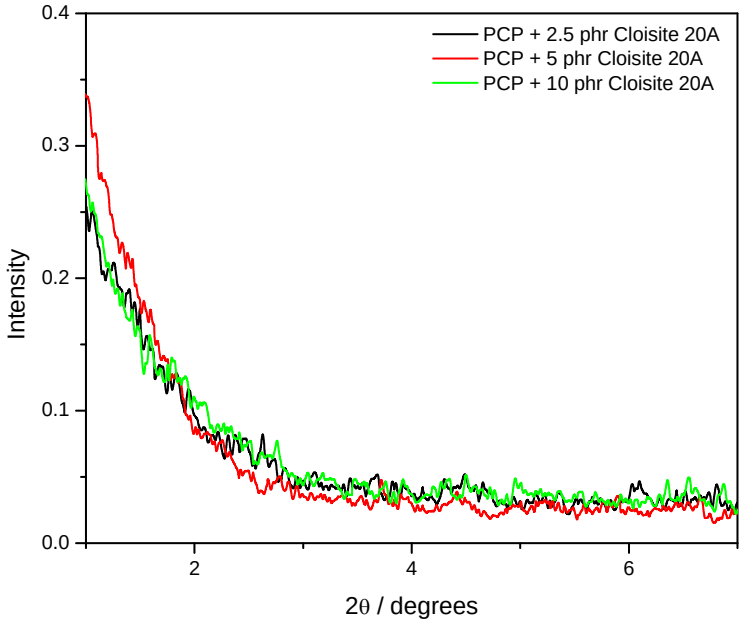

Figure 4.6 XRD diffractograms of PCP/Cloisite 20A nanocomposites

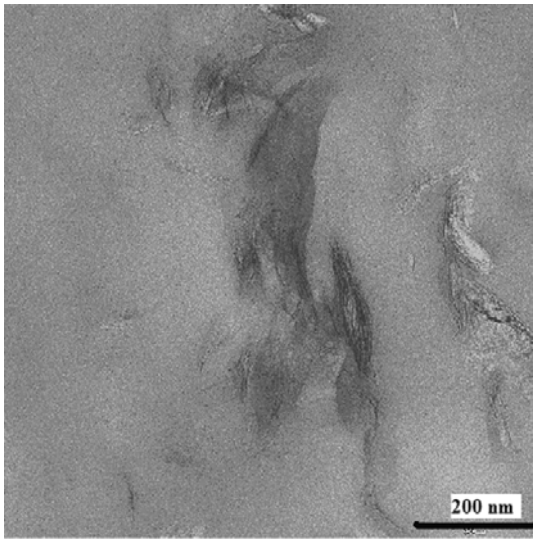

Figure 4.7 TEM micrograph of PCP + 5 phr Cloisite 20A

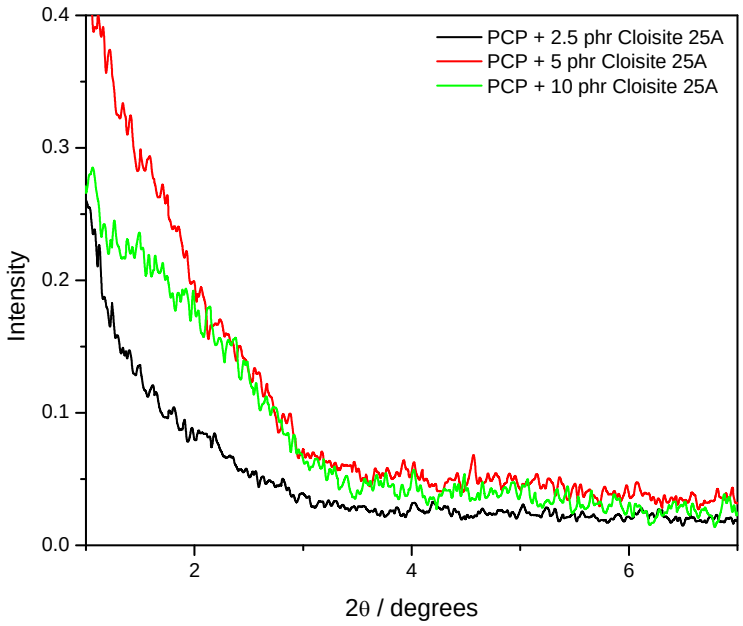

Figure 4.8 XRD diffractograms of PCP/Cloisite 25A nanocomposites

For Cloisite 25A filled nanocomposites, there are also no distinctive XRD peaks, although the 10 phr containing sample shows an indication of a peak around $2\theta = 2°$ (Figure 4.8), which is an indication of partial intercalation (Table 4.1). For the samples with lower clay contents no distinctive peaks are observed. The TEM micrographs of the 5 phr filler containing sample are presented in Figure 4.9. The stacking of some silicate layers is still observable. This is in line with the observations discussed above. According to Suprakas [4], who observed similar

behaviour in clay filled poly[(butylene succinate)-co-adipate] (PBSA) nanocomposites, the clay platelet starts exfoliating from the tactoids during the melt blending process, and as the clay particles become smaller with time, the resistance to further peeling away of the clay platelets from the parent tactoids gradually increases. Therefore, although the clay is not completely exfoliated, the remaining tactoids are too small for conventional XRD to detect clay layer stackings.

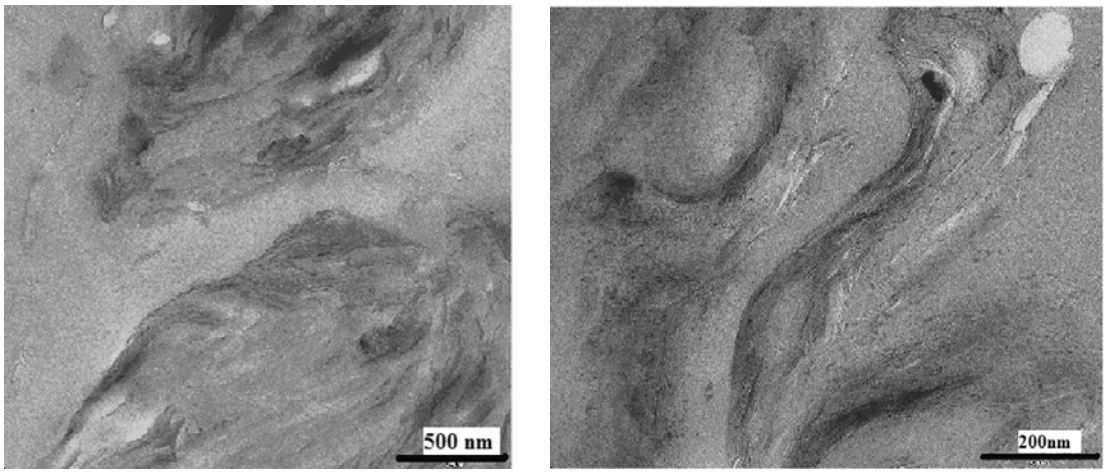

Figure 4.9 TEM micrographs of PCP + 5 phr Cloisite 25A: low magnification (left) high magnification (right)

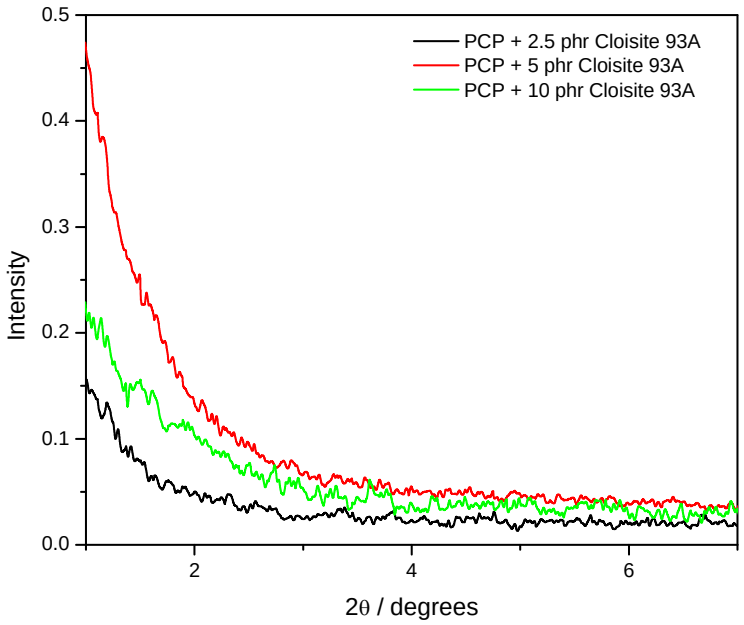

Figure 4.10 XRD diffractograms of PCP/Cloisite 93A nanocomposites

The x-ray diffractograms of the Cloisite 93A nanocomposites are shown in Figure 4.10. There are no clay diffraction (001) peaks observed for all the samples. Again the XRD results indicate that silicate layers are exfoliated within the PCP matrix. Both the TEM micrographs in Figure 4.11 show a good dispersion of the layered silicates in the PCP matrix, but in this case un-exfoliated clay stacks are clearly visible. This suggests that complete exfoliation of the silicate layers in the polymer matrix is difficult to achieve, even though there may be strong interactions between the polymer matrix and the clay surface.

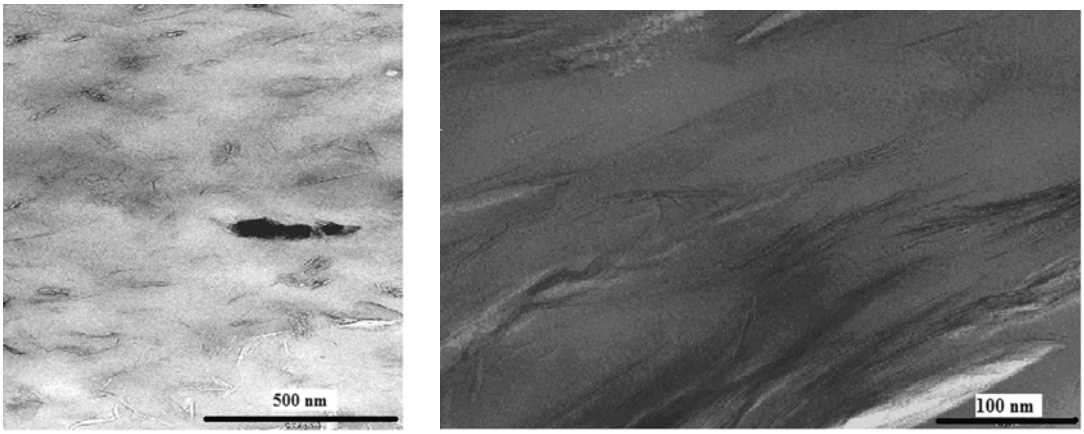

Figure 4.11 TEM micrographs of 5 phr Cloisite 93A: low magnification (left) high magnification (right)

In all five nanocomposite systems at lower filler content, the diffraction peaks were observed to shift to lower angles compared to those of the original organoclays, indicating that intercalation of PCP rubber into the organoclay layers occurred. The extent of intercalation depended on the type of organoclay and the structure of the modifier used. The reflections of Cloisite 10A and Cloisite 25A in the XRD patterns at 10 phr filler content show basal spacings of around 51.9-52.7 Å, indicating intercalation and partial exfoliation. Both these clays are modified with a modifier having only one tallow group. It is interesting that both the pure clays had relatively small basal spacings, and therefore there was not enough space for the rubber chains to completely penetrate the areas between the clay layers. Cloisite 15A, Cloisite 20A and Cloisite 93A did not show any diffraction peaks, even at 10 phr clay content. Cloisite 15A and Cloisite 20A were treated with the same modifier, containing two hydrogenated tallow groups, but at different modifier contents. Because of this, these clays

had larger basal spacings, which made it easier for the rubber chains to penetrate and separate the clay layers.

4.2 Fourier-transform infrared spectroscopy (FTIR)

The FTIR spectrum of only pure PCP is presented and discussed. This was done in order to ensure that there were no impurities in the pure PCP. Since all the properties of the nanocomposites were compared to that of pure PCP, it was important to ensure the pure PCP did not contain other solid impurities.

The FTIR spectrum of PCP gum is shown in Fig. 4.12. The observed vibrational frequencies in polychloroprene, along with their relative intensities and proposed assignments, are summarized in the Table 4.2.

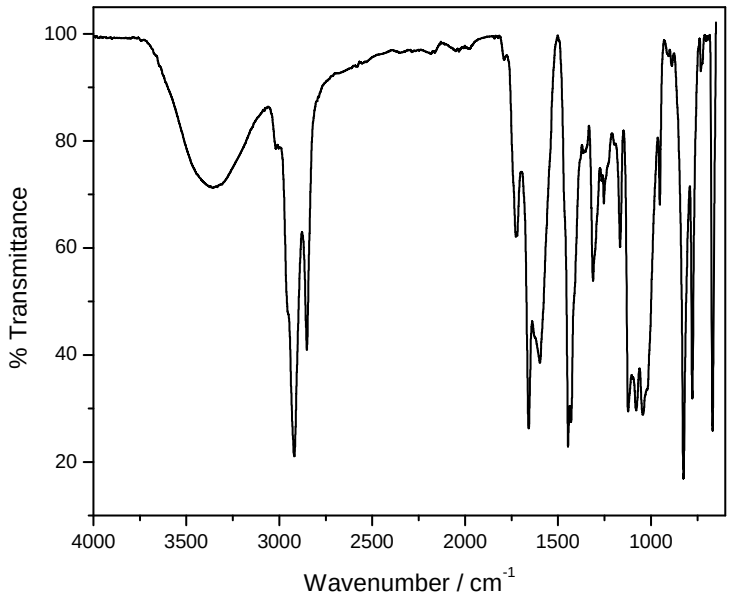

Figure 4.12 The FTIR spectrum of PCP gum

Table 4.2 Some important observed vibrations and wave numbers

Wavenumber / cm^{-1}	Assigned vibrations
3361	-OH group
2913	=C−H stretching mode
2853	=C−H stretching mode
1664	C=C stretching mode
1436	CH_2 deformation
1303	CH_2 wagging
1244	CH_2 twisting
1112-1009	C−C stretching vibrations
817	CH_2 rocking
766	CH_2 rocking
663	C−Cl stretching

The presence of a broad band in the region of 3361 cm^{-1} is assigned to the presence of hydroxyl groups. The C−H stretching vibration is normally observed between 3100 and 2800 cm^{-1}. The =C−H out-of-plane bending vibration normally occurs between 1000 and 800 cm^{-1}. This vibration is assigned to the peak at 887 cm^{-1} in Figure 4.11. The in-plane bending vibration of the methine C−H is at 1210 cm^{-1} in this spectrum. This vibration is also overlapped to some extent with the rocking and deformation vibrations of the methylene group. The methylene (CH_2) stretching vibration typically appears in the region 3000-2800 cm^{-1}. The medium band at 1436 cm^{-1} in the FTIR spectrum is assigned to the deformation (CH_2) modes of the methylene groups. The rocking mode of the CH_2 group gives rise to the strong bands at 817 and 766 cm^{-1} in the spectrum. This is moderately coupled with the deformational mode of the CH_2 group. The CH_2 wagging and twisting occur over a frequency range centered around 1300 cm^{-1}. The peak seen at 1302 cm^{-1} in the spectrum is considered to be the CH_2 wagging modes. The C=C stretching frequency typically appears between 1680 and 1630 cm^{-1}. The very strong band observed at 1664 cm^{-1} in the FTIR spectrum is assigned to the C=C stretching mode. The strong and medium intensity infrared bands at 1112 and 1009 cm^{-1} are ascribed to the C−C stretching vibrations. The C−Cl stretching region between 700 and 800 cm^{-1} is well known for its resonance specific to the conformational structures of polychloroprene. The strong band at 663 cm^{-1} in the FTIR spectrum is assigned to the C−Cl stretching mode [5-7]. All the bands observed in the spectrum indicate that the PCP was pure

without any impurities that may have influenced the observations on the PCP/clay nanocomposites.

4.3 Tensile properties

The tensile properties of the nanocomposites will be discussed based on polymer-clay interaction, dispersion of clay in the polymer matrix as observed in the TEM and XRD results, as well as the influence of organoclay filler content and its nature. Figure 4.13 shows typical stress-strain curves for the pure PCP and the Cloisite nanocomposites (see Appendix for all the stress-strain curves). Usually the tensile stress–strain curve for pure gum rubbers has an S-like shape. However, introduction of the filler influences the behaviour of the rubber and changes the shape of the curve [8]. The stress–strain curves in the figure are typical of a vulcanized gum which shows strain induced crystallization. This gives rise to a strain hardening effect. Das *et al.* [9] found similar strain-stress behaviour in a study of nanocomposites based on chloroprene rubber.

When the organoclay fillers are added into the polymer matrix, it is apparent that the nature of the surfactants plays a role in determining the mechanical properties of the PCP. Das *et al.* [9] found that MMT organoclay has the ability to enhance the crystallization tendency of chloroprene rubber chains. The samples investigated in this study show an effect similar to a yield point in thermoplastic polymers. The reason for this is not clear, but it may be related to the extent of vulcanization of these samples. This effect becomes less obvious in the clay-containing samples, which may be the result of reduced vulcanization as discussed by Das *et al*. [9].

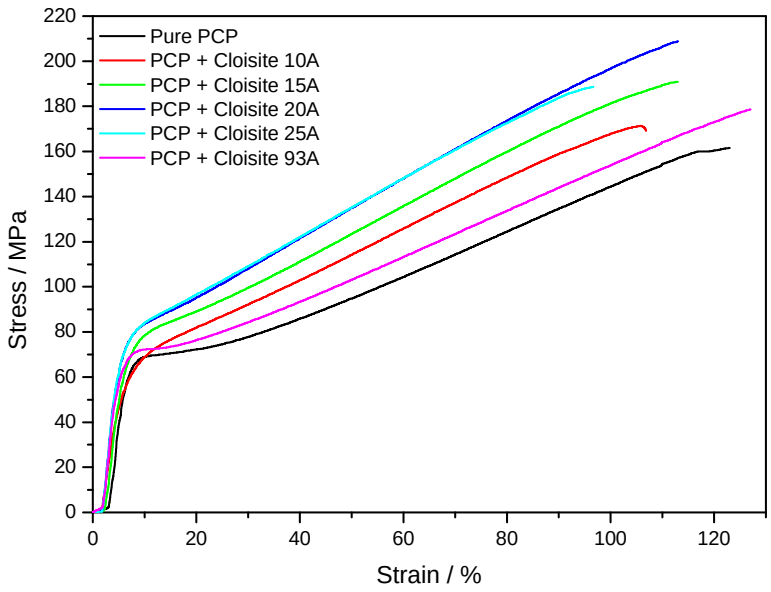

Figure 4.13 Typical stress-strain curves for PCP and its nanocomposites at 2.5 phr clay content

4.3.1 Stress at break

The stress at break values for all the PCP nanocomposites are listed in Table 4.3, and the influence of organoclay filler content on the tensile stress at break of the nanocomposite samples is shown in Figure 4.14. The tensile stress at break generally decreases with increasing clay content. The highest decrease at lower filler content is observed for Cloisite 10A, where more PCP matrix has penetrated the clay galleries and exfoliation is most pronounced. The decrease in tensile strength at break may be related to the clay particles acting as stress concentration sites, and the effect is much more pronounced at high filler contents for Cloisite 20A and 25A nanocomposites. Cloisites 20A and 25A containing samples exhibit a slight initial increase in tensile strength followed by a decrease with increasing amount of filler. For all the nanocomposites, at high clay content, the decrease in the tensile strength can be attributed to weak regions in the matrix-filler system, since the silicate layers may stack together to form tactoids. These stacked particles then deteriorate the properties of the nanocomposites by acting as defect points in the PCP matrix.

Table 4.3 Summary of mechanical properties

Sample	Stress at break / MPa	Elongation at break / %	Tensile modulus / MPa
Pure PCP	13.3 ± 0.8	425 ± 43	31.6 ± 9.3
PCP + 2.5 phr Cloisite 10A	9.9 ± 0.9	231 ± 52	40.5 ± 10.0
PCP + 5 phr Cloisite 10A	11.7 ± 0.2	405 ± 45	42.1 ± 3.7
PCP + 10 phr Cloisite 10A	10.4 ± 0.8	322 ± 49	53.7 ± 13
Pure PCP	13.3 ± 0.8	425 ± 43	31.6 ± 9.3
PCP + 2.5 phr Cloisite 15A	10.8 ± 0.6	260 ± 36	41.9 ± 7.8
PCP + 5 phr Cloisite 15A	15.9 ± 0.9	451 ± 67	58.9 ± 8.9
PCP + 10 phr Cloisite 15A	13.1 ± 0.6	260 ± 30	58.8 ± 9.4
Pure PCP	13.3 ± 0.8	425 ± 33	31.6 ± 9.3
PCP + 2.5 phr Cloisite 20A	14.1 ± 0.7	347 ± 29	43.9 ± 7.5
PCP + 5 phr Cloisite 20A	12.2 ± 0.6	495 ± 33	44.6 ± 6.1
PCP + 10 phr Cloisite 20A	8.2 ± 0.6	237 ± 37	45.6 ± 4.3
Pure PCP	13.3 ± 0.8	425 ± 43	31.6 ± 9.3
PCP + 2.5 phr Cloisite 25A	13.9 ± 0.7	371 ± 63	44.6 ± 9.6
PCP + 5 phr Cloisite 25A	11.7 ± 0.7	361 ± 64	49.2 ± 8.6
PCP + 10 phr Cloisite 25A	8.2 ± 0.4	235 ± 21	55.2 ± 12
Pure PCP	13.3 ± 0.8	425 ± 43	31.6 ± 9.3
PCP + 2.5 phr Cloisite 93A	10.6 ± 0.7	360 ± 59	42.1 ± 8.5
PCP + 5 phr Cloisite 93A	10.3 ± 0.7	349 ± 21	44.9 ± 3.4
PCP + 10 phr Cloisite 93A	10.1 ± 0.9	264 ± 45	50.6 ± 5.3

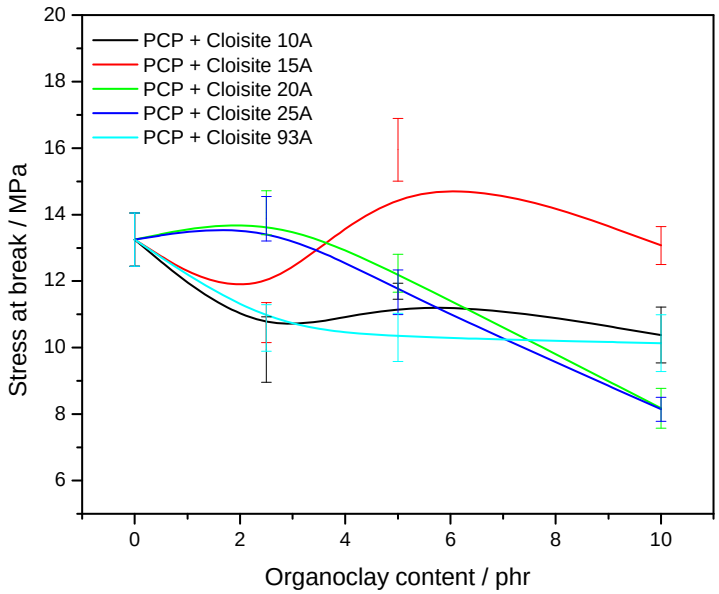

Figure 4.14 The influence of organoclay content on the tensile stress at break of the nano-composites

4.3.2 Elongation at break

The relationship between clay content and elongation at break of the nanocomposite samples is shown in Figure 4.15, and the elongation at break data of PCP and its nanocomposites are summarized in Table 4.3. The elongation at break generally decreases with up to 25% for the highest clay content. This decrease in elongation is characteristic of materials reinforced with stiff inorganic materials and this is particularly true for samples with an intercalated morphology [10]. Up to 2.5 phr clay content, all five organoclays have a similar influence on the elongation at break. The silicates may act as defect centres with lower stress transfer between the matrix and the filler, and hence the composites break at lower strains. Another possible reason is that the fillers reduced the polymer chain mobility [11]. Above filler contents of 2.5 phr, the elongation at break of the Cloisite 25A and 93A containing nanocomposites further decreases. Konstantinos *et al.* [12], in their study on the effects of primary and quaternary amine intercalants on the organoclay dispersion in a sulphur-cured EPDM rubber, also observed a decrease in elongation at break when the filler content was increased. They believe that this phenomenon is likely related to the agglomeration of

silicates layers in the polymer matrix. This agglomeration results in premature failure, owing to which both ultimate stress and elongation at break are reduced. This behaviour was also found by Ahmahdi *et al.* [13] in their investigation of the physical properties of EPDM–organoclay nanocomposites. Their results show that the elongation at break of EPDM-clay nanocomposites decreases with an increase in clay content. They attributed this observation to the fact that ductility decreases when stiffness is increased by reinforcement. The elongation at break values of the Cloisite 10A, 15A and 20A containing nanocomposites increases as the filler content was increased from 2.5 to 5 phr. Gao *et al.* [14] believe that the elongation at break increased because of reduced exfoliation in the formed nanocomposites. At high filler content the elongation at break decreased for all the investigated Cloisite nanocomposites. Gao *et al*. [14] also found that at higher clay particle contents more interactions between the clay and the polymer chains limit the motion of the rubber chains so that the tensile strength increased and the elongation at break decreased. They concluded that strong interaction between the clay and the polymer matrix constrains the motion of rubber chains.

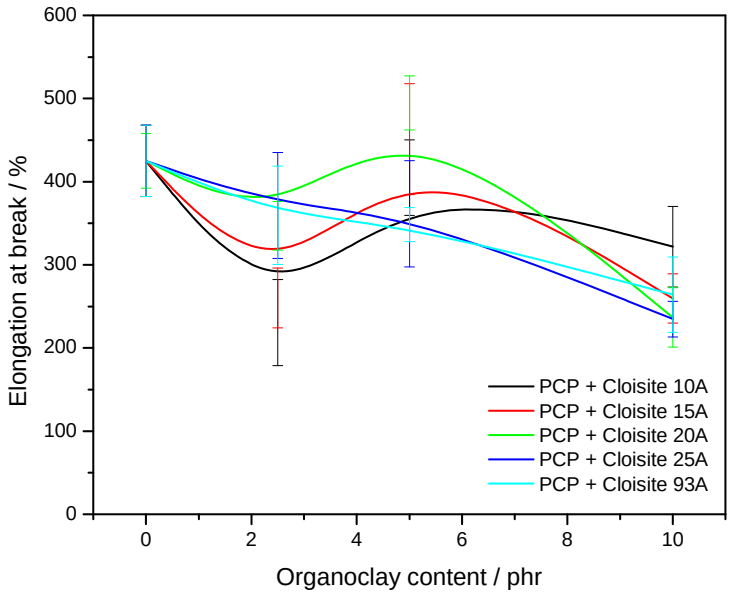

Figure 4.15 The influence of organoclay content on the elongation at break of the nano-composites

4.3.3 Tensile modulus

The tensile modulus of polymers normally increases when inorganic fillers are introduced into the polymer matrix. In the case of the PCP/clay nano-composites this also seems to be true, as is shown in Figure 4.16 and Table 4.3. It can be seen that the tensile modulus increases with increasing clay content. Since clay has a higher modulus and a more rigid structure, the modulus is expected to increase with increasing the clay content. No XRD diffraction peak was observed in all the nanocomposites at 2.5 and 5 phr filler content, which might indicate good dispersion of organoclay inside the polymer matrix. The increase in modulus that was observed also proves that there was a good interaction between the filler and the polymer matrix. Such polymer-filler interaction always helps to improve stress transfer through the interface and hence results in improved mechanical properties [11,15]. Zheng *et al* [16] investigated the influence of clay modification on the structure and mechanical properties of EPDM/montmorillonite nanocomposites. They found that the improvement in mechanical properties of EPDM/OMMT was due to the stronger interaction of the OMMT and the rubber matrix. The significant reinforcement of OMMT was caused by a good dispersion in the rubber matrix as proved by TEM and XRD. Figure 4.15 shows that Cloisite 15A is much more efficient in increasing the tensile modulus than the other organoclays. Cloisite 15A has the largest original inter-layer distance. This decreased the attraction between the silicate layers and led to more disordered nanolayers with high aspect ratio resulting in modulus enhancement [15,9]. These modulus increases also indicate a decrease in molecular mobility, which could be a consequence of the interaction of the polymer chains with the OMMT. At higher filler content, the moduli of the nanocomposites leveled off for Cloisite 15A and Cloisite 20A. This is probably due to the tendency of the clay particles to form agglomerates at higher filler contents.

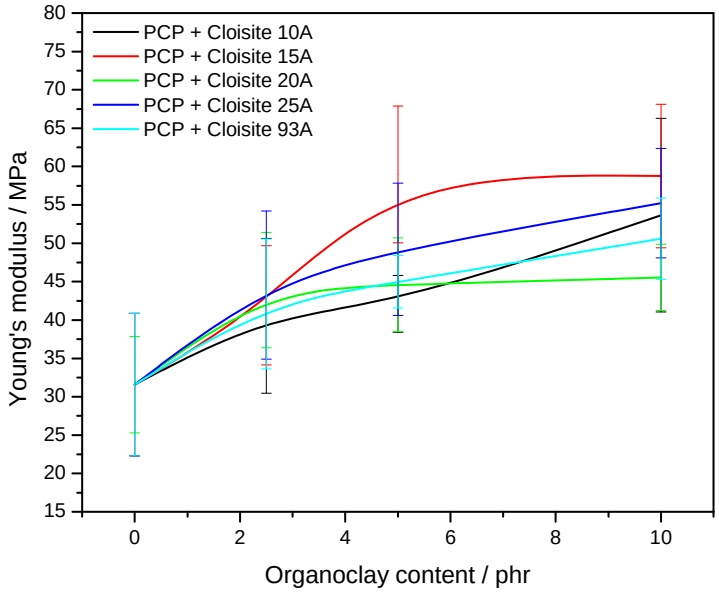

Figure 4.16 The influence of organoclay content on the tensile moduli of the nano-composites

4.4 Dynamic mechanical analysis (DMA)

Dynamic mechanical analysis (DMA) measures the response of a material to a cyclic deformation as a function of temperature. DMA results are expressed by three main parameters: (i) the storage modulus (*E*'), corresponding to the elastic response to the deformation; (ii) the loss modulus (*E"*), corresponding to the plastic response to the deformation, and (iii) the damping factor (tan δ), that is the *E*'/*E*" ratio, which indicates the energy dissipation by the sample, and which is useful for determining the occurrence of molecular mobility transitions such as the glass transition [17].

The DMA results will be discussed based on the nanocomposites morphology attained from the XRD and TEM analyses. It was found that both Cloisite 15A and 93A nanocomposites had better interaction with the rubber matrix and showed a more exfoliated morphology. Because of this, the presence of Cloisite 15A and Cloisite 93A in PCP had a more significant influence on some of the properties. Therefore the dynamic mechanical behaviour of these

nanocomposites is discussed separately from that of the nanocomposites based on Cloisite 10A, Cloisite 20A and Cloisite 25A.

4.4.1 Storage modulus and loss modulus

Figures 4.17 to 4.20 show the plots of storage and loss modulus as a function of temperature for pure PCP and the Cloisite 15A and 93A containing nanocomposites. There is a decrease in storage modulus with increasing temperature for these samples (Figures 4.17 and 4.19). This phenomenon is due to an increase in the segmental motion of the polymer chains as temperature is increased. A summary of the storage modulus values at -40 °C and 20 °C for each composite is shown in Table 4.4. The nanocomposite E' values below the glass transition are higher than that of pure PCP. This can be related to increased sample stiffness due to the presence of the nanoparticles. These results can also be related to the tensile modulus of PCP which increased with an increase in filler content. The storage modulus values are significantly lower at 20 °C than at -40 °C, as the PCP is now above its glass transition temperature. At temperatures above the T_g an increase in free volume occurs which allows space for molecular motions in the rubber matrix.

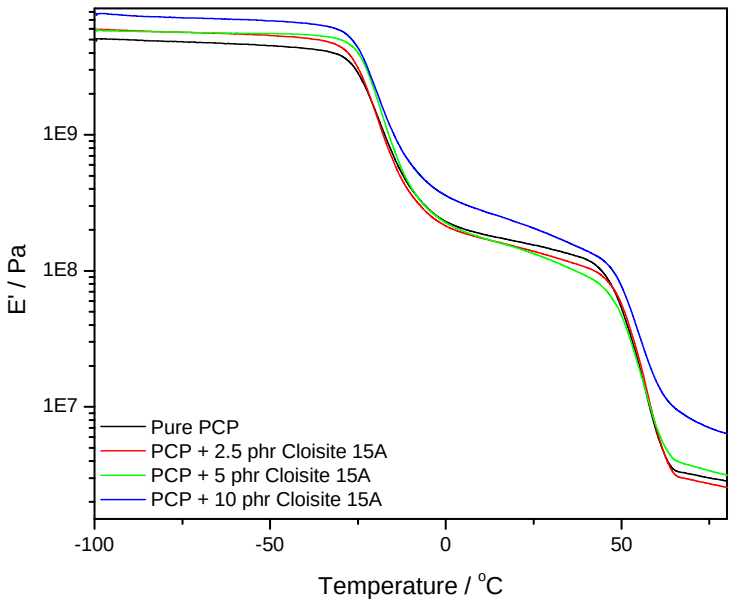

Figure 4.17 DMA storage modulus curves for pure PCP and the PCP/Cloisite 15A nanocomposites

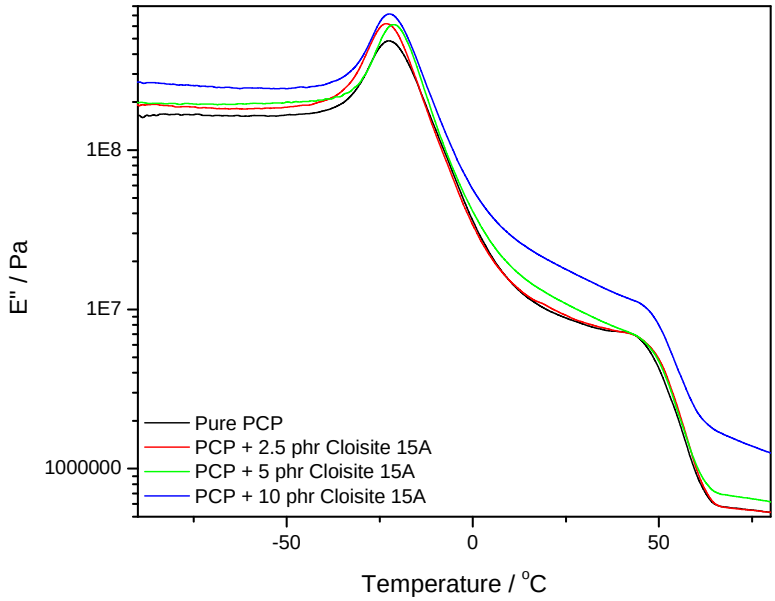

Figure 4.18 DMA loss modulus curves for pure PCP and the PCP/Cloisite 15A nanocomposites

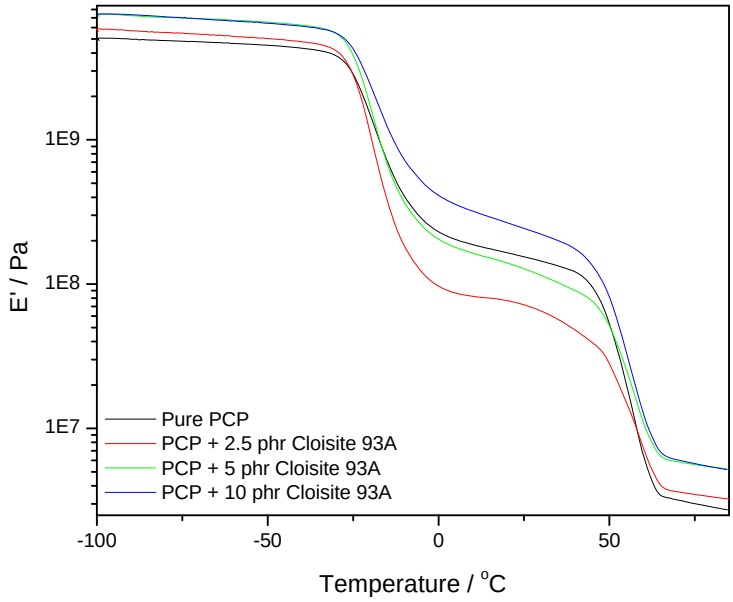

Figure 4.19 DMA storage modulus curves for pure PCP and the PCP/Cloisite 93A nanocomposites

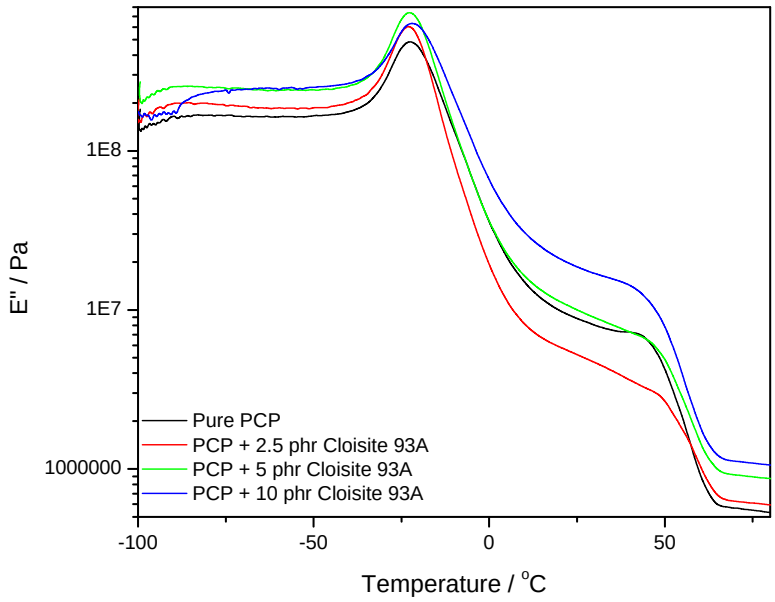

Figure 4.20 DMA loss modulus curves for pure PCP and the PCP/Cloisite 93A nanocomposites

The α-relaxation peaks at about -25 °C in Figures 4.18 and 4.20 for all the samples are correlated with the polymer glass transition which is caused by main chain motion, and the peak maxima are usually a measure of the glass transition temperature (T_g). At about 50 °C another relaxation occurs due to the melting of the crystalline domains in chloroprene rubber [9]. Table 4.4 summarizes the T_g values associated with the α-relaxation, measured from the maxima of the peaks in the loss modulus curves for pure PCP and the nanocomposites. The presence of the Cloisite 15A and 93A does not significantly change this temperature. This result means that the glass transition temperature is not significantly affected by the presence of nano-clay particles. The nanocomposite *E"* values below the glass transition temperature are, like the *E'* values, generally higher than that of pure PCP.

Table 4.4 Dynamic mechanical properties of PCP and its nanocomposites

Sample	T_g from tan δ curve / °C	T_g from loss modulus curve / °C	10^9 E' / Pa (at -40 °C)	10^8 E' / Pa (at 20 °C)
Pure PCP	-14.4	-21.9	4.3	1.6
PCP + 2.5 phr Cloisite 10A	-13.5	-21.1	5.9	1.8
PCP + 5 phr Cloisite 10A	-15.4	-22.3	5.6	1.6
PCP + 10 ph Cloisite 10A	-14.3	-21.7	5.7	1.8
PCP + 2.5 phr Cloisite 15A	-15.9	-22.7	5.1	1.5
PCP + 5 phr Cloisite 15A	-14.4	-21.7	6.2	1.5
PCP + 10 phr Cloisite 15A	-15.2	-22.3	6.6	2.2
PCP + 2.5 phr Cloisite 20A	-13.1	-20.8	6.1	2.1
PCP + 5 phr Cloisite 20A	-13.8	-22.9	5.4	1.4
PCP + 10 phr Cloisite 20A	-15.3	-22.1	6.6	2.3
PCP + 2.5 phr Cloisite 25A	-14.2	-21.5	5.8	2.2
PCP + 5 phr Cloisite 25A	-15.7	-22.8	4.9	1.2
PCP + 10 phr Cloisite 25A	-13.2	-21.6	7.2	3.4
PCP + 2.5 phr Cloisite 93A	-15.1	-23.1	4.7	0.8
PCP + 5 phr Cloisite 93A	-15.2	-22.5	6.2	1.4
PCP + 10 phr Cloisite 93A	-14.2	-21.8	6.1	2.6

The storage and loss modulus curves for pure PCP and the Cloisite 10A, 20A and 25A nanocomposites are shown as a function of temperature in Figures 4.21 to 4.26. There is also a decrease in storage and loss modulus with increasing temperature for all these samples. There is no clear trend in the storage and loss moduli with increasing clay content for Cloisite 10A, 20A and 25A. The *E′* curves show a decrease in modulus and the *E″* curves show a peak for all the samples in the temperature region of the glass transition. The α-relaxation peak maximum values from the loss modulus curves show a similar trend than the Cloisite 15A and 93A samples as a function of clay content. The *E'* and *E"* values of the composites below the glass transition are also higher than that of pure PCP, as observed for the Cloisite 15A and 93A nanocomposites. The steep drop in *E′* and *E″* at about 50 °C is associated with the melting of the crystalline regions in PCP.

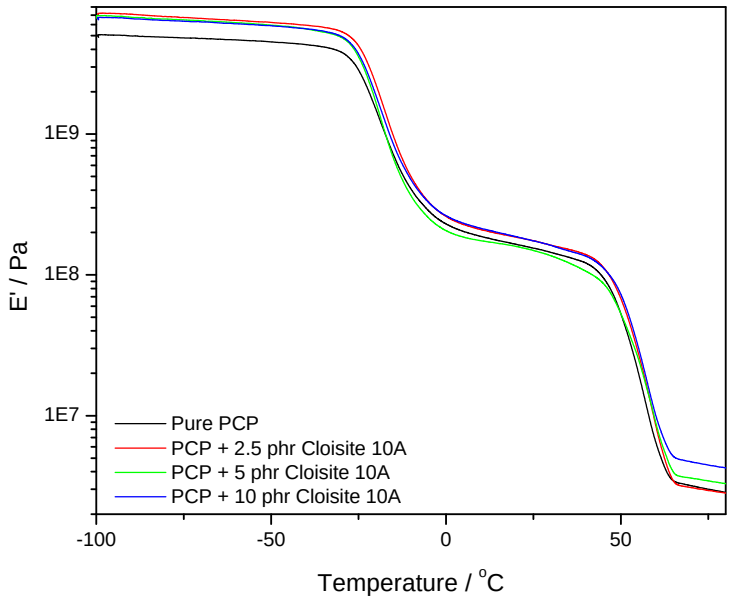

Figure 4.21 DMA storage modulus curves for pure PCP and the PCP/Cloisite 10A nanocomposites

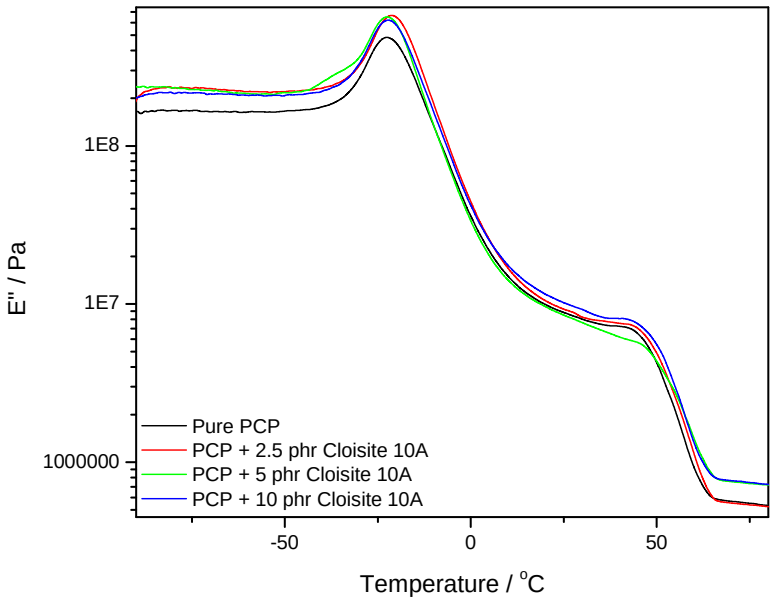

Figure 4.22 DMA loss modulus curves for pure PCP and the PCP/Cloisite 10A nanocomposites

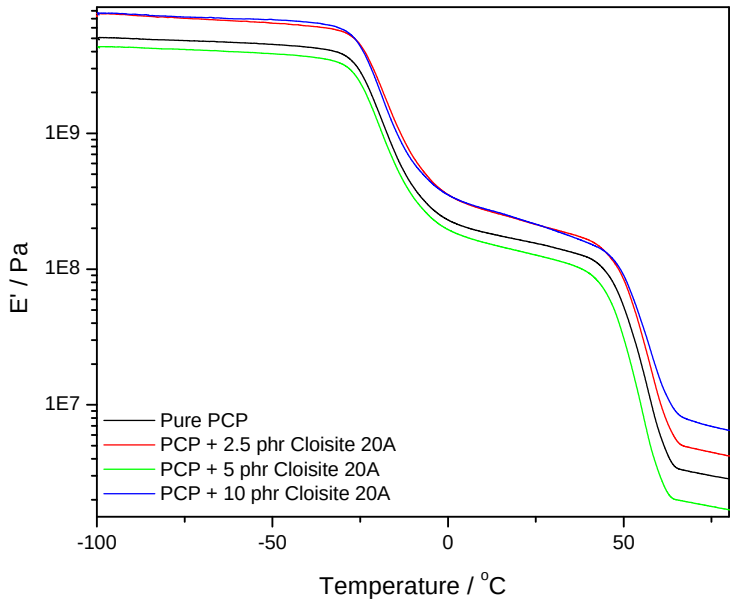

Figure 4.23 DMA storage modulus curves for pure PCP and the PCP/Cloisite 20A nanocomposites

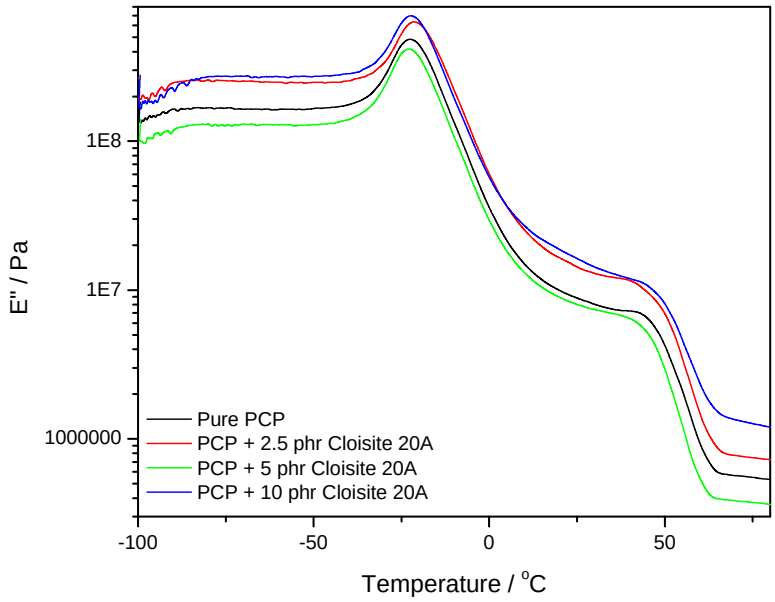

Figure 4.24 DMA loss modulus curves for pure PCP and the PCP/Cloisite 20A nanocomposites

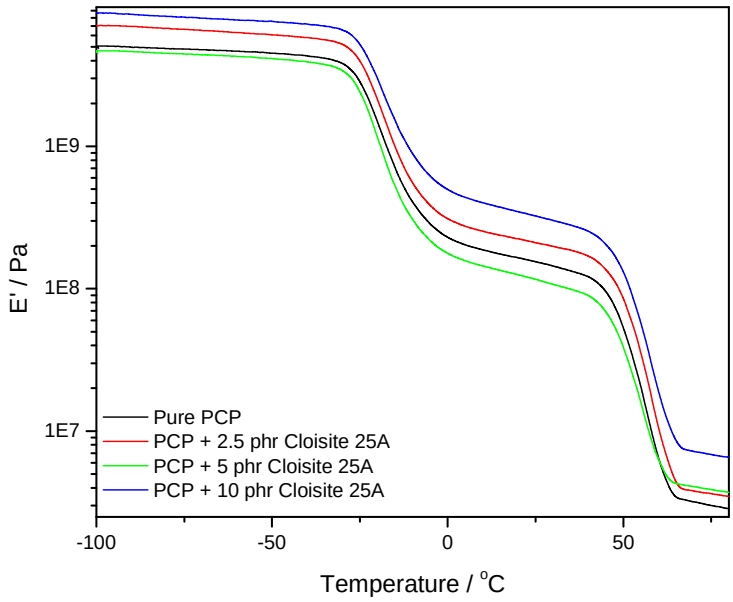

Figure 4.25 DMA storage modulus curves for pure PCP and the PCP/Cloisite 25A nanocomposites

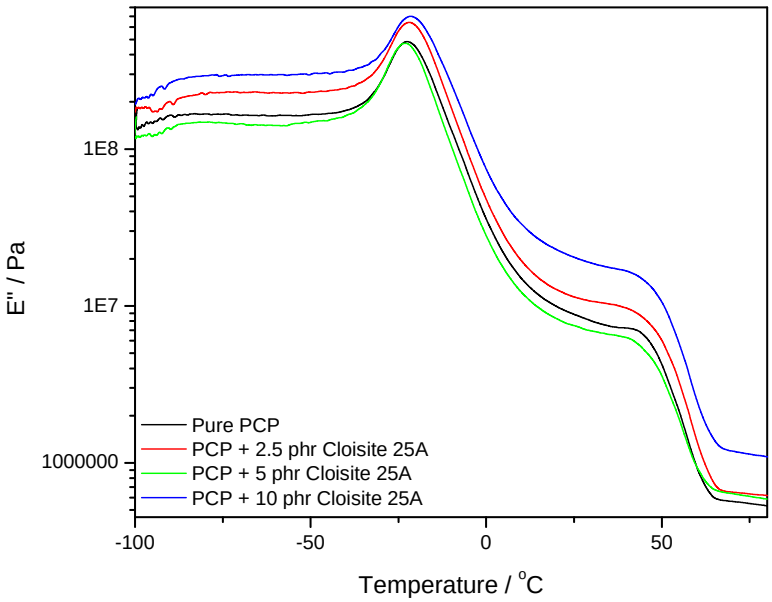

Figure 4.26 DMA loss modulus curves for pure PCP and the PCP/Cloisite 25A nanocomposites

4.4.2 Damping factor

Figures 4.27 and 4.28 show the plots of the damping factor (tan δ) of PCP and the Cloisite 15A and 93A nanocomposites as a function of temperature. All the plots show only one transition peak (α-transition) in this temperature range, which is indicative of the glass transition (T_g). Closer examination of the tan δ peaks reveals a trend of gradual decrease in peak height with increasing filler content for these nanocomposites. The tan δ value decrease is more pronounced for the Cloisite 93A samples, probably because there is a stronger interfacial interaction between the rubber and the filler. At higher filler content the tan δ peak for pure PCP is higher than those for the nanocomposites. Table 4.4 summarizes the T_g values associated with the α-relaxation measured from the maxima of the tan *δ* curves for pure PCP and the nanocomposites. There is no significant shifting in the loss maximum of the PCP nanocomposites as organoclay content in the composites increases. This means that the glass transition temperature, related to the maximum of tan δ, is not significantly affected by the presence of nanofillers or by the extent of clay dispersion. The strong intermolecular interactions between Cloisite 93A and PCP reduced the mobility of the PCP chain segments and caused high energy dissipation.

Figures 4.29 to 4.31 depict the damping factor (tan δ) curves for pure PCP and the Cloisite 10A, 20A and 25A nanocomposites as a function of temperature. Only one transition in this temperature range is observed, which is associated with the α-transition. There is no clear trend of tan δ peak positions with increasing filler content. It is also clear from Table 4.4 that there is no significant shifting in the loss maximum of the PCP nanocomposites as organoclay content in the nanocomposites increases. At about 50 °C, in all the damping factor curves, there is an increase in tan δ.

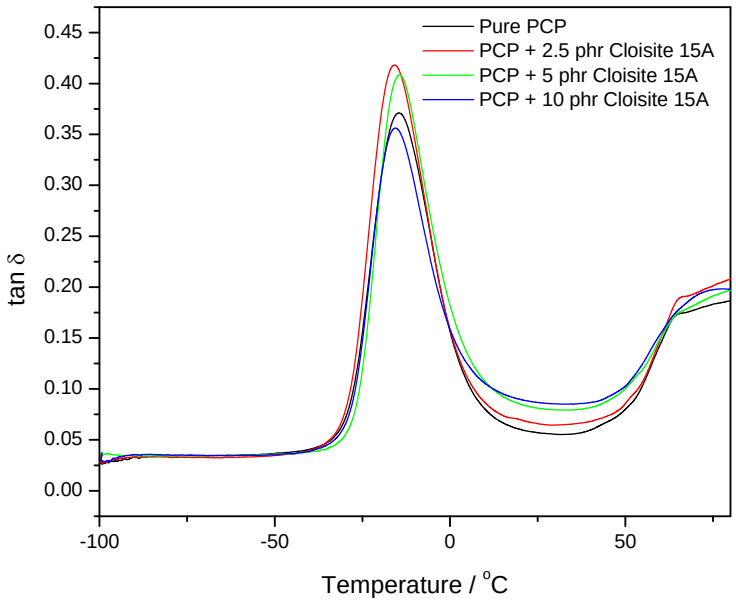

Figure 4.27 DMA damping factor curves for pure PCP and the PCP/Cloisite 15A nanocomposites

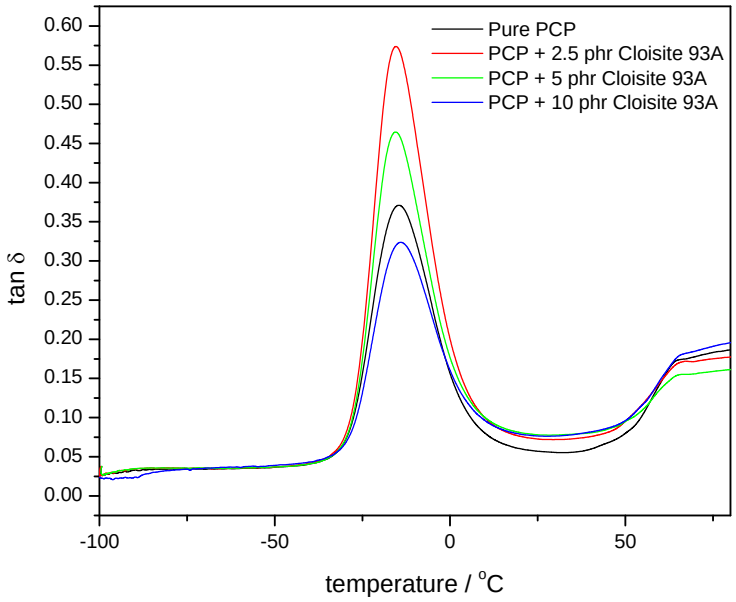

Figure 4.28 DMA damping factor curves for pure PCP and the PCP/Cloisite 93A nanocomposites

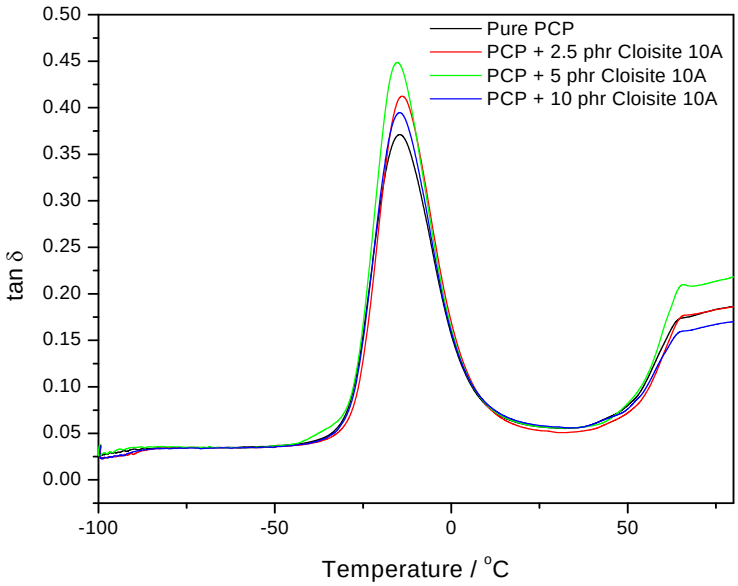

Figure 4.29 DMA damping factor curves for pure PCP and the PCP/Cloisite 10A nanocomposites

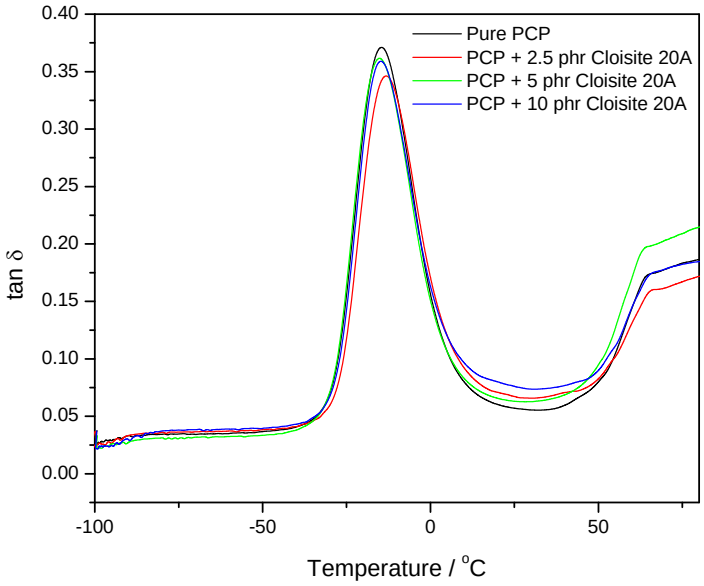

Figure 4.30 DMA damping factor curves for pure PCP and the PCP/Cloisite 20A nanocomposites

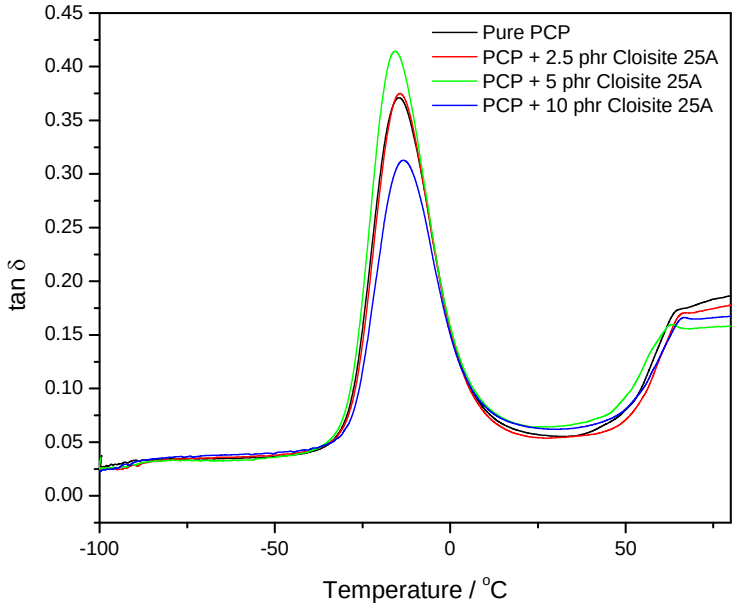

Figure 4.31 DMA damping factor curves for pure PCP and PCP/Cloisite 25A nanocomposites

4.5 Thermogravimetric analysis (TGA)

Thermogravimetric analysis was used to determine the thermal stability of the PCP nanocomposites. The weight loss due to the formation of volatile products after degradation was monitored as a function of temperature**.** The thermal degradation of pure PCP occurred in two stages as observed in Figure 4.32. The first weight loss occurred around 300 °C. This stage was attributed to the elimination of HCl molecules, leaving behind the polyene chains. This is followed by a gradual decrease in weight between 300 and 450 °C, with a second clearly defined weight loss step around 450 °C. Nair *et al.* [26], in their study of the thermogravimetric analysis of PVC/ELNR blends, associated this step with the thermal degradation of the polyene sequences and the evolution of volatile aromatic and aliphatic compounds by the intramolecular cyclisation of the conjugated sequences. The thermal degradation products yielded in PVC in this stage are similar to the decomposition products produced in PCP [28]. Above 500 °C there was a further gradual decrease in sample weight, which is explained as the release of tar and volatiles as a result of condensation reactions. The

30% sample still present at 600 °C is a black carbonaceous char which cannot degrade further [21-22].

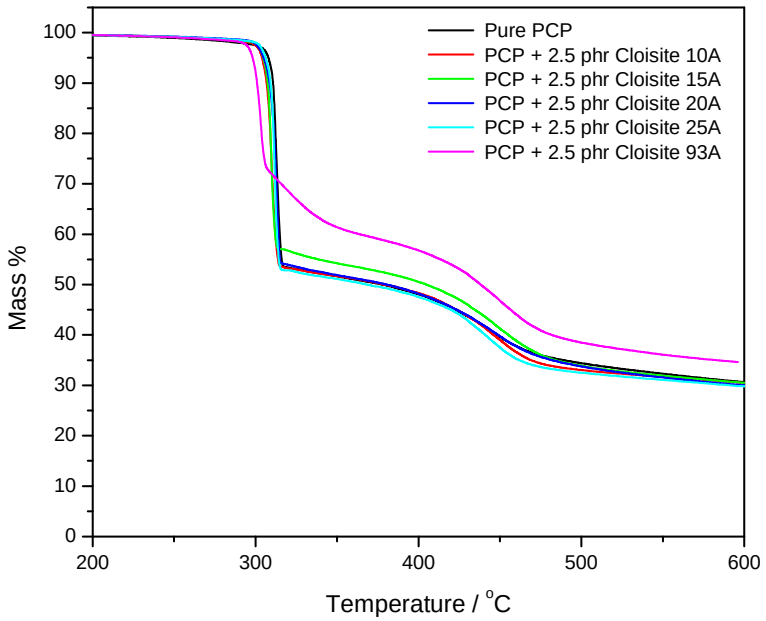

Figure 4.32 TGA curves of PCP/organoclays at 2.5 phr

The Hoffman reaction, depicting the mechanism of the reaction occurring during organoclay degradation, is shown in Figure 4.33. The alkyl ammonium modified clays decompose between 200 and 300 °C to produce α-olefins and amines. This leads to the elimination of the ammonium modifier which results in a substitution of the ammonium linkages on the clay with hydrogen protons due to β-carbon fracture that should be acting as Brønsted acidic sites that accelerate polymer degradation. Ultimately, the α-olefins, by-products, or intermediates produced in this reaction could attack the polymer and promote polymer degradation [27]. Figures 4.32, 4.34 and 4.35 show the weight loss as a function of temperature for the different PCP/Cloisite nanocomposites, having filler contents of respectively 2.5, 5 and 10 phr. Table 4.5 presents the temperatures at 5% degradation of the nanocomposite samples and pure PCP.

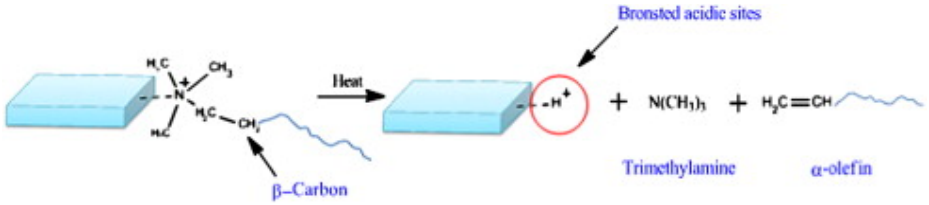

Figure 4.33 The Hoffman elimination reaction mechanism [27]

Table 4.5 Temperatures at 5% degradation of all the investigated samples

Sample	2.5 phr clay	5 phr clay	10 phr clay
Pure PCP	307.5 °C	307.5 °C	307.5 °C
PCP + Cloisite 10A	303.2 °C	296.8 °C	305.1°C
PCP + Cloisite 15A	304.1 °C	305.9 °C	309.4 °C
PCP + Cloisite 20A	304.7 °C	303.5 °C	309.7 °C
PCP + Cloisite 25A	305.3 °C	304.4 °C	313.6 °C
PCP + Cloisite 93A	298.2 °C	302.3 °C	302.9 °C

Figure 4.32 depicts the TGA curve of the PCP/Cloisite samples at 2.5 phr clay. All samples started degrading around 300 °C and the temperatures of the initial stage of degradation shifted to lower values for all the nanocomposites. The presence of a quaternary ammonium anion in the nanocomposite systems is probably responsible for the acceleration of the polymer decomposition in this stage, according to the Hoffman reaction proposed above. Because of the more efficient exfoliation observed for Cloisite 93A, there should be better interaction between the clay and PCP, hence more HCl might have been adsorbed during the first stage of degradation. This explains the smaller mass loss observed during the first degradation stage, which indicates that less HCl initially diffused out of the sample. The Cloisite 15A based nanocomposite also shows a smaller weight loss when compared to the other samples**.** This could be due to the Cloisite 15A and 93A having stronger interactions between the surfaces of the clay particles and the functional groups on the polymer chains.

There is a second degradation step during the first stage for the Cloisite 93A containing sample around 300-350 ºC, which might be related to retarded dehydrochlorination of PCP. Dick *et al.* [22] studied the char forming processes in polychloroprene through solid state ^{13}C

NMR. They observed that initially the dehydrochlorination was rapid, followed by second and third slower steps. They observed that the rapid dehydrochlorination (stages 1 and 2) occurred below 300 ºC due to the dehydrochlorination of the isomerised 1,2 unit, which contains the most labile chlorine. The third stage was due to the dehydrochlorination of the more stable 3,4 and 1,4 units and occurred at 357–365 ºC. The other nanocomposite samples displayed similar behaviour to pure PCP, and yielded similar char contents at 600 °C. At higher temperatures the linear polyenes are predicted to disappear through two competing processes: intramolecular cyclization and intermolecular crosslinking. The intermolecular crosslinking produces only unsubstituted aromatics while intramolecular cyclization leads to the formation of crosslinked polyene chains. At higher temperatures the crosslinked polyene chains undergo one or both of two competing processes: further decomposition to produce char and intramolecular cyclization to produce alkyl aromatics [23]. When there is a strong interaction between PCP and the organoclay, the Brönsted acidic sites present in the clay layers accelerate the crosslinking reactions, and suppress the evolution of the unsubstituted aromatics [33]. This probably led to the formation of more residue or char in the case of the Cloisite 93A samples.

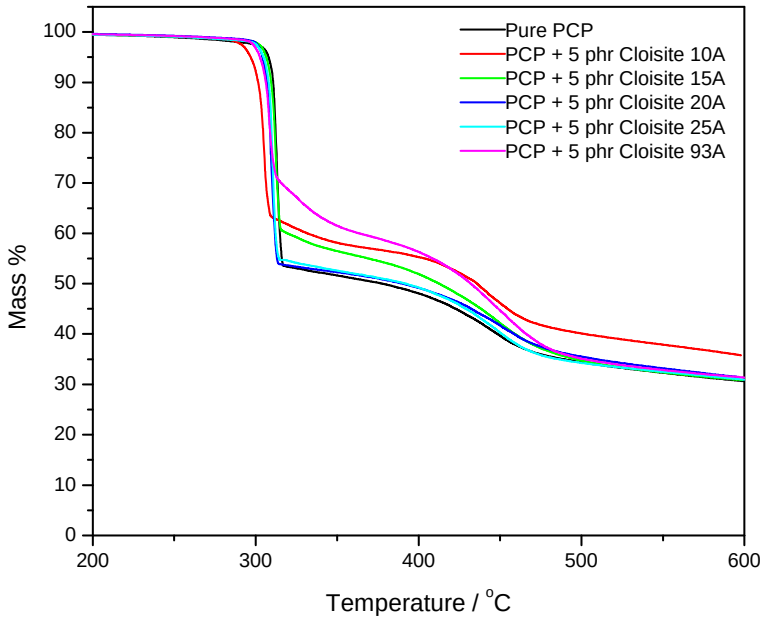

Figure 4.34 TGA curves of PCP/organoclays at 5 phr

Figure 4.34 shows the TGA curves of the PCP nanocomposites at 5 phr nanoclay content. The onset of degradation of all the nanocomposites has lower values than that of pure PCP. In this

case it is not only the Cloisite 15A and the Cloisite 93A containing samples that show different degradation behaviour. At this higher clay content the Cloisite 10A containing sample shows similar behaviour. By increasing the filler content from 2.5 phr to 5 phr for Cloisite 10A, the clay becomes more intercalated because of the presence of the phenyl group, resulting in more interactions between the clay and the rubber. The third stage of HCl evolution due to dehydrochlorination of the more stable 3,4 and 1,4 units also probably occurs because of stronger interaction between the organoclay and PCP. There are no observed differences in the amount of char formed at higher temperatures, except for Cloisite 10A. The higher char formation in Cloisite 10A is probably due to a strong interaction between PCP and the organoclay, which suppressed the evolution of unsubstituted aromatics in PCP.

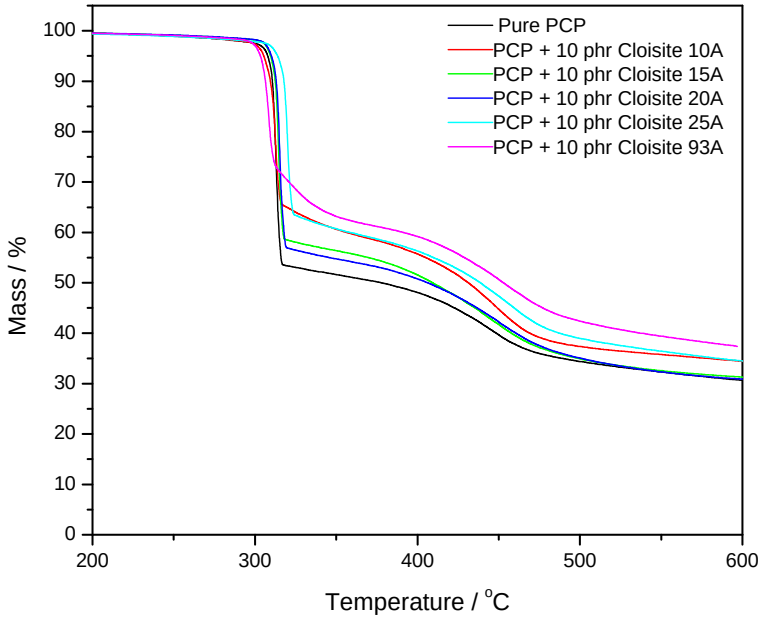

Figure 4.35 TGA graphs of PCP/organoclays at 10 phr

Figure 4.35 displays the TGA curves of the PCP nanocomposites at 10 phr nanoclay content. There is not much difference between the TGA curves for these samples up to 300 °C, and for all the samples the first transition occurs at almost the same temperature. There are significant differences in initial mass loss compared to pure PCP. At lower filler content, the organoclay filler normally acts as a nucleating agent, reducing polymer chain mobility and affecting the kinetics of the oxidation process. With a 10 phr loading, the catalyzing effect of all the nanocomposite samples rapidly rises because of concentration of active centres (i.e. metal ions). This effect increases the interaction at the interface between the filler and the matrix,

which causes a decrease in the rate of evolution of the volatile products. The higher char content observed for the Cloisite 93A, 10A and 25A indicates that this sample improves the thermal stability of the nanocomposites at higher filler content. The nanocomposites based on Cloisite 15A and 20A, which use the same intercalant, show similar behaviour at higher temperatures. The Cloisite 20A and 15A were treated with the same modifier containing two hydrogenated tallow groups, but at different modifier contents.

It is clear from the TGA results that some filler already have a significant influence on the PCP degradation mechanism at low clay contents, while other clays only start showing an influence at 5 phr and others only at 10 phr clay content. Both Cloisite 93A and Cloisite 15A had an influence on the polymer degradation at 2.5 phr. Both of them are derived from a two-tailed hydrogenated tallow organoclay and have no characteristic x-ray reflection, which suggests a highly exfoliated structure containing dispersed silicate platelets. Cloisite 20A and Cloisite 25A begin showing observable differences at high filler content. Both of them are derived from a single-tailed structure which resulted in intercalated composites having moderate stiffness improvements.

4.6 Stress relaxation

Stress relaxation was used to investigate the time-dependent viscoelastic properties of the polymer and its nanocomposites. The stress relaxation of polymers is attributed to chain motion and orientation, disentangling of polymer chain network strands, and deformation and rupture of micro domains and crosslinks. If stress relaxation occurs, part of the energy stored in the materials is dissipated and part of the deformed chains cannot retract. Therefore, more pronounced stress relaxation may cause a lowering of the recovery stress [29]. The stress decay of all the samples was monitored at a constant strain of 20%. Figures 4.36 to 4.45 show the stress relaxation curves of PCP and its different nanocomposites.

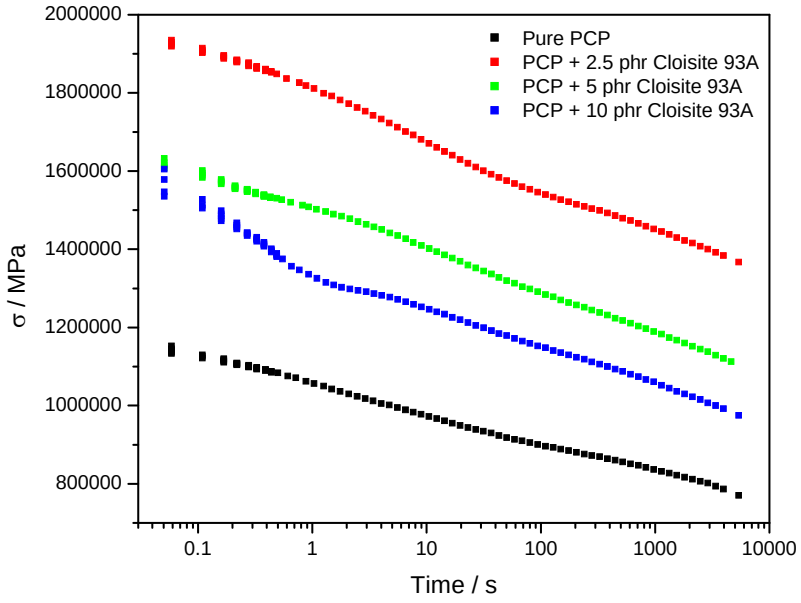

Figure 4.36 Stress relaxation curves of Cloisite 93A-filled PCP nanocomposites

The stress relaxation plots of the PCP-Cloisite 93A nanocomposites are shown in Figures 4.36 and 4.37. In both figures the stress decay slows down with time as the system approaches equilibrium. The initial change is consistent with the physical relaxation caused by the relaxation of the polymer chains and fillers, while the long-term relaxation occurs due to chemical reactions over time [30]. The addition of organoclay reinforces the matrix, thus the relaxation curves of the nanocomposites lie at a higher level compared to pure PCP (Figure 4.36). The highest initial stress is observed in the sample with 2.5 phr clay, and decreases with an increase in filler content. This is probably due to a tendency of clay particles to form large agglomerates at higher filler contents, thus deteriorating the mechanical properties. The higher residual stress was also found at 2.5 phr clay content (Figure 4.37). The samples with higher filler contents have lower residual stresses than the pure PCP. The higher relaxation rate obtained for samples at higher filler content may be attributed to the breakdown of filler-filler aggregates and weak polymer-filler networks [31].

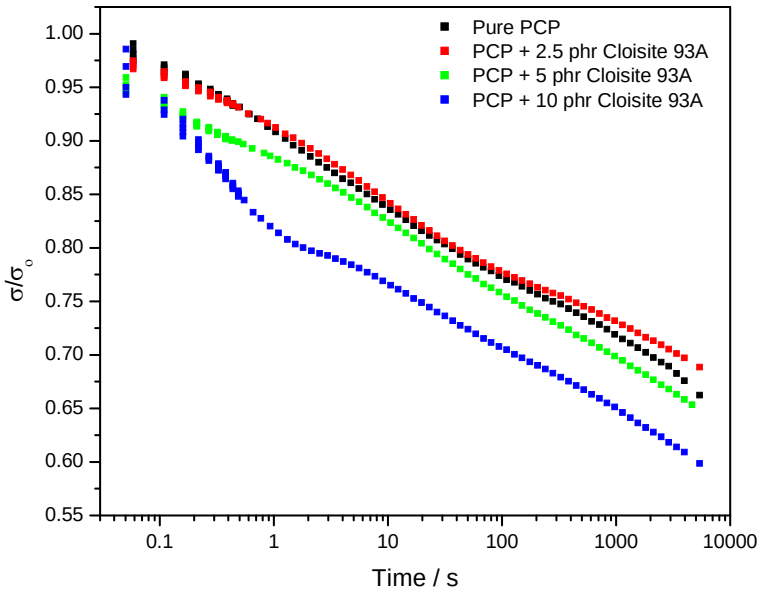

Figure 4.37 Rate of stress decay for Cloisite 93A-filled PCP nanocomposites

Figures 4.38 and 4.39 represent the stress relaxation plots of nanocomposites with different Cloisite 25A loadings. The initial stresses of all the nanocomposites are higher than that of pure PCP, and further decreases with an increase in filler content (Figure 4.38). The pure PCP and the nanocomposite samples with 5 and 10 phr clay have comparable residual stresses at the end of the relaxation time (Figure 4.39). The 2.5 phr clay containing sample has the highest residual stress of all the samples investigated. At low loadings the chances of forming aggregates are comparatively low and hence good dispersion of the filler is normally achieved, increasing the stress recovery. However, at 5 and 10 phr clay loadings, due to the breakdown of the aggregates, the energy stored in the materials dissipated more and the recovery became less pronounced. Hence, they displayed similar behaviour to pure PCP.

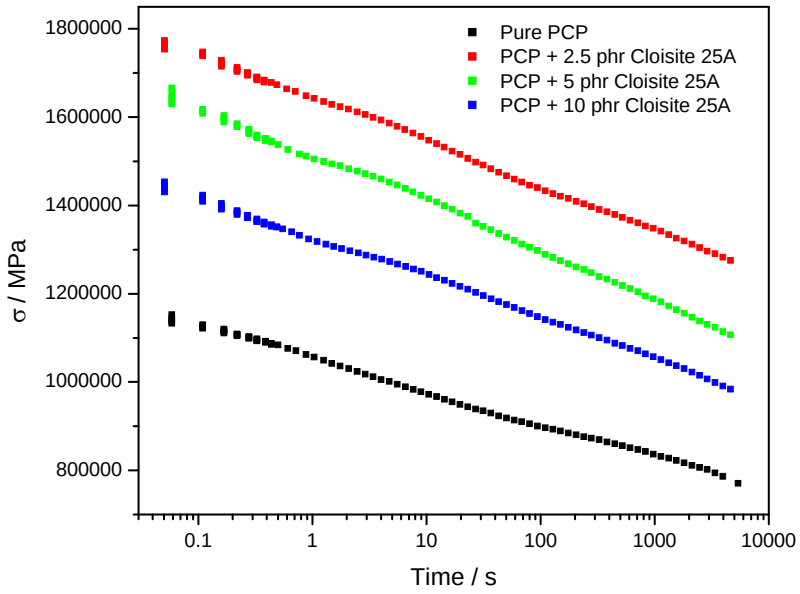

Figure 4.38 Stress relaxation curves of Cloisite 25A-filled PCP nanocomposites

The stress relaxation curves of the Cloisite 10A containing nanocomposites are depicted in Figures 4.40 and 4.41. The influence of the addition of organoclay can be seen in Figure 4.40. All the nanocomposite samples have higher initial stresses than pure PCP, which decrease with an increase in clay content. The normalized residual stresses and relaxation rates of the Cloisite 10A containing nanocomposites are shown in Figure 4.41. Pure PCP and the nanocomposite samples with 5 and 10 phr clay loadings have comparable residual stresses left at the end of the relaxation time. The relaxation behaviour of the 5 phr sample does not show the same trend as the other samples.

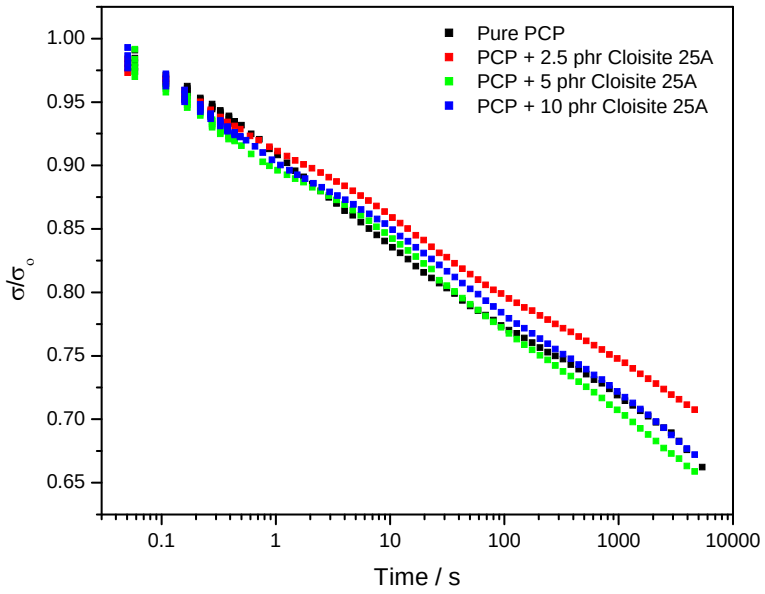

Figure 4.39 Rate of stress decay for Cloisite 25A-filled PCP nanocomposites

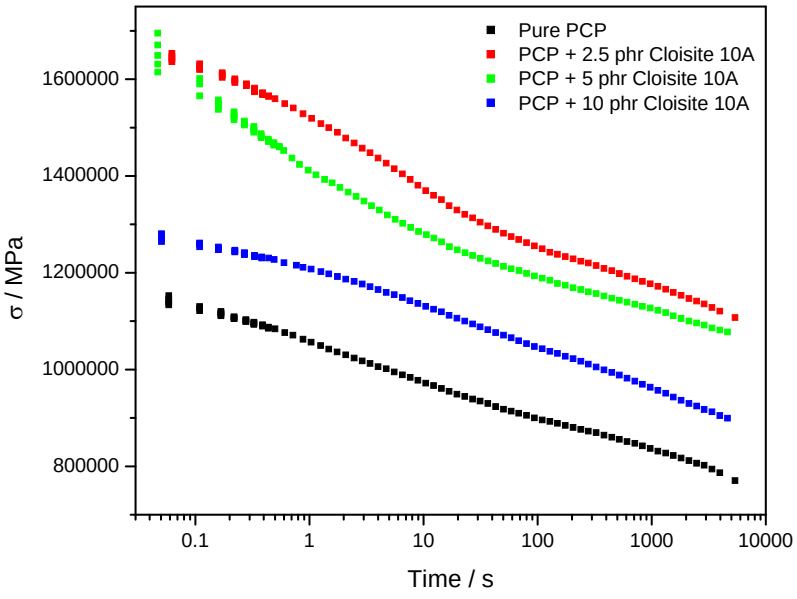

Figure 4.40 Stress relaxation curves of Cloisite 10A-filled PCP nanocomposites

Figures 4.42 and 4.43 show the stress relaxation curves of the Cloisite 15A containing nanocomposites. As in the previous cases, the stress decay decreases with an increase in time, and the addition of filler reinforces the rubber matrix (Figure 4.42). The initial stresses follow the change in the elastic modulus with an increase in organoclay content. Furthermore, the residual stresses (Figure 4.43) do not follow the same dependence on organoclay content as was observed in Figure 4.42. The higher relaxation rates for the 5 and 10 phr clay containing samples are associated with the breakdown of filler-filler and weak polymer-filler networks during the course of the relaxation process [32]. At low loadings, the chances of forming aggregates are smaller and hence a good dispersion is achieved. The rate of stress relaxation is therefore typically lower at low filler content.

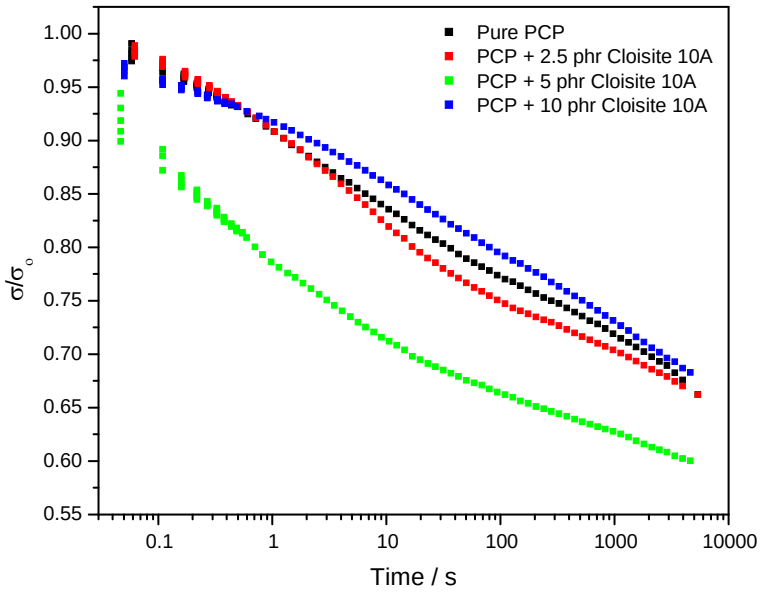

Figure 4.41 Rate of stress decay for Cloisite 10A-filled PCP nanocomposites

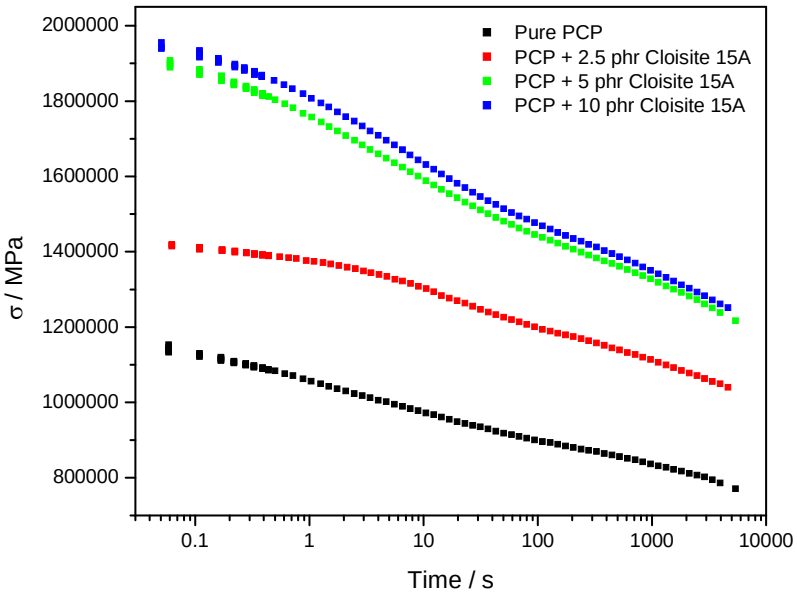

Figure 4.42 Stress relaxation curves of Cloisite 15A-filled PCP nanocomposites

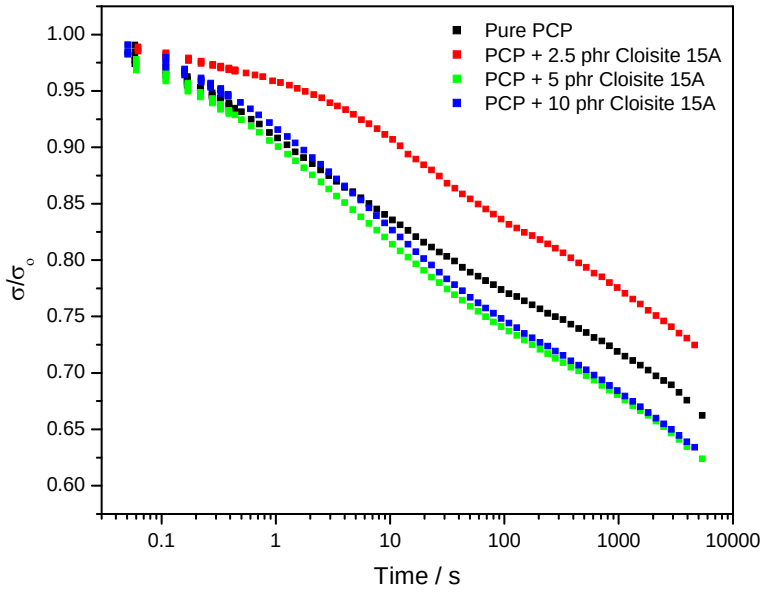

Figure 4.43 Rate of stress decay for Cloisite 15A-filled PCP nanocomposites

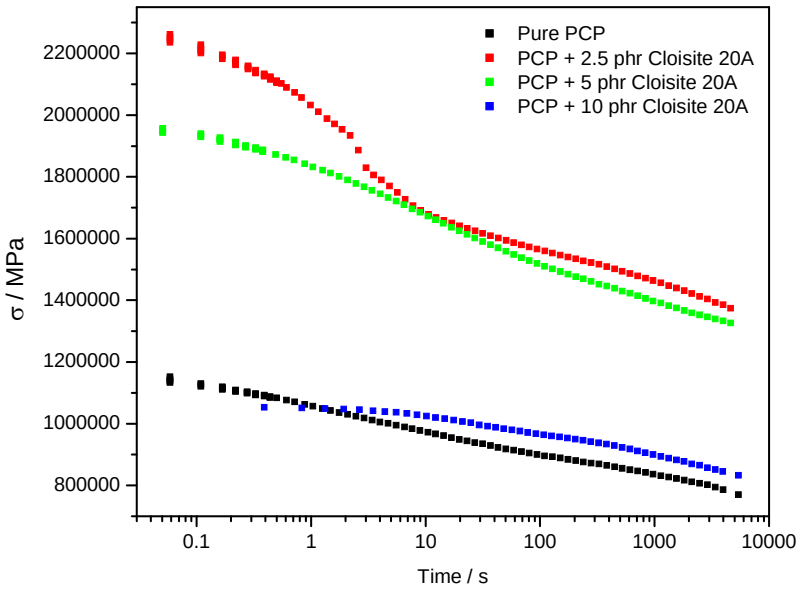

Figure 4.44 Stress relaxation curves for Cloisite 15A-filled PCP nanocomposites

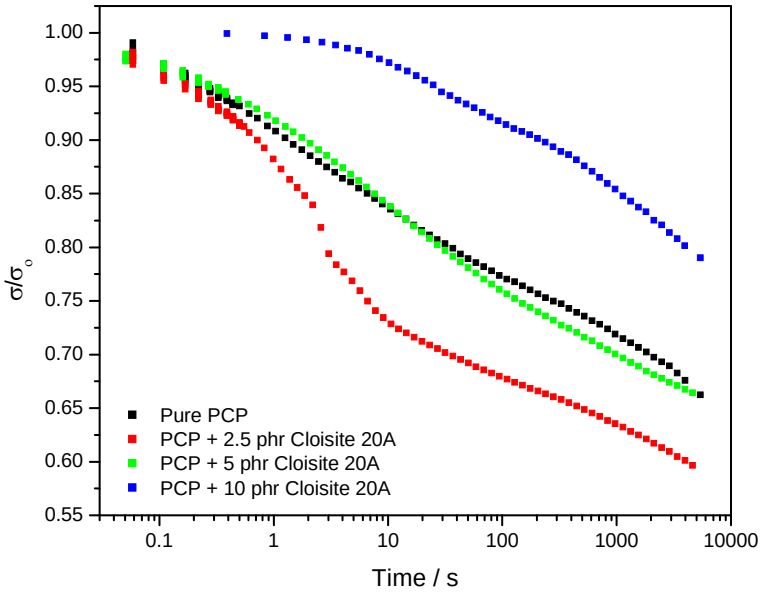

Figure 4.45 Rate of stress decay for Cloisite 15A-filled PCP nanocomposites

Figures 4.44 and 4.45 represent the stress relaxation plots of the nanocomposites prepared with various Cloisite 20A filler loadings. The samples containing 2.5 and 10 phr clay show unusual relaxation behaviour. It is believed that these samples slipped in the tensile test clamp during the stress relaxation analyses. The results show that the elastomeric material with 5 phr clay loading has a higher initial stress than pure PCP. Both PCP and the 5 phr clay containing sample have comparable residual stress left at the end of the relaxation time. Conclusive results about the impact of organoclay loading on PCP relaxation could not be reached for this type of organoclay.

4.7 References

1. L. Szazdi, A. Pozsgay, B. Pukanszky. Factors and processes influencing the reinforcing effect of layered silicates in polymer nanocomposites. European Polymer Journal 2007; 43:345-359.
2. B. Pukanszky. Interfaces and interphases in multicomponent materials: past, present, future. European Polymer Journal 2005; 41:645-662.
3. J. Moczo, B. Pukanszky. Polymer micro and nanocomposites: Structure, interactions, properties. Journal of Industrial and Engineering Chemistry 2008; 14:535-563.
4. S.R Suprakas. Visualisation of nanoclay dispersion in polymer matrix by high-resolution electron microscopy combined with electron tomography. Macromolecular Materials and Engineering 2009; 294:281-286.
5. F.R. Adley, E.C. Muniz, A.R. Freitas. Degradation of polychloroprene/natural rubber (PCP/NR) blends by photo-Fenton process. Polymer Degradation and Stability 2008; 93:601-607.
6. R.K. Gunasekaran, A. Natarajan, A. Kala. FTIR spectra and mechanical strength analysis of some selected rubber derivatives. Spectrochimica Acta: Part A 2007; 68:323-330.
7. V. Arjunan, S. Subramanian, S. Mohan. Vibrational spectroscopic studies on trans-1,4-polychloroprene. Turkish Journal of Chemistry 2003; 27:423-431.
8. S. Sun, C. Li, L. Zhang, H.L. Du, J.S. Burnell-Gray. Effects of surface modification of fumed silica on interfacial structures and mechanical properties of poly(vinyl chloride) composites. European Polymer Journal 2006; 42:1643-1652.

9. A. Das, F.R. Costa, U. Wagenknecht, G. Heinrich. Nanocomposites based on chloroprene rubber: Effect of chemical nature and organic modification of nanoclay on the vulcanizate properties. European Polymer Journal 2008; 44:3456-3465.
10. S. Subramani, J.Y. Lee, J.H. Kim, I.W. Cheong. Crosslinked aqueous dispersion of silylated poly(urethane–urea)/clay nanocomposites. Composites Science and Technology 2007; 67:1561-1573.
11. R.R. Maharsia, H.D. Jerro. Enhancing tensile strength and toughness in syntactic foams through nanoclay reinforcement. Materials Science and Engineering A 2007; 454:416-422.
12. G.G Konstantinos, J. Karger-Kocsis. Effects of primary and quaternary amine intercalants on the organoclay dispersion in a sulfur-cured EPDM rubber. Polymer 2005; 46:3069–3076.
13. S.J. Ahmadi, Y. Huang, W. Li. Fabrication and physical properties of EPDM-organoclay nanocomposites. Composites Science and Technology 2005; 65:1069-1076.
14. J. Gao, Z. Gu, G. Song, P. Li, W. Liu. Preparation and properties of organo-montmorillonite/fluoroelastomer nanocomposites. Applied Clay Science 2008; 42:272-275.
15. L. Zhu, R.P. Wool. Nanoclay reinforced bio-based elastomers: Synthesis and characterization. Polymer 2006; 47:8106-8115.
16. H. Zheng, Y. Zhang, Z. Peng, Y. Zhang. Influence of clay modification on the structure and mechanical properties of EPDM/montmorillonite nanocomposites. Polymer Testing 2004; 23:217–223.
17. G. Sui, W.H. Zhong, X.P. Yang, Y.H. Yu. Curing kinetics and mechanical behavior of natural rubber reinforced with pretreated carbon nanotubes. Materials Science and Engineering A 2008; 485:524–531.
18. D. Fragiadakis, P. Pissis. Glass transition and segmental dynamics in poly(dimethylsiloxane)/silica nanocomposites studied by various techniques. Journal of Non-Crystalline Solids 2007; 353:4344–4352.
19. R. Rajasekar. K. Pal, G. Heinrich, A. Das, C.K. Das. Development of nitrile butadiene rubber–nanoclay composites with epoxidized natural rubber compatibilizer. Materials and Design 2009; 30:3839–3845.

20. X.Y. Zhao, P. Xiang, M. Tian, H. Fong, R. Jin, L.Q Zhang. Nitrile butadiene rubber/hindered phenol nanocomposites with improved strength and high damping performance. Polymer 2007; 48:6056-6063.
21. T. Kameda, Y. Watanabe, G. Grause, T. Yoshioka. Dehydrochlorination behavior of polychloroprene during thermal degradation. Thermochimica Acta 2008; 476:28–32.
22. C. Dick, J.J. Liggat, C.E. Snap. Solid state 13C NMR study of the char forming processes in polychloroprene. Polymer Degradation and Stability 2001; 74:397–405.
23. T. Karayildirim, J. Yanik, M. Yuksel, M. Saglam, C. Vasile, H. Bockhorn. The effect of some fillers on PVC degradation. Journal of Analytical and Applied Pyrolysis 2006; 75:112-119.
24. F.L. Jin, K.Y. Rheeb, S.J. Park. Surface treatment of montmorillonite on the thermal stabilities of bisphenol-A diglycidyl dimethacrylate nanocomposites. Materials Science and Engineering A 2006; 436:429–433.
25. A. Laachachi, D. Ruch, F. Addiego, M. Ferriol, M. Cochez, J.M. Lopez-Cuesta. Effect of ZnO and organo-modified montmorillonite on thermal degradation of poly(methyl methacrylate) nanocomposites. Polymer Degradation and Stability 2009; 94:670–678.
26. M.N. Radhakrishnan Nair, G.V. Thomas, M.R. Gopinathan Nair. Thermogravimetric analysis of PVC/ELNR blends. Polymer Degradation and Stability 2007; 92:189-196.
27. X. Xu, Y. Ding, Z. Qian, F. Wang, B. Wen, H. Zhou, S. Zhang, M. Yang. Degradation of poly(ethylene terephthalate)/clay nanocomposites during melt extrusion: Effect of clay catalysis and chain extension. Polymer Degradation and Stability 2009; 94:113–123.
28. C.M. Dick, J.J. Liggat, C.E. Snape. Solid state ^{13}C NMR study of the char forming processes in polychloroprene. Polymer Degradation and Stability 2001; 74:397-405.
29. H. Xia, M. Song, Z. Zhang, M. Richardson. Microphase separation, stress relaxation, and creep behavior of polyurethane nanocomposites. Journal of Applied Polymer Science 2006; 103:2992-3003.
30. A. P. Meera, S. Said, Y. Grohens, A. S. Luyt, S. Thomas. Tensile stress relaxation studies of TiO_2 and nanosilica filled natural rubber composites. Industrial and Engineering Chemistry Research 2009**;** 48:3410-3416.

31. S. Ray, A. M. Shanmugharaj, A. K. Bhowmick. A new parameter for interpretation of polymer-filler and filler-filler interactions in rubber vulcanizates. Journal of Materials Science Letters 2002; 21:1097-1100.
32. J. Fröhlich, W. Niedermeier, H.D. Luginsland. The effect of filler–filler and filler–elastomer interaction on rubber reinforcement. Composites Part A: Applied Science and Manufacturing 2005; 36:449-460.

Chapter 5: Conclusions and recommendations

This thesis focused on the effects of organoclay type and filler content on the thermal, mechanical, and morphological properties of PCP/Cloisite clay nanocomposites. Nanocomposite samples with five different types of montmorillonite organoclay, Cloisite 10A, 15A, 20A, 25A, and 93A, were prepared *via* melt intercalation and analysed with TEM, XRD, DMA, FTIR, TGA, tensile testing and stress relaxation.

TEM and XRD analyses indicated very good dispersion of Cloisite 15A in the rubber matrix at all the filler contents. It was found that the disappearance of the clay reflection from the XRD pattern does not necessarily indicate complete exfoliation, since some stacks of clay were still observed in the TEM micrographs at high filler loading. The mechanical properties of the Cloisite 15A nanocomposites were improved with the incorporation of Cloisite 15A filler. The initial stresses in stress relaxation, as well as the elastic modulus increased with an increase in organoclay content. The improved reinforcement was due to good interaction between the organic modifier and the polymer chains. The nanocomposites' tensile strength and elongation decreased with an increase in filler content. This was attributed to the restricted mobility of the polymer chains. The DMA results showed improvements in the storage modulus. The improvements were related to increased sample stiffness due to the presence of the nanoparticles. There was no significant shifting in the loss maximum of the PCP nanocomposites with increasing Cloisite 15A filler content. This means that the glass transition temperature, related to the maximum of the glass transition peak in the tan δ curve, was not significantly affected by the presence of the nanofillers. There was not much difference between the TGA thermal stability for the Cloisite 15A nanocomposites and pure PCP. At different filler contents, all the samples showed similar residue contents compared to pure PCP. There was an influence of Cloisite 15A on the degradation mechanism of PCP, especially at 2.5 phr filler content, probably because of better dispersion of the filler.

The XRD and TEM results of Cloisite 93A depicted an exfoliated structure and a well-dispersed morphology in the polymer matrix at all filler contents. The TEM micrographs showed a good dispersion of the layered silicates in the PCP matrix, but in this case un-exfoliated clay stacks were also seen. The tensile testing results showed that the presence of organoclay reinforced the matrix, which was evident in the relaxation behaviour where the

nanocomposite curves lied at a higher level than that of pure PCP. The tensile modulus considerably improved with clay loading due to the stronger interfacial adhesion between the polymer and the exfoliated clay layers. The nanocomposites' tensile strengths and elongations at break decreased with an increase in filler content, and the DMA results showed a considerable increase in storage and loss modulus below the glass transition, and a slight decrease in the glass transition with organoclay loading. The α-relaxation peak maximum values in the loss modulus curves showed a similar trend for the Cloisite 15A and 93A samples as a function of clay content. The TGA results showed that there was more intimate contact between the Cloisite 93A and PCP, hence more HCl might have been adsorbed during the first stage of the degradation at all filler contents. The higher decrease in the rate of evolution of the volatiles might have been due to strong interactions at the interface between the filler and the matrix. This explains the smaller mass loss that was observed during the first degradation stage.

The morphological analyses of Cloisite 10A containing nanocomposites indicated that better polymer-filler interaction were obtained at 2.5 and 5 phr clay contents. A silicate (001) diffraction peak was not visible in the XRD spectrum at 2.5 phr clay content, but the TEM image for the 5 phr filler content showed individual silicate layers dispersed in the PCP matrix and some stacks of clay platelets. An improvement in the tensile modulus with increasing clay content was observed for the Cloisite 10A containing samples. The tensile strength and elongation at break decreased with an increase of organoclay content due to better polymer-filler interaction that restricted the mobility of polymer chains. The recovery of stress was also higher at 2.5 phr filler content due to the enhanced clay dispersion observed in the TEM micrographs. The DMA results showed that the E' and E" values of the composites below the glass transition were higher than that of pure PCP. The glass transition temperature was not affected when Cloisite 10A was mixed with PCP. There was also an increase in char content at 5 phr filler content, the formation of which was ascribed to more interactions between the clay and the rubber.

There was better dispersion of the Cloisite 25A clays in PCP at 2.5 and 5 phr filler content. At 10 phr filler content distinctive particulates of aggregates were observed which indicated partial intercalation of the sample. The mechanical properties were enhanced with the addition of as low as 2.5 phr Cloisite 25A clay. The initial stresses of all the nanocomposites were higher than that of pure PCP, and they further decreased with an increase in filler content

indicating strong reinforcement. Cloisite 25A containing samples exhibited a slight initial increase in tensile strength and elongation at break, followed by a decrease with increasing amount of filler. The DMA results showed an improvement in storage modulus below the glass transition temperature with increasing Cloisite 25A loading. There was no significant shifting in the loss maximum of the PCP nanocomposites with increasing Cloisite 25A content. This means that the glass transition temperature was also not significantly affected by the presence of nanofillers.

The (001) diffraction peaks of the Cloisite 20A nanocomposites were observed to shift to lower angles compared to that of the original organoclay. However, the TEM micrographs showed a distinct particulate structure of the filler in the PCP matrix. The tensile tests showed that there was a decrease in the elongation at break as well as the ultimate strength with increasing clay content, while a considerable increase in Young's modulus was observed. These properties agreed well with the observed morphologies. The E' and E" values of the composites below the glass transition were higher than that of pure PCP. There was no clear trend in the storage and loss moduli with increasing clay content. The α-relaxation peak maximum values from the loss modulus curves showed a similar trend to the Cloisite 10A and 15A samples as a function of clay content.

The results showed some improvements in the mechanical and dynamic mechanical properties with the incorporation of as little as 2.5 phr organoclay in all the samples. With increasing organoclay content in all the samples the tensile strength and elongation at break decreased. The drop in tensile stress at break was assigned to the fact that the filler became less delaminated and formed aggregates with an increase in filler content. The decrease in elongation at break was attributed to the clay particles acting as defect centres in the PCP matrix. The largest decrease was observed for the Cloisite 20A and 25A clay containing samples. Both these clays were derived from a single-tailed structure, which resulted in intercalated composites having moderate stiffness improvements. The Young's modulus also increased in all compositions with an increase in filler content. The biggest improvements were observed for Cloisite 15A and 93A. Both these clays contain a two-tailed hydrogenated tallow organo-modifier and showed no characteristic x-ray reflection at all filler contents in the nanocomposites. The recovery of stress was higher at 2.5 phr organoclay filler content for the Cloisite 15A containing samples due to enhanced clay dispersion. The better clay dispersion also resulted in higher quantities of carbonaceous char because of the restricted

evolution of volatile degradation products. The Cloisite 10A and 93A containing samples showed higher char contents at 5 phr clay content.

Most of the available literature on PCP focused on the pyrolysis and degradation of PCP, and little information on PCP based nanocomposites is available. Therefore it is recommended that further research be undertaken in the area of PCP based nanocomposites to better understand the relationship between the nano-morphology and its properties. Evidence from this investigation indicated that some organoclays were not well dispersed at the nano-level, and there still seem to be poor interaction between the polymer and the filler. Future research should concentrate on improving the organoclay dispersion and the polymer-filler interaction in the case of the PCP matrix. Work should also focus on the role that quartenary salts play in the decomposition of the PCP matrix, as well as the influence of the filler on the degradation mechanism of PCP.

AKNOWLEDGEMENTS

It has been an eventful journey of four years, during which I have learned a lot and have hopefully contributed towards the advancement of the field of Polymer Nanocomposites. I am thankful to my supervisor, Prof. Riaan Luyt, for introducing me to this fascinating research area and for guiding me through the entire process. His encouragement and constructive criticisms have played a major role not only in this work but in the overall development of my research aptitude. I would also like to express my gratitude to Prof. Sabu Thomas, Unmesh K.B, Dr. Vladimir Djokovic and Mr. Essa Ahmad for providing useful input in my research.

I am also thankful to all my friends and fellow students in the Polymer Research Group for their cooperation, guidance, friendship and valuable inputs in this work.
Mr. Lefu Nhlapo
Dr. Spirit Molefi
Mr. Tshwafo Motaung
Mr. Mfiso Mngomezulu
Ms. Julia Mofokeng
Mr. Tsietsi Tsotetsi
Mrs. Moipone Mokoena
Mrs. Dorine Mosiangaoko
Mrs. Mpondi Molefe
Mr. Dumisane Gamede

Special thanks go to University of Free State at large and the National Research Foundation for providing financial assistance.

APPENDIX

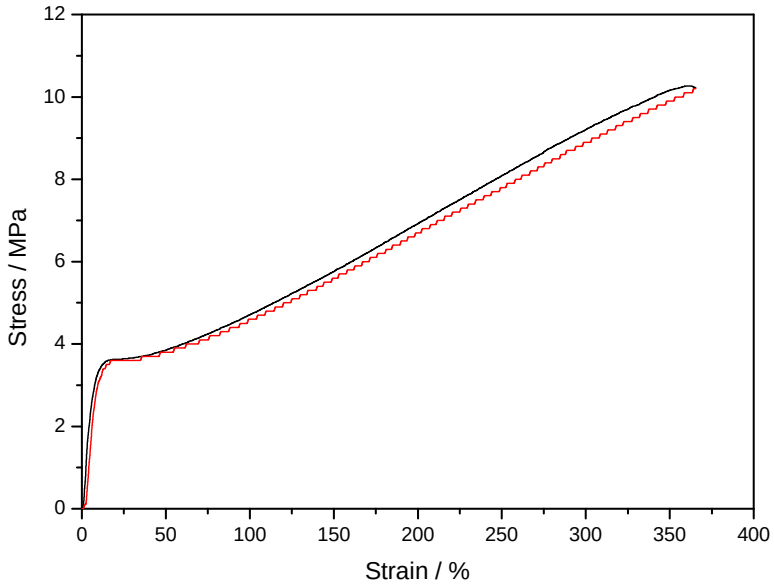

Figure A.1 Stress-strain curves for pure PCP

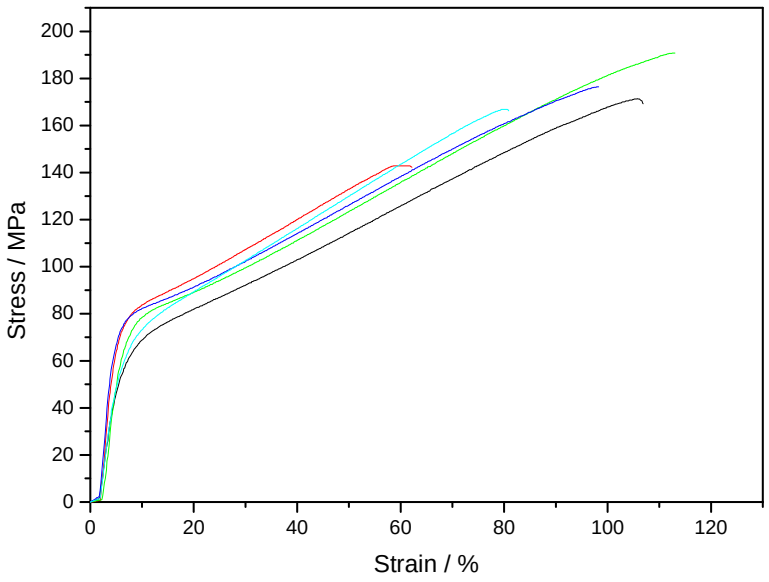

Figure A.2 Stress-strain curves for PCP + 2.5 phr Cloisite 10A nanocomposites

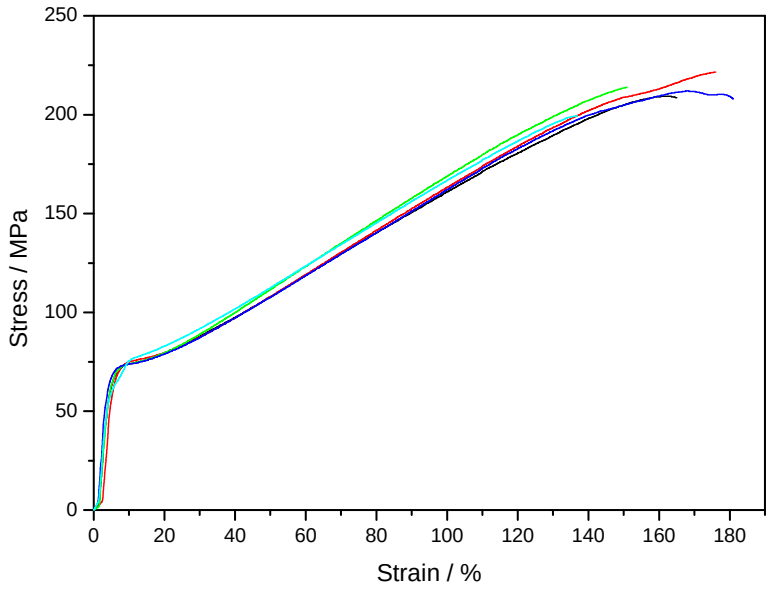

Figure A.3 Stress-strain curves for PCP + 5 phr Cloisite 10A nanocomposites

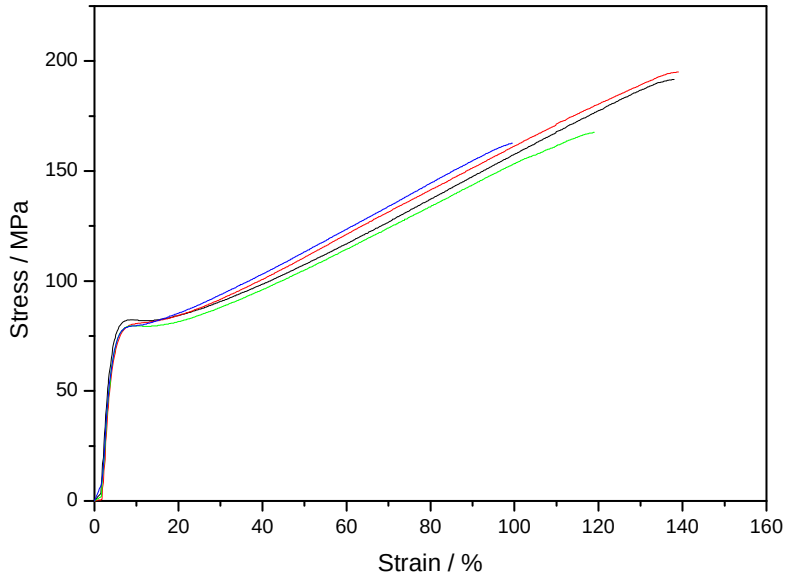

Figure A.4 Stress-strain curves for PCP + 10 phr Cloisite 10A nanocomposites

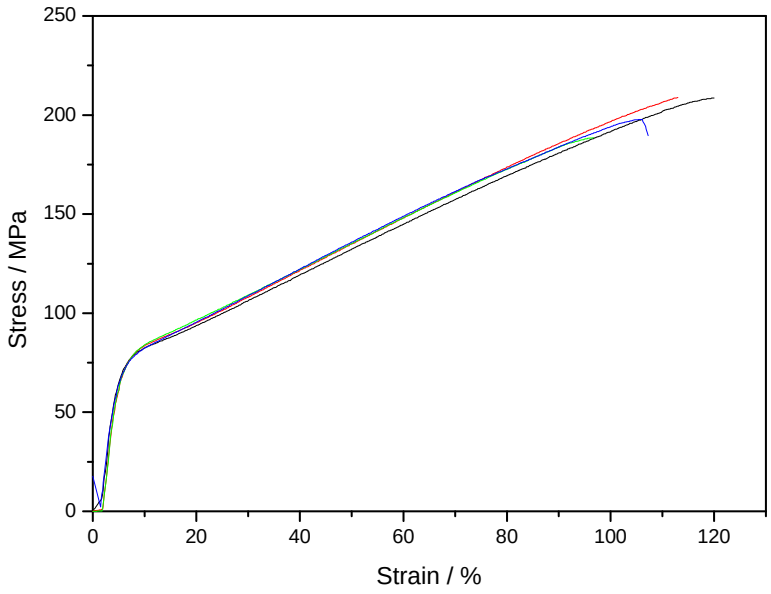

Figure A.5 Stress-strain curves for PCP and 2.5 phr Cloisite 15A nanocomposites

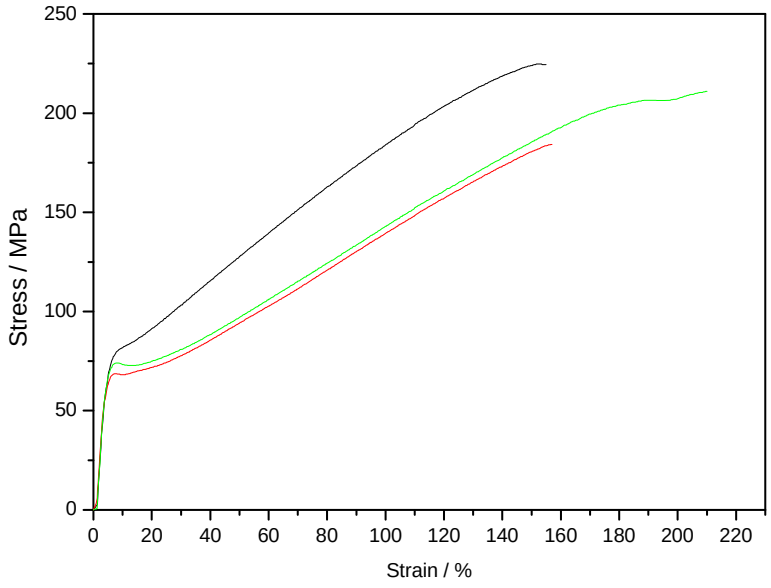

Figure A.6 Stress-strain curves for PCP + 5 phr Cloisite 15A nanocomposites

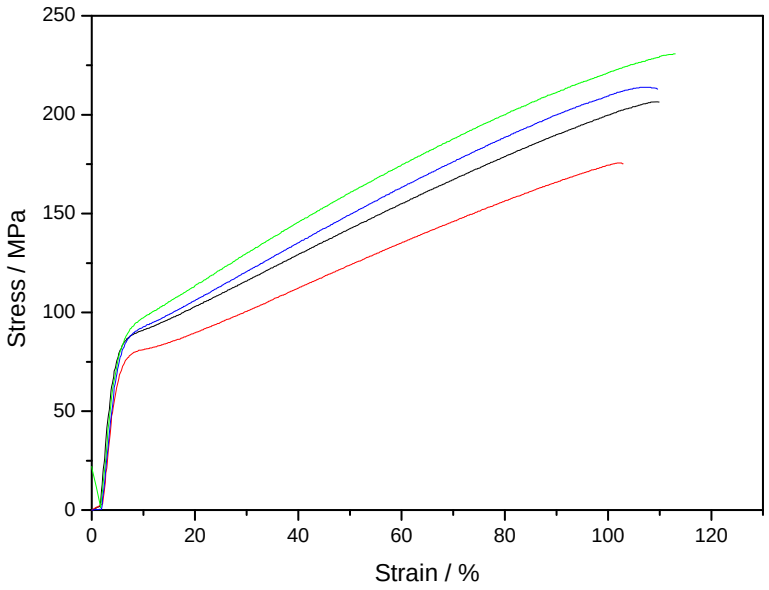

Figure A.7 Stress-strain curves for PCP + 10 phr Cloisite 15A nanocomposites

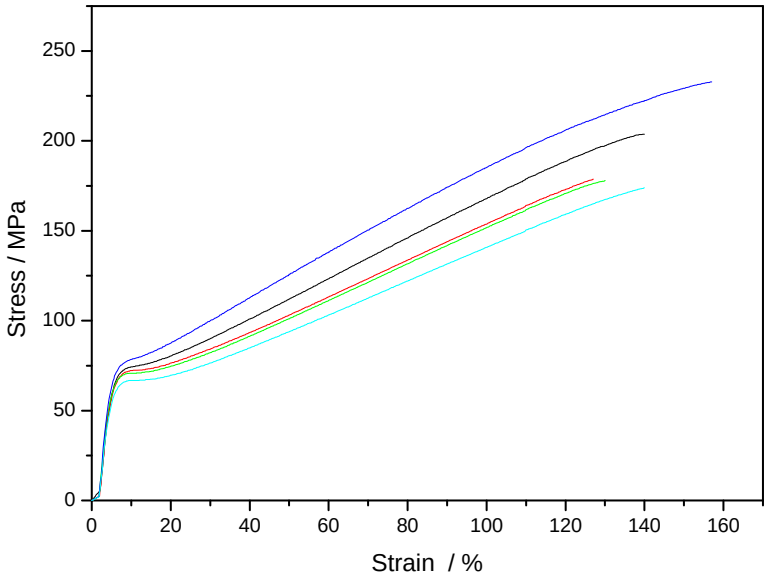

Figure A.8 Stress-strain curves for PCP + 2.5 phr Cloisite 20A nanocomposites

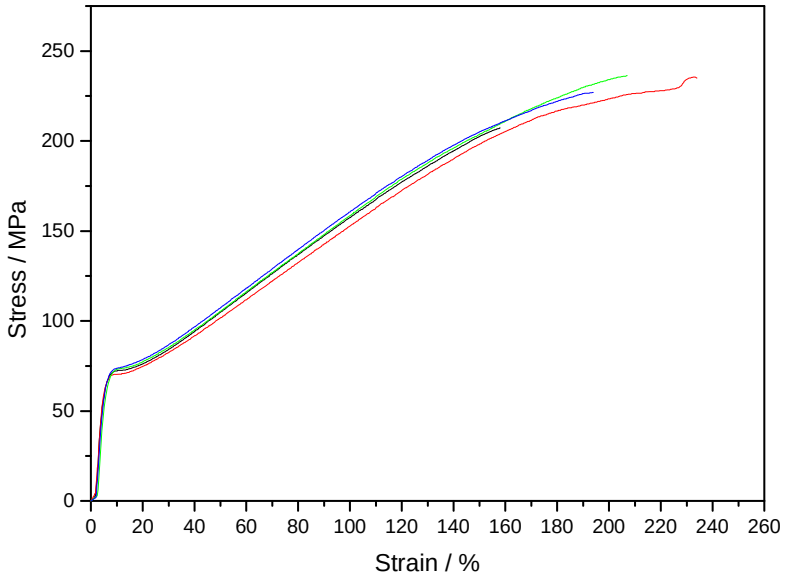

Figure A.9 Stress-strain curves for PCP + 5 phr Cloisite 20A nanocomposites

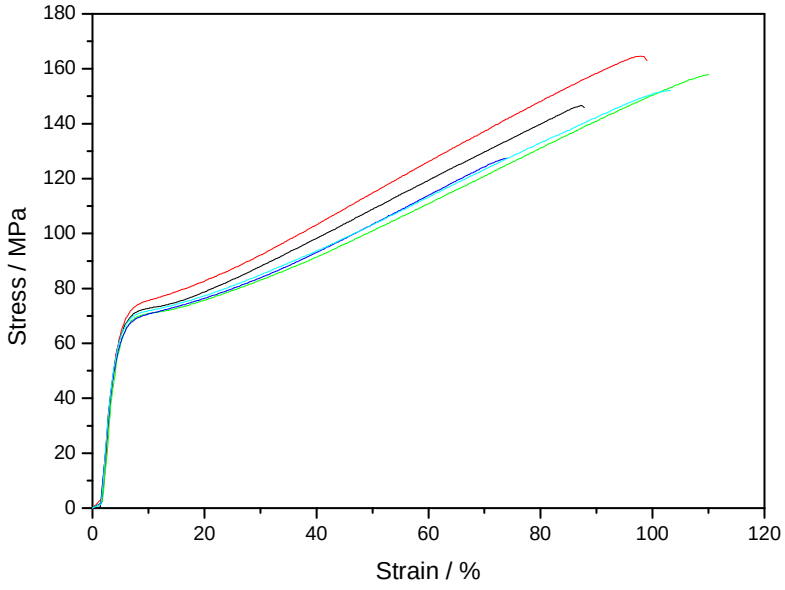

Figure A.10 Stress-strain curves for PCP + 10 phr Cloisite 20A nanocomposites

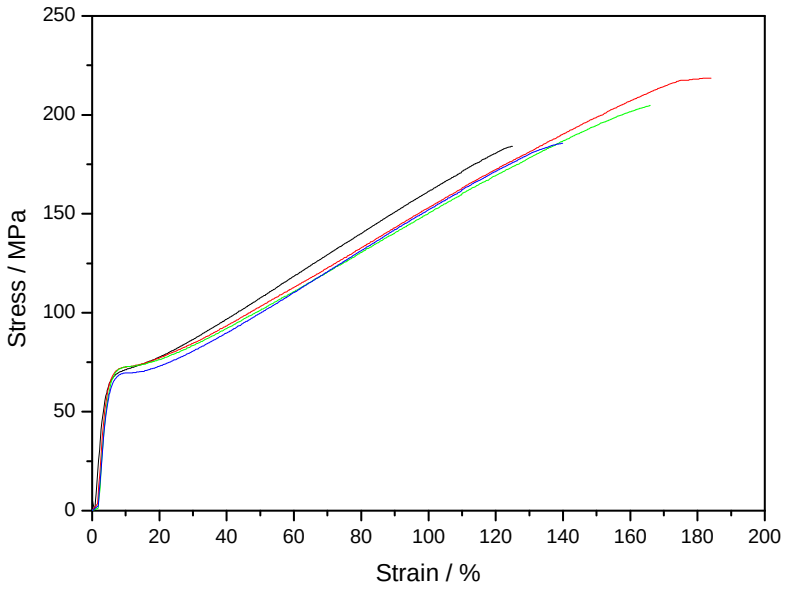

Figure A.11 Stress-strain curves for PCP + 2.5 phr Cloisite 25A nanocomposites

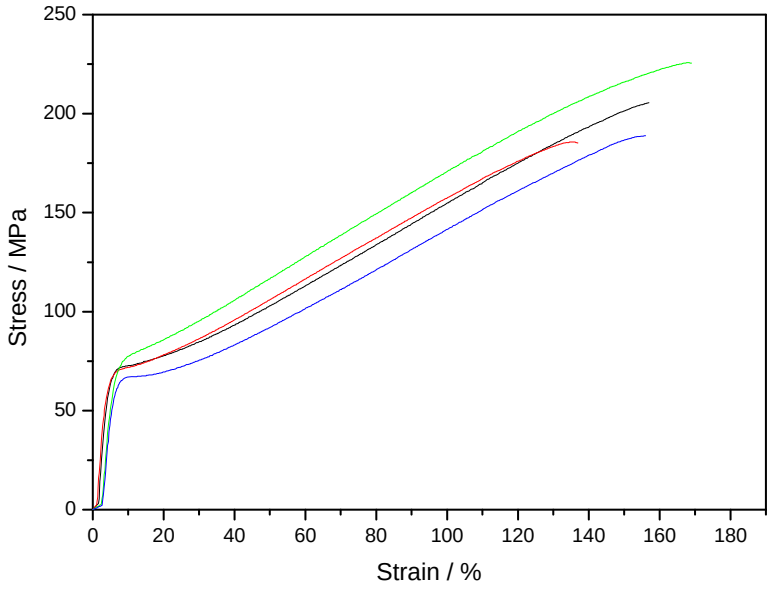

Figure A.12 Stress-strain curves for PCP + 5 phr Cloisite 25A nanocomposites

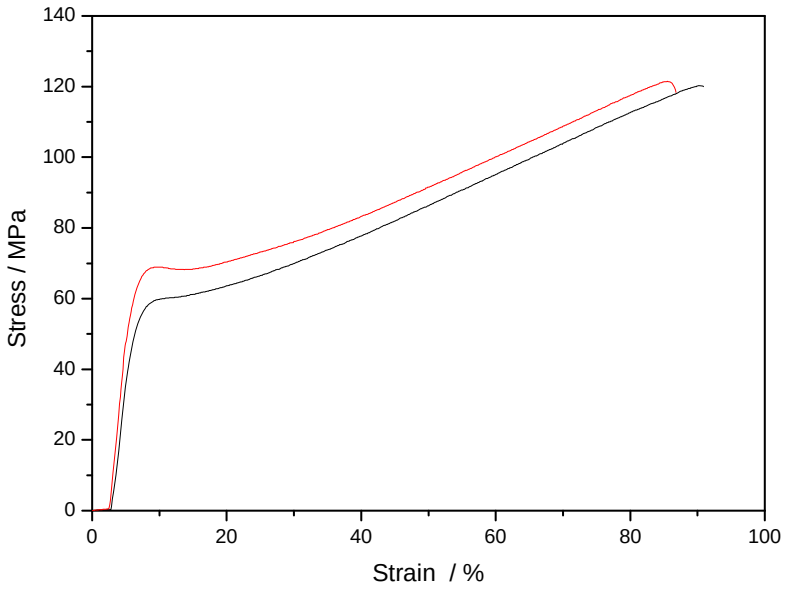

Figure A.13 Stress-strain curves for PCP + 10 phr Cloisite 25A nanocomposites

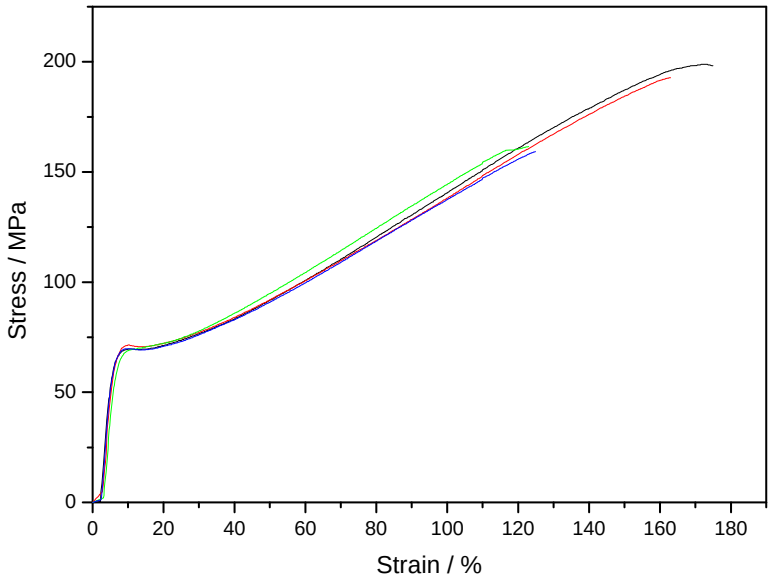

Figure A.14 Stress-strain curves for PCP + 2.5 phr Cloisite 93A nanocomposites

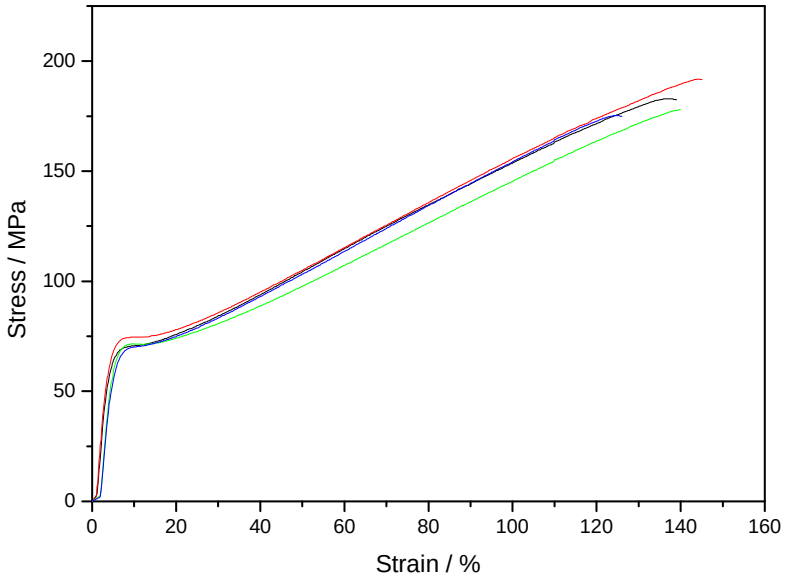

Figure A.15 The stress-strain curves for PCP and 5 phr Cloisite 93A nanocomposites

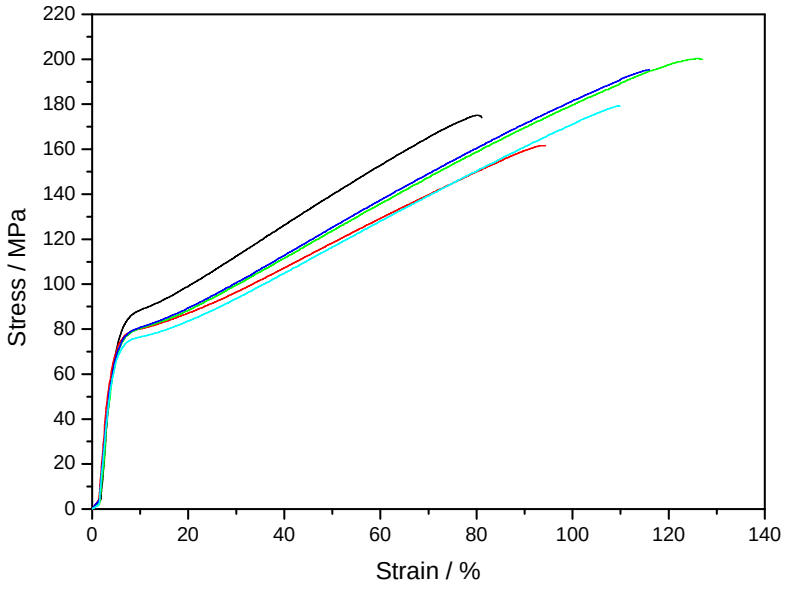

Figure A.16 Stress-strain curves for PCP + 10 phr Cloisite 93A nanocomposites